

# Overall voltage stability with the presence of distributed energy resources in a low voltage DC network

Giel Van den Broeck

Thesis submitted for the degree of  
Master of Science in de  
ingenieurswetenschappen: energie

**Thesis supervisor:**

Prof. dr. ir. Johan Driesen

**Assessors:**

Prof. dr. ir. Ruth Vazquez Sabariego

Dr. ir. Barry Rawn

**Mentor:**

Ir. Tuan Dat Mai

© Copyright KU Leuven

Without written permission of the thesis supervisor and the author it is forbidden to reproduce or adapt in any form or by any means any part of this publication. Requests for obtaining the right to reproduce or utilize parts of this publication should be addressed to Faculteit Ingenieurswetenschappen, Kasteelpark Arenberg 1 bus 2200, B-3001 Heverlee, +32-16-321350.

A written permission of the thesis supervisor is also required to use the methods, products, schematics and programs described in this work for industrial or commercial use, and for submitting this publication in scientific contests.

# Preface

Five years ago, I started as a bachelor engineering student at the university of Leuven. After obtaining my bachelor degree in mechanical and electrical engineering, I decided to further specialize in energy sciences, a relatively new education programme at our faculty. To my opinion, the energy programme is unique in the sense that it involves technical, economical as well as political aspects. I furthermore believe that technology will play an important role in facing the energy challenges that are ahead of us. The master Energy allowed me to widen my vision on energy, while still deepening my technical skills.

This master thesis concludes my five-year study in engineering sciences. In this preface, I would like to thank all that helped me to achieve this master thesis.

First of all, I would like to thank my supervisor, TuanDat Mai, for carefully reviewing my thesis texts, the daily supervision and the advice. TuanDat, I would like to especially thank you for giving me the opportunity to publish my first technical paper.

Secondly, special thanks go to my promotor Prof. Johan Driesen, for offering me this interesting subject in the field of renewable energy and smart distribution grids. I would like to thank you especially because you gave me the freedom to explore and find my own way.

Thirdly, I would like to thank the assessors, Prof. Ruth Sabariego and Dr. Barry Rawn for reading this thesis text.

Finally, I would like to thank my family and friends for supporting me, not only this year but also the last five years. You were always there when I needed a pat on the back. Especially, I would like to thank my grandfather and father for passing on their passion for electronics and technology. You were always prepared to listen and discuss with me on technical and energy-related topics.

*Giel Van den Broeck*

# Contents

<b>Preface</b>	<b>i</b>
<b>Abstract</b>	<b>iv</b>
<b>Dutch abstract</b>	<b>v</b>
<b>List of Figures and Tables</b>	<b>vi</b>
<b>List of Abbreviations and Symbols</b>	<b>viii</b>
<b>1 Introduction</b>	<b>1</b>
1.1 Context and motivation . . . . .	1
1.2 Thesis objectives and constraints . . . . .	4
1.3 Thesis outline . . . . .	5
<b>2 Low-voltage DC networks</b>	<b>7</b>
2.1 Structure of LVDC networks . . . . .	7
2.2 DC versus AC distribution networks . . . . .	10
2.3 Protection of DC distribution networks . . . . .	16
2.4 Conclusion . . . . .	18
<b>3 DC voltage stability and static control</b>	<b>19</b>
3.1 A definition of DC voltage stability . . . . .	19
3.2 System-theoretical framework for stability . . . . .	24
3.3 Control of the DC voltage . . . . .	36
3.4 Conclusion . . . . .	38
<b>4 Time-domain models of DC systems</b>	<b>41</b>
4.1 Models of power electronic converters . . . . .	42
4.2 Models of distributed energy resources . . . . .	60
4.3 Model of a photovoltaic system . . . . .	61
4.4 Switched simulation of a small LVDC system . . . . .	63
4.5 Conclusion . . . . .	64
<b>5 MatLVDC</b>	<b>65</b>
5.1 Capabilities of MatLVDC . . . . .	65
5.2 Structure of the toolbox . . . . .	67
5.3 Application Example: circuit including a constant-power load . . . . .	69
5.4 Conclusion . . . . .	73

<b>6 DC voltage stability of a LVDC network</b>	<b>75</b>
6.1 Description of the network . . . . .	75
6.2 Influence of power variations . . . . .	79
6.3 Conclusion . . . . .	89
<b>7 Conclusion and future work</b>	<b>91</b>
<b>A Maximum power through a line</b>	<b>95</b>
A.1 Assumptions . . . . .	95
A.2 Maximum power through a line . . . . .	96
<b>B MatLVDC User Guide</b>	<b>99</b>
<b>C Modeling Dynamics of Electric and Electronic Components in DC Distribution Grids</b>	<b>109</b>
<b>References</b>	<b>117</b>

# Abstract

Although alternating current (AC) networks are well established today, modern power electronics have enabled an increasing number of direct current (DC) loads. Additionally, increasing environmental concerns and uncertain investment policies for centralized electricity generation are causing a shift towards distributed energy resources (DER). Most DER require DC in the power conversion chain. The increasing number of DC loads and generation consequently encourages the power industry to develop DC networks that can avoid AC/DC conversion steps which reduce the system efficiency.

This thesis addresses voltage stability in low-voltage DC networks, since it is of utmost importance to ensure the safe and reliable operation of DC networks. A definition for LVDC voltage stability is proposed, based upon the existing definition of AC power system stability. The major contribution of this master thesis is a Matlab® toolbox that facilitates the dynamic simulation and linear system analysis of DC networks. Furthermore, a comprehensive overview of DC networks is provided, including a SWOT analysis and an overview of nominal voltage levels.

# Dutch abstract

## **Nederlandstalige titel:**

### **Spanningsstabiliteit in laagspanning gelijkstroomnetten met inbegrip van verspreide energie-opwekking**

Omwille van historische redenen, maakt het huidige elektriciteitsdistributienet gebruik van wisselstroom -en spanning om elektriciteit naar de verbruikers te verdelen. Nochtans is het aantal verbruikers die werken op gelijkstroom fors toegenomen door de ontwikkelingen in de vermogenelektronica vanaf midden vorige eeuw. Daarnaast leiden het toegenomen milieubewustzijn en een onzeker investeringsklimaat voor centrale energie-opwekking, tot meer verspreide energie-opwekking in het distributienet. Deze verspreide energiebronnen leveren vaak gelijkstroom die moet worden omgezet in wisselstroom door vermogenelektronische convertoren, wat gepaard gaat met verliezen.

Gelijkstroomnetten kunnen ook meer vermogen overbrengen over dezelfde kabels voor wisselstroom. Daarnaast laten ze ook toe de efficiëntie van het systeem te verbeteren door het aantal vermogenelektronische convertoren te verminderen.

Het gebruik van gelijkstroomnetten is niet beperkt tot elektriciteitsdistributie, maar ze worden ook toegepast in de scheepvaart en luchtvaart, data centers en het laden van elektrische voertuigen.

Deze thesis behandelt spanningsstabiliteit in gelijkstroomnetten, omdat dit belangrijk is voor de veilige en betrouwbare werking van gelijkstroomnetten. Een definitie voor spanningsstabiliteit is niet voorhanden en daarom stelt deze thesis een definitie voor. Een voorname bijdrage van deze thesis is de ontwikkeling van een Matlab toolbox om tijdsdomeinsimulaties en kleinsignaalanalyse van gelijkstroomnetten uit te voeren. Deze analyse-methoden zijn toegepast om de stabiliteit na te gaan van een laagspanning gelijkspanningsnet.

# List of Figures and Tables

## List of Figures

2.1	DC and AC network configurations . . . . .	8
2.2	AC and DC waveforms . . . . .	10
2.3	AC versus DC current distribution [4] . . . . .	12
2.4	Number of converters in DC and AC distribution networks[3] . . . . .	12
3.1	Stability in the state-phase plane . . . . .	20
3.2	Transient voltage envelope MIL-STD-704-F (270 V DC system) [15] . . . . .	22
3.3	DC voltage stability classification[43] . . . . .	23
3.4	Overview of the stability analysis techniques . . . . .	24
3.5	Envelope of a normal voltage transient for 28 V buck converter [41] . . . . .	26
3.6	DC system comprising a constant-power load (P) . . . . .	26
3.7	Steady-state source and load characteristic of the circuit in fig. 3.6 . . . . .	28
3.8	Stability of equilibria . . . . .	28
3.9	Stability limits for the CPL example network fig. 3.6 . . . . .	32
3.10	Minor loop gain criteria [57] . . . . .	33
3.11	Subsystem interconnection [57] . . . . .	33
3.12	Stability assessment of the CPL example by the minor-loop gain Nyquist plot . . . . .	35
3.13	DC voltage control possibilities . . . . .	37
3.14	DC voltage droop control characteristic . . . . .	38
4.1	Overview of a DC system . . . . .	41
4.2	Overview of the modeling techniques for power electronic converters . . . . .	44
4.3	DC/DC converter . . . . .	45
4.4	DC/DC converter inductor voltage and current waveforms . . . . .	45
4.5	Overview of the modeling techniques for power electronic converters . . . . .	51
4.6	A comparison between the different models w.r.t. computation time and error for the inductor current (left) and capacitor voltage (right) . . . . .	53
4.7	Case 1 — Variation of the switching frequency . . . . .	54
4.8	Case 2 — Variation of the inductance . . . . .	55
4.9	Case 3 — Variation of the capacitance . . . . .	56
4.10	Case 4 — Variation of the duty cycle . . . . .	57

4.11	AC/DC interface converter . . . . .	58
4.12	Control scheme of a PV generator interfaced via a DC/DC boost converter . . .	61
4.13	Circuit diagram of the investigated DC system . . . . .	63
4.14	Comparison between averaged and switched DC bus voltage waveforms at bus 3	64
5.1	Possible network topologies . . . . .	66
5.2	Class overview of MatLVDC . . . . .	67
5.3	Overview of a DC system . . . . .	68
5.4	Application example to demonstrate MatLVDC . . . . .	69
5.5	Input data for MatLVDC . . . . .	71
6.1	Unipolar DC network . . . . .	77
6.2	Bipolar DC network . . . . .	78
6.3	Linearized system poles . . . . .	79
6.4	Simulation results for a PV input power 50% step change . . . . .	80
6.5	Unipolar bus voltage transients for varying PV power generation . . . . .	82
6.6	Bipolar bus voltage transients for varying PV generation . . . . .	83
6.7	Bode plot for the linearized DC system around the initial operating point w.r.t. the PV irradiance inputs (dashed line for unipolar network; solid line for bipolar network) . . . . .	84
6.8	Unipolar bus voltage transients for varying microturbine power generation . .	85
6.9	Bipolar bus voltage transients for varying microturbine power generation . . .	86
6.10	Unipolar bus voltage transients for varying resistive load (BUS 4) power demand	87
6.11	Bipolar bus voltage transients for varying resistive load (BUS 4) power demand	88

## List of Tables

2.1	Proposed voltage levels for LVDC distribution networks . . . . .	9
2.2	SWOT analysis of DC grids . . . . .	11
3.1	The circuit parameters for fig. 3.6 . . . . .	29
4.1	Model parameters . . . . .	53
4.2	References to the models of distributed energy resources and power converters that are applied in this thesis . . . . .	60
5.1	Stable and unstable values of $R$ . . . . .	70
6.1	Main component parameters . . . . .	76

# List of Abbreviations and Symbols

## Abbreviations

AC	Alternating Current
DC	Direct Current
DER	Distributed energy resources
EPRI	European Power Research Institute
HVDC	High Voltage Direct Current
ICT	Information and communication technology
IEA	International Energy Agency
LV	Low-voltage
PEC	Power electronic converter
PV	Photovoltaic
RES	Renewable energy sources
SS	State-space representation

---

## Symbols

A	Ideality factor
C	Capacitance
d	Duty cycle
L	Inductance
i	Current
$I_{ph}$	Photo-current
$I_s$	Reverse diode saturation current
k	Boltzmann constant
$K_i$	Integral controller gain
$K_p$	Proportional controller gain
$n_p$	Number of PV array strings in parallel
$n_s$	Number of PV modules in series
P	Power
q	Electron charge or switching function
S	Solar irradiance
t	Time
v	Voltage
V	Voltage
$\theta$	Temperature
$\tau$	Time constant



# Chapter 1

## Introduction

### 1.1 Context and motivation

In the recent years, governments and the power industry are fundamentally rethinking the ways of generating and using the available energy resources, because they have increased environmental concerns, want to decrease their dependency on fossil fuels, and all this in a context of liberalized electricity markets. Meanwhile, the mission of the power industry remains to assure secure and reliable electricity supply, because the cost of the energy-not-served significantly exceeds the cost of supplying a unit of electricity. Although this mission remains the same as in the early days of power systems, the operating boundary conditions are changing and the existing grid is not designed for that.

#### **Distributed energy resources**

Today, electricity is generated by large, centralized generators and then delivered to the customer via the transmission and distribution grid. Although this paradigm was favored in the early days of power systems, a transition has begun. Policy incentives and technical advancements enabled the rapid deployment of distributed energy resources (DER) that are connected directly to the distribution network or on the customer side of the power meter. This definition of DER includes renewable energy sources (RES) as small-scale photovoltaic generation (PV) and wind power, but also cogeneration and fuel cells [2].

While policy incentives aim at reducing greenhouse gas emissions and air pollution, DER present several technical challenges to assure the secure and reliable operation of the power system in the future. For instance, since the electric power system is the ultimate *just-in-time* system [49], demand and generation should at all times remain in balance. This balance is at stake, due to the intermittent nature of RES like PV and wind, of which the power output varies according to weather conditions. Moreover, a large number of DER may cause overloading of equipment in the distribution network. Consider for example Germany, where approximately 80% of the PV generation is connected at low-voltage: it is not uncommon for the PV power to exceed the peak load by three to four times on feeders that are not designed to accommodate PV [65]. DER also have a lower reliability and availability than the utility service [49].

Apart from technical challenges, the deployment of DER will require new market mechanisms. Today, for instance, utilities recover the fixed costs that are due to network services via the variable tariffs per unit electricity. Thus although customers with a PV installation profit from the network services, their annual electricity bill is low since it is only determined by their net electricity consumption.

To overcome these technical and economical challenges, the European Power Research Institute (EPRI) advises an integrated approach [16], where the presence of DER is incorporated in network development plans, network codes and market mechanisms.

### **Increasing demand for electricity**

Apart from a shift towards DER at the generation side, the electricity infrastructure will also have to deal with an increased demand. For instance, the International Energy Agency (IEA) expects that in 2020, 20 million electric vehicles (EVs) will be on the road [30]. Since the current distribution network is not able to handle these large numbers, coordinated charging will be required [13]. Moreover, the IEA expects a 300% increase in ICT-related electricity consumption [29].

### **Increasing application of DC**

While the original grid transmits electricity by means of alternating current (AC), the interest to apply direct current (DC) for electricity distribution and transmission increases. In fact, this situation resembles the battle of the currents at the end of the 19th century when the first power systems were developed. At that time, Thomas Edison promoted the use of DC, while George Westinghouse advocated the use of AC. Eventually, the trend towards building large, centralized generation facilities required high voltages to transmit electricity over long ranges. Only AC could at that time be easily transformed to high voltages by means of the transformer, invented in 1886 by William Stanley [53], which is one of the main reasons why AC transmission and distribution systems are widespread today.

Although electricity is transmitted using AC, a lot of loads today operate at DC or at least require DC somewhere in the power conversion chain: personal computers, cellphones, induction motors that are driven by a variable-speed drive, electronic ballasts for fluorescent lighting, LEDs. Moreover, the successful development of modern power electronics since the 1950's, has also enabled DC/AC conversion and DC/DC conversion. Apart from the low-voltage applications, High-Voltage DC (HVDC) has gained importance, because this technology allows to transmit bulk power over long distances and to construct submarine transmission links [5].

Apart from the loads, also PV generation operates at DC and wind generators require an intermediate DC bus to inject power into the grid that matches the phase angle and frequency of the grid. The logical next step would then be to extend this DC bus up to the network level and construct a DC grid. This would reduce (or at least simplify) the number of converters in the power system, and therefore the efficiency increases. Moreover, DC enables to transmit more power across the conductors that are in place or permits to use thinner conductors. A more detailed discussion on the advantages and disadvantages of DC networks is provided in Chapter 2.

DC power although is not new: the first commercial high-voltage DC (HVDC) connection was installed in Sweden [5] and the International Space Station is equipped with a DC power distribution network [26]. In April 2013, ABB equipped a Norwegian vessel with a full onboard DC network to improve the fuel efficiency [1]. Moreover, equipping future aircraft with an onboard DC network allows to reduce conductor cross-sections and consequently save weight [11].

### **Low-voltage DC distribution networks**

Since low-voltage DC (LVDC) networks offer potential advantages and cost savings, this has been a subject of research. The research mainly focused on possible network configurations and static stability (i.e. the stable and acceptable operation of DC networks in steady-state) and control, although no definition for voltage stability in LVDC networks exists to the author's knowledge. While the subject of static stability and control has attracted great attention, the transient stability (i.e. stability following disturbances that have occurred) is under-investigated. Moreover, the available stability criteria that are available in the literature are inherently conservative and difficult to apply to larger DC networks.

## 1.2 Thesis objectives and constraints

This thesis primarily focuses on following objectives:

- Define DC voltage stability for LVDC distribution networks and justify the importance of DC voltage stability
- Develop a Matlab toolbox to assess the stability of LVDC networks by using small-signal analysis
- Apply the developed toolbox to analyze the stability of a reference LVDC network that comprises distributed energy resources

This thesis focuses on the voltage stability of LVDC networks and does not consider the interactions between the AC and DC network. Therefore, the AC network is modeled as an infinite bus that by definition has a constant voltage magnitude, a constant frequency and the three phases are symmetric.

DC networks consist of a large number of power electronic converters, that have nonlinear dynamics. This thesis will apply the small-signal linearization technique to assess the stability of LVDC networks. This thesis focusses on small-signal stability of steady-state operating equilibria. Therefore, the start-up behavior of DC systems is not treated.

## 1.3 Thesis outline

Following this introductory chapter, this thesis consists of five chapters.

Chapter 2 gives a conceptual overview of DC networks. The structure of DC networks is introduced and the strengths, weaknesses, opportunities and threats of DC networks are discussed. The chapter concludes with the protection of DC networks.

A definition of DC voltage stability is proposed in chapter 3, based on the accepted definition of power system stability. The importance of DC voltage stability is highlighted and the mathematical tools to assess stability are revised. This chapter also provides an example of DC voltage instability by means of a DC network that contains a constant-power load. The different stability analysis techniques are reviewed and are subsequently applied to the example network. Chapter 3 ends with a discussion on static voltage control to ensure the power balance in steady-state.

Chapter 4 addresses the time-domain modelling techniques that are appropriate to assess DC voltage stability. Because of the nonlinear switching behavior of power electronic converters, the dynamic simulation requires numerically stiff-ODE solvers. Typically, these solvers apply small time steps that lead to long computation times. To overcome this issue, the first part of this chapter gives an overview of the available dynamic modelling techniques that smooth out the switching behavior of the power electronic converters and therefore decrease the computation time. The second part of this chapter discusses the modelling and control of distributed energy resources, that are present in DC networks. This chapter concludes with a time-domain simulation of an LVDC network that shows that averaged converter models are a good approximation to assess the stability of a DC network that includes distributed energy resources.

Chapter 5 discusses MatLVDC, a Matlab® toolbox that the author has developed to assess the voltage stability of DC networks. This is the major contribution of this master thesis, since MatLVDC allows to easily set up a state-space representation of DC networks that can subsequently be simulated and analyzed by using small-signal analysis. This toolbox can serve a wide variety of applications, such as DC distribution networks, data centers and DC networks onboard ships and aircraft. An overview of the capabilities of the toolbox, the structure of the program code and an application example is provided in Chapter 5. A user guide is provided in the appendix.

Chapter 6 analyzes the stability of a unipolar and bipolar DC distribution network that comprises distributed energy resources. The toolbox MatLVDC is applied here to obtain the results, for three simulation scenarios of realistic disturbances that may occur.

The last chapter provides the conclusions of this thesis and suggestions for future work.



## Chapter 2

# Low-voltage DC networks

Low-voltage DC (LVDC) networks have drawn the attention of the power industry: a large number of loads operate at DC or require DC in the power conversion chain and, in addition, LVDC distribution systems can facilitate the increasing number of distributed energy resources (DER) that regularly output DC power.

This chapter introduces LVDC networks. The first section will introduce the structure of DC networks, including a discussion on the possible network configurations and possible voltage levels. The second section will discuss differences between AC and DC distribution networks. In particular, this section analyzes the strengths, weaknesses, opportunities and threats (SWOT) of DC networks and discusses whether the existing AC infrastructure is suited for DC distribution. The last section will discuss the protection system for DC distribution grids.

## 2.1 Structure of LVDC networks

### 2.1.1 Distribution network configurations

The technical literature proposes two network *configurations* for LVDC distribution networks: the unipolar and bipolar configuration (Figure 2.1). The unipolar configuration consists of a positive (+) and negative (-) phase conductor (+) that carry the load current, while the bipolar configuration provides an additional neutral (0) return conductor at an intermediate voltage level.

The bipolar configuration offers advantages over the unipolar configuration in terms of:

1. *Increased reliability*: two conductors can remain in service when the third conductor would fail[33, 37]
2. *Increased power transfer capability*: this will be elaborated in section 2.2.1.

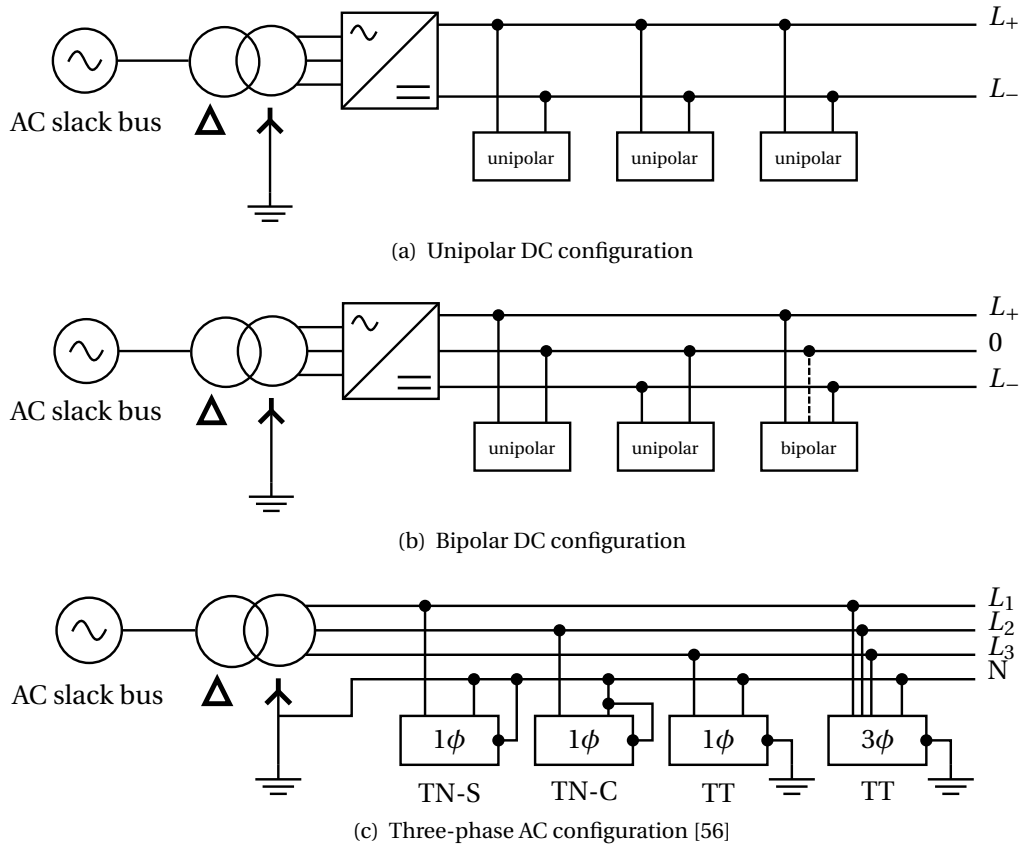


FIGURE 2.1: DC and AC network configurations

### 2.1.2 DC distribution network components

A DC network requires an AC/DC inverter as an interface between DC and AC distribution networks. Moreover, bipolar DC networks apply additionally converters to balance phase voltages and currents.

#### AC/DC interface inverter

Both the unipolar and bipolar configuration will require an inverter at the interface between the DC and AC distribution networks. This inverter should enable bi-directional power flow, especially when distributed energy resources are implemented [10, 31]. A forced-commutated voltage-source (VSC) inverter (VSC) is therefore preferred to a line-commutated current-source inverter (LCC). A VSC requires smaller harmonic filters than a LCC because of the higher switching frequencies [6]. Furthermore, a VSC can provide reactive power support to the AC system, or operate at unity power factor to minimize transmission losses in the AC system [4].

DC networks are also capable of operating as a microgrid. Microgrids are electrical networks that can run either in grid-connected mode or in islanding mode. In islanding mode, the microgrid is disconnected from the utility grid and demand and generation need to be balanced locally. In DC microgrids, the AC/DC inverter should provide the smooth transition between grid-connected and islanding mode [37].

### Voltage and current balance converters

A bipolar configuration will require a *voltage balancer* to balance the voltage between the phase conductors and the neutral conductor. When no voltage balancer is installed, the voltage between the positive terminal and neutral will differ from the voltage between the negative terminal and neutral.

In bipolar configurations, when the load currents that flow through the positive and negative line differ, the current in the neutral conductor will not be zero. Therefore losses arise in the neutral conductor, which can be avoided by a *current balancer*. This current balancer can additionally participate to dampen oscillations in DC networks [45].

### 2.1.3 Nominal voltage levels

The nominal voltage level will determine the conductor insulation level and cross-section, the rating of the power semiconductor devices and the protection devices. According to the EU Low-Voltage Directive [21], this voltage level should range between 75 V and 1500 V. Table 2.1 provides an overview of the voltage levels that are proposed.

At the moment of writing, no nominal voltage standard exists for LVDC distribution networks [45].

Voltage level	Proposed by	Motivation
$\pm 170\text{V}$	[35]	Low voltage to the ground and 340V available for loads that require more power. Matches the Japanese AC power network.
326V	[19]	326 V is the peak voltage of the utility network in Europe, that allows to reconstruct AC voltage waveforms.
380V	[8]	Limit of the AC wiring infrastructure and power semiconductors
400V	[39]	Covers most existing consumer loads and indoor appliances
More studies are reported in [32]		

TABLE 2.1: Proposed voltage levels for LVDC distribution networks

## 2.2 DC versus AC distribution networks

### 2.2.1 Strengths, weaknesses, opportunities and threats

Table 2.2 outlines the strengths, weaknesses, opportunities and threats (SWOT) of DC distribution networks as compared to AC distribution. The strengths and weaknesses of DC distribution networks are the inherent advantages and disadvantages. The opportunities and threats take into account the external factors, like the increasing number of distributed energy resources. The following paragraphs will motivate this SWOT analysis more in detail and compare DC to AC distribution systems.

#### Strengths

**Transfer more power** In contrast to AC, DC distribution networks enable to transfer more power through the same cable infrastructure and involve less conduction losses [34, 3, 9].

When comparing the cable infrastructure of three-phase AC networks (Figure 2.1(c)) to DC networks (Figure 2.1(a), Figure 2.1(b)), DC networks are able to operate around the peak voltage level that is  $\sqrt{2}$  higher than the AC rms voltage [3, 34]. This is illustrated by the voltage and current waveforms in Figure 2.2. The filled grey and blue area indicate the energy that the current and voltage waveforms contain within one AC period, while the current and voltage are at the operating limits. Since the grey area is larger than the blue area, the average DC power is higher. Also note that the blue area further decreases when the AC waveforms are not in phase ( $\cos \phi = 1$ ). Figure 2.3 illustrates this effect on the maximum power that can be transmitted across a three-phase AC, a unipolar and a bipolar configuration [4].

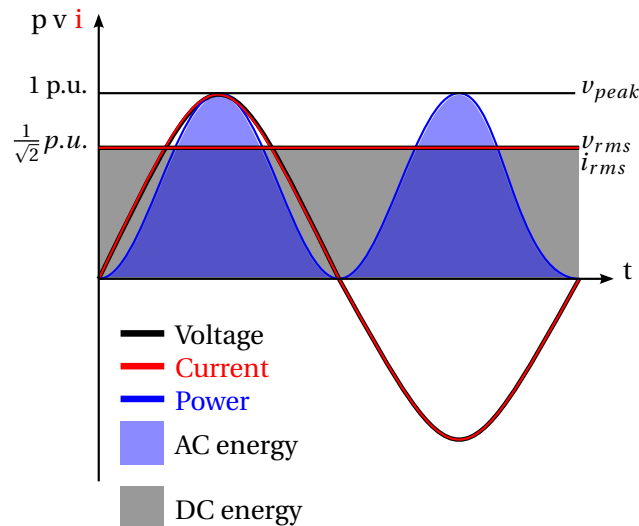


FIGURE 2.2: AC and DC waveforms

Strengths	Weaknesses
<ul style="list-style-type: none"> <li>• DC networks can transfer more power through the same cable as compared to AC</li> <li>• DC networks involve less losses</li> <li>• DC DER do not require frequency synchronization by means of a phase-locked loop (PLL)</li> <li>• More control is possible in the context of smart grids since DC grids consist of controllable power electronic converters: <ul style="list-style-type: none"> <li>– The AC/DC interface inverter can operate at unity power factor to minimize the losses in the transmission network</li> </ul> </li> <li>• The power quality increases <ul style="list-style-type: none"> <li>– The AC/DC interface inverter provides better fault-ride through capability</li> <li>– The controllable DC converters can regulate the load voltage, when a voltage fluctuation occurs in the DC distribution network</li> </ul> </li> </ul>	<ul style="list-style-type: none"> <li>• Protection is more difficult</li> <li>• More power electronics affect the reliability and filters are needed to reduce the harmonics</li> <li>• Relatively new technology: uncertainty in reliability, technology and costs evolution</li> <li>• The AC/DC inverter, at the point-of-common-coupling between AC and DC networks, has converter losses.</li> </ul>
Opportunities	Threats
<ul style="list-style-type: none"> <li>• DC networks can facilitate the increasing number of DER</li> <li>• DC grids are suited for an increasing amount of DC loads</li> <li>• DC microgrids can operate in remote areas, that AC distribution lines cannot reach</li> </ul>	<ul style="list-style-type: none"> <li>• The existing distribution network infrastructure uses AC, a reliable and trusted technology</li> <li>• No standards for DC grids are available</li> </ul>

TABLE 2.2: SWOT analysis of DC grids

**Less losses** At the network level, conduction losses are lower since DC networks do not transmit reactive current [36]. Moreover, no inductive voltage drop appears across the line [62, 33, 37]. At the system level, DC distribution systems allow to reduce the number of power conversion steps and hence increases the efficiency [3, 8]. Moreover, the power electronic converters for DC have a smaller footprint. A comprehensive analysis in [36] proves to be 15% more efficient at a system level.

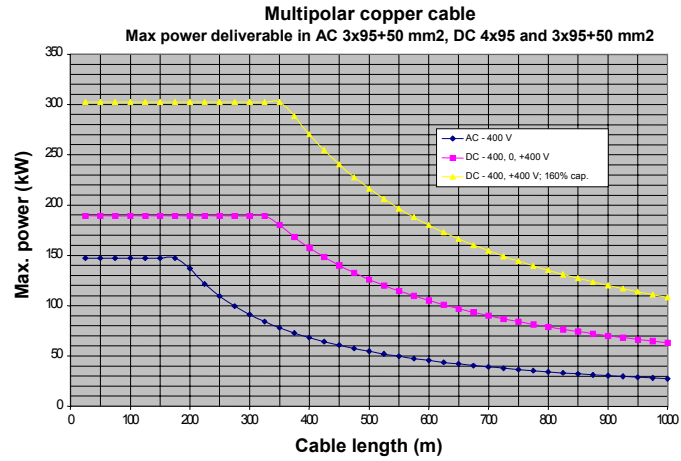


FIGURE 2.3: AC versus DC current distribution [4]

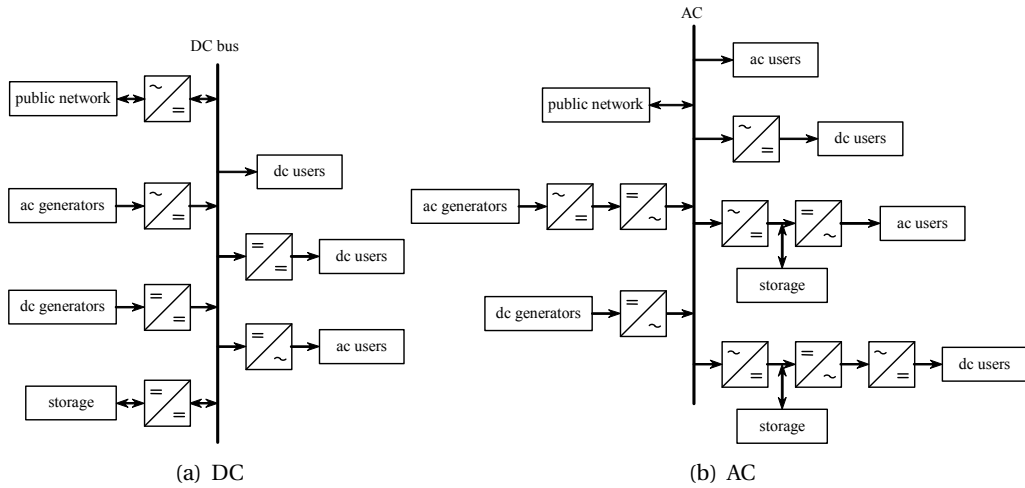


FIGURE 2.4: Number of converters in DC and AC distribution networks[3]

**No frequency synchronization** In AC networks, the frequency is an indicator of the power balance in the network. This role is taken over by the DC voltage in DC networks, which means that the DC voltage will rise (fall) when more power is injected (withdrawn) than withdrawn (injected) [3]. This simplifies the control of the converters that connect distributed energy resources and loads to the network, since no phase-locked loop<sup>1</sup> is necessary [37]. Similar to frequency droop control, different distributed voltage control schemes exist to balance the load and generation [32].

<sup>1</sup>A phase-locked loop synchronizes the converter to the grid frequency

**More control** The increased number of *controllable* converters allows to optimize the network flows or other system variables. Therefore the DC network aligns with smart distribution grids, that will apply (distributed or centralized) control strategies to regulate bi-directional power flows in the network [55].

**Increased power quality** The interface inverter between the AC and DC network improves the fault-ride through capability of the DC network, since the interface inverter can avoid that AC voltage fluctuations propagate to the DC network. Moreover, the interface converter can regulate the reactive power that is withdrawn from the AC grid to zero and hence operate at unity power factor, which consequently reduces the losses in the transmission network [36].

### Opportunities

**Distributed energy resources** Policy incentives, technical advancements and uncertain investment prospects on centralized power generation (like fossil fuels and nuclear power) promote the use of distributed energy resources (DER) that are connected at low and medium voltage levels. Especially decentralized renewable energy sources like solar photovoltaics and wind power are gaining importance. In most cases, a power electronic converter interfaces DER with the AC distribution network, since DER produce DC power or incompatible AC power. A DC network can simplify the interfaces between DER and the distribution network, since less power semiconductor devices are necessary [32]. Moreover, the increased power transfer capability of DC networks allows to re-use the existing infrastructure closer to the limits. Implementing a DC distribution network thus facilitates the increasing number of distributed energy resources.

**DC loads** While DC DER are deployed in distribution networks, the development of power electronics has resulted in numerous loads that require DC power in the power conversion chain. Examples are computers, fluorescent lighting, variable-speed drives [32] and LED lighting. Since DC loads are mostly interfaced to AC systems using uncontrollable diode rectifiers, DC systems can eliminate this inefficient conversion stage (Figure 2.4).

DC networks are also suited to connect DC battery energy storage systems (BESS). In particular, there is an opportunity for DC networks to charge electric vehicles, that can be considered a mobile BESS [30]. DC networks thus enable the integration of vehicle-to-grid concepts (V2G).

**Electrically undeveloped areas** DC networks can also be installed in electrically undeveloped areas where no electricity infrastructure is present yet, especially if the local generation comprises DER.

### **Weaknesses**

Although DC networks are promising as explained above, there are still some technical challenges that need to be overcome.

**Protection** Protection devices in DC networks need to operate faster than in AC networks [58]. Due to no zero-crossing of the voltage, current interruption is an issue with High-Voltage DC (HVDC). However, at low-voltage levels, AC protection devices are suited for DC protection systems [61, 59]. This is elaborated further in section 2.3.

**More power electronics affect the reliability** DC networks contain more controllable power converters, which implies that the number of power semiconductor devices will increase. Power semiconductor devices typically have shorter lifetimes as compared to the existing AC network equipment and therefore may affect the reliability of DC networks [34]. These power electronic converters will also need harmonic filtering, but applying high switching frequencies (order of 10 kHz) reduces the filter size.

**Uncertainty** Since LVDC networks provide an alternative lay-out for power distribution in contrast to the established AC networks, the reliability has not been proven. DC networks also imply uncertainty with respect to the technology and future cost projections.

### **Threats**

**AC is established** The established AC network infrastructure is reliable and secure, widely spread and difficult to adapt: most of the distribution cables in Belgium are older than 20-30 years, since replacement requires extensive planning, permitting and collaboration with other utilities (water suppliers, telephone operators).

**No standards** To assure interoperability between different component manufacturers, standards need to be developed. A voltage standard for LV and MV DC networks is not available at the moment of writing. Standards enable the industry to produce equipment that is interoperable, so that DC systems can be interconnected and overlaid.

### **2.2.2 Re-use of the existing AC network infrastructure**

Re-using the existing AC distribution network infrastructure for LVDC networks is feasible and even profitable to transmit more power through the same lines, as is elaborated above.

The existing AC network cables or overhead lines<sup>2</sup> can be arranged in a unipolar or bipolar configuration for DC electricity distribution:

- The three phase conductors compose a bipolar configuration. Since there are in total 4 conductors available, one conductor will in essence not be used. This conductor can serve as a spare conductor.
- Two pairs: a pair of two phase conductors and a phase and neutral conductor pair can compose 2 unipolar configurations. Note that the second pair contains the neutral conductor that regularly has a smaller cross-section and consequently has a lower rated current.

The existing AC network cables have following operating limits [3]:

- To avoid thermal overloading, the maximum rms current is limited
- The cable insulation level determines the maximum line-line and line-ground voltage

As explained in section 2.2.1 and shown in fig. 2.3, DC permits to transfer more power through the same lines. The flat part of the curves in fig. 2.3 is due to the rms current limit of the cable. The second, decreasing part of the curve is due to the maximum voltage drop across a cable.

---

<sup>2</sup>In Flanders: rural medium-voltage feeders regularly apply BXB 3x95+54.6mm<sup>2</sup> and urban feeders apply EAXVB 4x150mm<sup>2</sup> [14]

### 2.3 Protection of DC distribution networks

DC networks require a well-functioning protection system that ensure reliable and secure power distribution. While AC protection systems are well-established, DC protection systems are under-investigated. Salomonsson et al. [59] designs a protection system for LVDC distribution networks.

#### 2.3.1 Grounding

Grounding allows to detect ground faults that ensure personnel and equipment safety [19]. Since metallic parts of consumer appliances are connected to the ground via a protective earth conductor, they cannot become energized: a ground current will flow when a phase conductor touches the metallic parts. While AC distribution networks are grounded (Figure 2.1(c)), LVDC networks can be ungrounded or grounded by connecting the neutral or one of the phase conductors. The positive phase is preferably connected to ground compared with the negative one to reduce the impact of corrosion.

High-impedance and low-impedance grounding are feasible for LVDC networks and affect the behavior of the network during faults. Low-impedance grounding results in large fault currents and consequently large DC voltage transients. Large fault currents facilitate the fault detection, but large DC voltage transients will affect the power quality. A high-impedance grounding prevents large DC voltage transients, but measuring and detecting the fault current is more difficult.

[3] notes that, when connecting the neutral conductor of a bipolar DC network to the star point of the AC transformer, the DC current can drive the transformer into saturation. Consequently, a voltage balancer (Section 2.1.2) is essential to avoid a DC current in the transformer.

#### 2.3.2 Protection devices

The protection devices that constitute the protection system are (1) voltage and current measurements, (2) protective relays to process the measurements and (3) current interrupters. It should be stressed that measurement devices need to be able to measure DC values and therefore electromechanical residual current relays cannot be applied[32].

Current interrupters for AC are also suited for DC: fuses and molded-case circuit breakers (MCCB)[58]. Fuses have rated rms currents and voltages that are equally applicable to DC and AC. MCCB will interrupt the current when the instantaneous or rms value of the current exceeds a preset value. The instantaneous value is tracked using a magnetic tripping device, while the rms current is tracked by a thermal tripping device. MCCB current ratings always specify rms values and therefore the magnetic tripping device should be able to handle the peak value of the DC current.

When fuses and MCCB have too large time constants and are consequently too slow, power-electronic switches can be applied that operate faster at the expense of more losses. To compensate for the losses, a switch is proposed in [51], that is a compromise between a mechanical and power-electronic switch.

### **2.3.3 Protection system design**

The objective of the protection system is to detect and isolate faults fast and accurately to ensure personnel and equipment safety. The protection system needs to act fast, since faults influence the DC bus voltage and consequently the power quality of DC networks. Designing a protection system will have to take into account following considerations [58]:

1. the type of faults that can occur
2. the consequences of a particular fault type
3. the required protection devices
4. back-up protection devices
5. detection methods
6. measures to prevent faults and measures to prevent incorrect operation of the protection system

### **2.4 Conclusion**

This chapter introduced the structure of DC networks, including the unipolar and bipolar configuration and possible voltage levels. The strengths, weaknesses and opportunities were subsequently discussed:

DC networks allow to transmit more power than an AC network that uses the same infrastructure. Moreover, DC distribution systems require less power converters, since numerous loads require DC and most DER generate DC power or incompatible AC power that needs to be converted via an intermediate DC voltage bus. These power semiconductor devices typically have shorter lifetimes than AC network components, which affects the reliability of DC networks. The main treats to DC distribution networks are the lack of standardization and uncertainties regarding the reliable operation.

This chapter ended with the protection of DC networks, which is still subject for debate. The aspects of grounding, the ability to re-use AC current interrupters and the considerations of protection system design were discussed.

## Chapter 3

# DC voltage stability and static control

Chapter 2 introduced the structure and advantages of DC networks. This chapter introduces a definition of DC voltage stability, since it is essential to assure the proper operation of a DC network.

The DC bus voltage plays an important role: it is an indicator of the power balance in DC networks. The DC bus voltage will increase when more power is supplied than withdrawn and vice versa. Consequently, the role of the DC bus voltage in a DC network is comparable to the role of the frequency in AC networks.

The aim of this chapter is to propose a definition for DC voltage stability, that is based upon the accepted definition of power system stability. The first section will introduce a definition and stress the importance of DC voltage stability. The second section will discuss the system-theoretical framework of system stability, while the third section outlines control of the DC voltage to ensure power balance in steady-state.

### 3.1 A definition of DC voltage stability

Stability is related to the dynamics of systems. Intuitively, stability means that a system reaches an equilibrium state and remains there [40]. Frequently, the concept of stability is illustrated by a rolling ball that starts top-hill and rolls down into a valley, i.e. a stable equilibrium point.

In this section, a formal definition of DC voltage stability is introduced, based on the accepted definition of *power system stability*. According to the author's knowledge, no definition exists at the moment of writing.

### 3.1.1 Power system stability

Kundur et al. [43] define power system stability as:

**Definition 1. Power system stability** is the ability of an electric power system, for a given initial operating condition, to regain a state of operating equilibrium after being subjected to a physical disturbance, with most system variables bounded so that practically the entire system remains intact.

This definition focuses on the *dynamical behavior* of power systems: the state of the power system will change over time due to varying inputs and disturbances. Stability in particular, considers the trajectory that a system state travels along between an initial and final condition following a disturbance. Examples of disturbances in AC networks are network reconfiguration (e.g. line disconnection to interrupt a fault current) and changes in load and generation. Similar disturbances can occur in DC networks, especially when more distributed energy resources are involved [16]. It is concluded that stability and dynamics are strongly interlinked.

From the system-theoretical viewpoint, a system is stable if the system state remains bounded, starting from a bounded initial condition (Figure 3.1). However, the definition of power system stability is more strict in the sense that it not only requires the state to be bounded, but also that the state is confined within a subspace that is bounded by the operating limits of the components. This of course makes sense from a practical point of view, since voltage and current limits apply for the components constituting a DC system. Apart from requiring the system state to remain stable, the system state should thus also be *acceptable*, meaning that operating limits should not be violated.

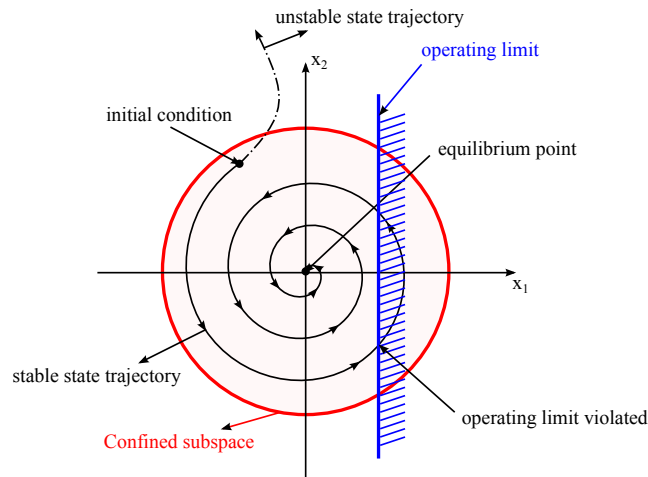


FIGURE 3.1: Stability in the state-phase plane

The definition makes an interesting nuance by stating that “..., with *most* system variables bounded ...”. The question arises here whether or not *all* system variables should be bounded. A first remark is that stability in practice does not require *all* state variables to be stable, assuming that the disregarded state variables will not alter the stability of the power system appreciably. Needless conservative designs can be avoided this way. A second remark is that every stability assessment model requires assumptions and approximations which subsequently result into *reduced order models*. So requiring all state variables to be bounded, would involve complex models and it is never guaranteed that the model incorporates all conceivable dynamics. Both remarks relate to the concept of *partial stability*, that requires only a subset of the system variables to remain stable. The remarks indicate that every stability analysis will be inherently focused on partial stability.

It is worthwhile to emphasize that the definition of power system stability refers to the ability of an electric power *system* to regain a state of operating equilibrium after a disturbance has occurred; the focus thus lies on the stability of the entire system, rather than the individual components that constitute the system.

#### 3.1.2 DC voltage stability

Following definition for DC voltage stability is proposed:

**Definition 2.** DC voltage stability is the ability of a DC power system to maintain the DC voltage within an *acceptable operating margin* at *all* DC buses constituting the DC system before and after a *disturbance* has occurred.

##### Discussion of the definition

Similar to the definition of power system stability, DC voltage stability is also approached from a system point of view, but also draws the attention to the individual components since every DC bus voltage is required to be acceptable, i.e. within operating limits.

The definition is more strict than stability in the mathematical sense, since the DC voltage should remain within an *acceptable operating range*. The operating limits should therefore not be violated. Standards ETSI EN 300 132-3-1 [22] and MIL-STD-704-F [15] define nominal voltages and voltage transient envelopes in case of disturbances for telecommunication systems and aircraft systems respectively. An example of a transient voltage envelope is shown in fig. 3.2.

The acceptable operating range in practice will depend on the type of equipment. Therefore the boundaries of the acceptable operating range are still to be determined and can vary depending on the type of equipment. The acceptable operating range can also be defined as a voltage envelope that limits the transient voltage waveform following a disturbance.

### 3. DC VOLTAGE STABILITY AND STATIC CONTROL

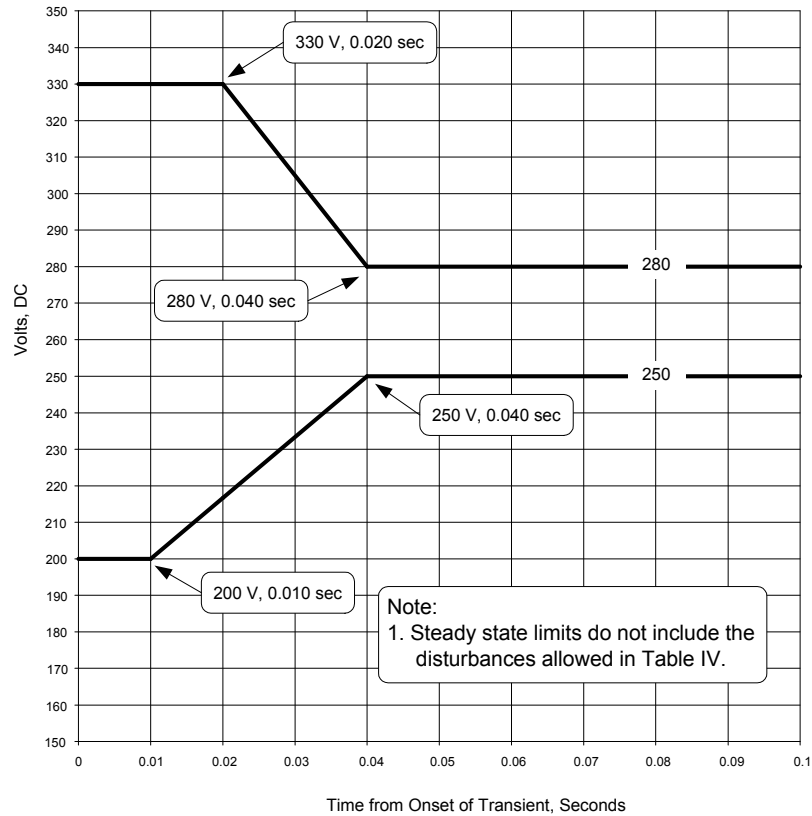


FIGURE 3.2: Transient voltage envelope MIL-STD-704-F (270 V DC system) [15]

DC system variables other than DC voltages (e.g. current and power) also need to remain within their operating limits. Stability of these system variables is covered by the general definition of power system stability (Definition 1), which requires each of these state variables to regain an acceptable operating equilibrium after a disturbance has occurred.

Since the DC bus voltage is an indicator for the power balance in the system, DC voltage stability is important from a control perspective [7, 45, 39].

#### Classification

Although power system stability is essentially a single problem, distinguishing different classes of power system stability intends to properly understand, analyze and finally effectively treat the phenomena related to stability [43]. The concept of *partial stability* (explained in section 3.1.1) justifies this approach. Also for DC power system stability a similar classification holds.

AC power system stability is categorized into 3 groups:

- *Rotor angle stability* refers to the ability of synchronous machines of an interconnected power system to remain in synchronism after being subjected to a disturbance.
- *Frequency stability* refers to the ability of a power system to maintain steady frequency following a severe system upset resulting in a significant imbalance between generation and load.
- *Voltage stability* refers to the ability of a power system to maintain steady voltages at all buses in the system after being subjected to a disturbance from a given initial operating condition.

DC power system stability differs from AC power system stability in the sense that the classes rotor angle stability and frequency stability are not present. These system variables are not present in a pure DC system that is not interconnected with an AC system. When studying the interaction between AC and DC systems, of course these concepts come back into play. Only the class of voltage stability remains.

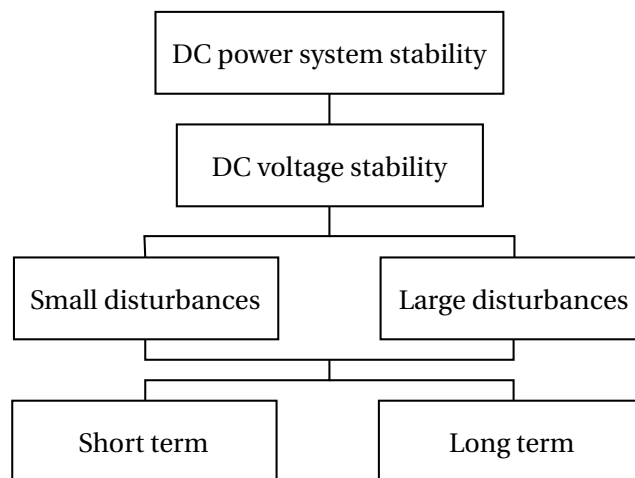


FIGURE 3.3: DC voltage stability classification[43]

DC voltage stability is further classified according to the type and the time frame of the disturbance that is subject to study (Figure 3.13). Disturbances can be either large or small, which are relative concepts. In general, small disturbances refer to disturbances which allow to apply small-signal analysis techniques. Large disturbances are outside of the region where small-signal analysis techniques are appropriate. In stead, it requires for instance time-domain simulations or nonlinear stability assessment techniques. The second subdivision is based on the time frame and distinguishes short and long term phenomena. Short term phenomena are typically within the time frame of less than a second to several seconds. Long term phenomena extend from several seconds to minutes, even hours. Long term stability can also be considered as static stability, referring to steady-state behavior, as will be elaborated in section 3.3.

### 3.2 System-theoretical framework for stability

To comply with the proposed definition of DC voltage stability (Definition 2), the DC system variables should not violate their operating limits. This section reviews the system-theoretical framework for stability of operating points, since a prior requirement for acceptability is that the operating point is stable, from a system-theoretical point of view.

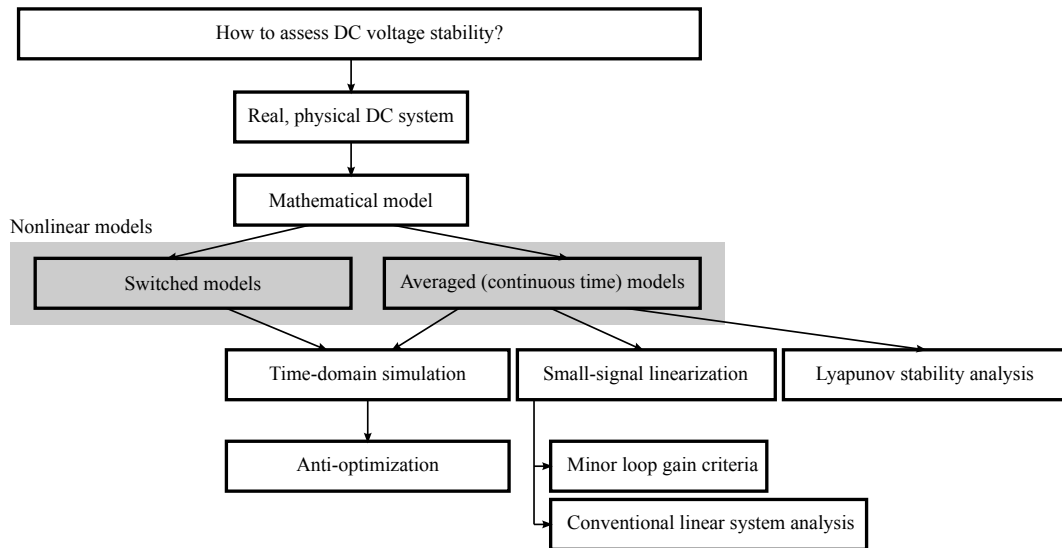


FIGURE 3.4: Overview of the stability analysis techniques

It is important to note that every stability analysis technique is based upon a mathematical model of the real, physical DC system (Figure 3.4). This mathematical model will always be an approximation to the physical DC system, and therefore will not include all conceivable system dynamics. The mathematical model should incorporate those dynamics that are important to ensure voltage stability, without containing overdetailed system dynamics. Therefore, the mathematical model will always be a trade-off between the available computational resources and the required level of detail.

A large number of power converters will be present in DC networks, that have (nonlinear) switching dynamics. Chapter 4 will elaborate further on the mathematical time-domain modelling techniques, and explain the use of switched models and averaged models. For the remainder of this section, it is sufficient to know that switched models will incorporate the switching dynamics, while averaged models do not. Therefore, switched models have a higher level of detail, but require much more computational resources to simulate a power converter.

Both switched and averaged models present nonlinear dynamics, that do not allow to apply the regular linear system analysis techniques, unless the equations are linearized around a steady-state operating equilibrium. This linearization process is referred to as *small-signal linearization* and allows to apply conventional linear system analysis and minor loop gain criteria that are developed for DC networks. It is important to emphasize, that small-signal linearization is only applicable for small deviations around the operating equilibrium. Therefore, stability is not guaranteed for large deviations (i.e. large-signal stability). However, when the linearized system is unstable around a specified operating equilibrium, also the nonlinear system will be unstable, which allows to detect *instability* using small-signal linearization.

Since small-signal linearization is inherently limited to small deviations from the operating equilibrium, time-domain simulations are regularly applied in daily practice. Test scenarios that are likely to occur in practice are set-up and subsequently simulated. The advantage of time-domain simulations is that large-signal behavior is included. The drawback of time-domain simulations is that it is time-consuming and not necessarily includes all possible causes of instability. To partially overcome these drawbacks, [41] applies a technique called *anti-optimization* to the control design of a buck converter. There the stability problem is transferred to an optimization problem for finding worst performance regarding stability criteria for a parameters range. This technique matches the needs and practice of industry, that specify transient envelopes and operating limits (Figure 3.5), and can be automated. The drawback of the methodology presented in [41] is that detailed switched models are applied that require extensive computational resources.

Throughout this chapter, the concepts are illustrated using the example DC circuit that is depicted in fig. 3.6. The circuit comprises a source, typically followed by a LC filter, and a load that consists of a resistor and a constant-power load (CPL). Typical constant power loads in practice are for instance constant-speed drives. Buck converters that control the output power also operate as a CPL.

CPL are known to destabilize DC systems, as will be shown in the subsequent discussion [18].

Envelope of a normal voltage transient for 28 V Buck converter

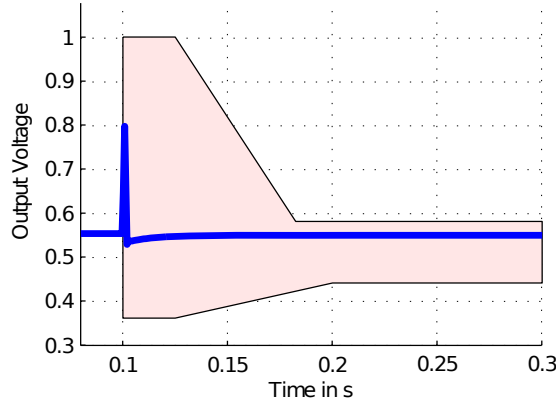


FIGURE 3.5: Envelope of a normal voltage transient for 28 V buck converter [41]

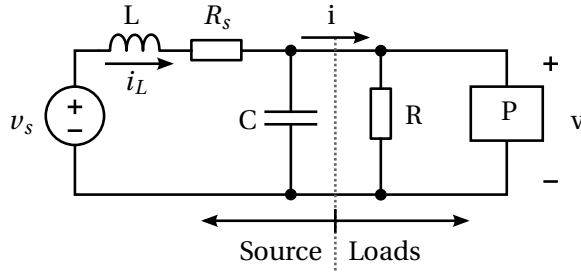


FIGURE 3.6: DC system comprising a constant-power load (P)

### 3.2.1 System dynamics

In general, system dynamics are mathematically described by a set of differential equations:

$$\frac{d\mathbf{x}}{dt} = \mathbf{f}(\mathbf{x}, t) \quad (3.1)$$

where  $\mathbf{x} \in R^n$  is the state vector that contains the  $n$  state variables of the system and  $\mathbf{f}(\mathbf{x}, t)$  is a vector-valued function that will govern the system dynamics at time  $t$ . When  $\mathbf{f}$  depends only implicitly on the time, i.e.  $\mathbf{f}(\mathbf{x}, t) = \mathbf{f}(\mathbf{x})$ , the system is *time-invariant*.

Points  $\mathbf{x}_0$  where  $\mathbf{f}(\mathbf{x}) = 0$  are *equilibrium points*, since the derivative of the state vector is zero and consequently, the system will remain there. In the remainder of this section, without loss of generality, the origin will be the equilibrium point of the system. Since a set of state variables is not uniquely determined, every equilibrium point can be located at the origin by a proper transformation of the state variables [40].

Conventional circuit analysis techniques lead to the equations that describe the system dynamics of the example circuit (Figure 3.6):

$$\begin{cases} L \frac{dx_1}{dt} = f_1(x_1, x_2) = V_s - x_2 - V - R_s x_1 - R_s I_L \\ C \frac{dx_2}{dt} = f_2(x_1, x_2) = x_1 + I_L - \frac{P}{x_2 + V} - \frac{x_2 + V}{R} \end{cases} \quad (3.2)$$

where  $L$ ,  $C$ ,  $R$ ,  $R_s$  are the circuit elements as in fig. 3.6,  $P$  is the power of the CPL and  $x_1$  and  $x_2$  are the state variables that are related to the inductor current and the capacitor voltage:  $x_1 = i_L - I_L$ ,  $x_2 = v - V$ , where  $I_L$  and  $V$  denote the steady-state equilibrium values of the inductor current and capacitor voltage respectively. By defining  $x_1$  and  $x_2$  this way, the origin ( $x_1 = 0$ ,  $x_2 = 0$ ) will be the steady-state equilibrium of the phase-plane.

### 3.2.2 An example of instability in DC networks: constant-power load

To intuitively understand the influence of a CPL on the stability of DC networks, consider the example in fig. 3.6. (Table 3.1 contains the circuit parameters that are used to obtain the results in this section.)

The source and load characteristic (in steady-state) are shown in fig. 3.7 for varying values of the load resistor. Consider the load characteristic that is highlighted in red and operating points A and B. When, following a small disturbance, the voltage decreases (increases) in point A, the load current will decrease (increase) as well. Therefore the voltage drop across the resistor  $R_s$  will decrease (increase), and consequently the voltage across the load will increase (decrease) back again. Finally the voltage settles back in equilibrium point A, that is stable. This is not the case for point B: when the voltage decreases (increases), the current will increase (decrease) and therefore the load voltage will decrease (increase) even more, since the voltage drop across  $R_s$  increases (decreases). The voltage will thus move away from operating point B, and consequently point B is an unstable equilibrium point.

The load characteristic shows a turning point (where the current  $i$  attains a minimum) that separates the unstable equilibrium points that lie below and the stable equilibrium points that lie above. At this turning point, the power that is withdrawn by the CPL equals the power that is withdrawn by the resistive load ( $P = V^2/R$ )<sup>1</sup>. Above the turning point, the resistive load power exceeds the CPL and the equilibrium points are stable and vice versa [18].

When the resistance value increases, the power that is drawn by the resistive load consequently decreases and therefore the turning point occurs at a higher voltage as is shown in fig. 3.7.

<sup>1</sup>Actually, the CPL power can be a little higher, because in this example  $R_s$  is included. However, since  $R_s$  is small, this can be neglected as will be clarified in section 3.2.4

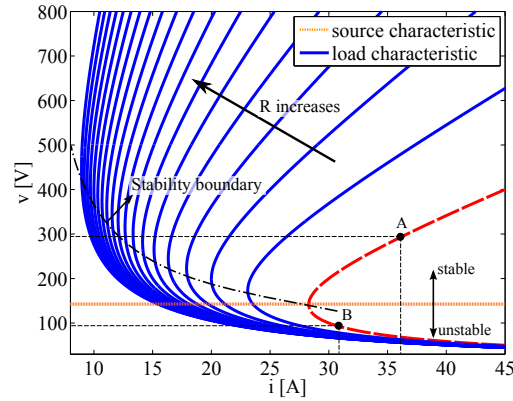


FIGURE 3.7: Steady-state source and load characteristic of the circuit in fig. 3.6

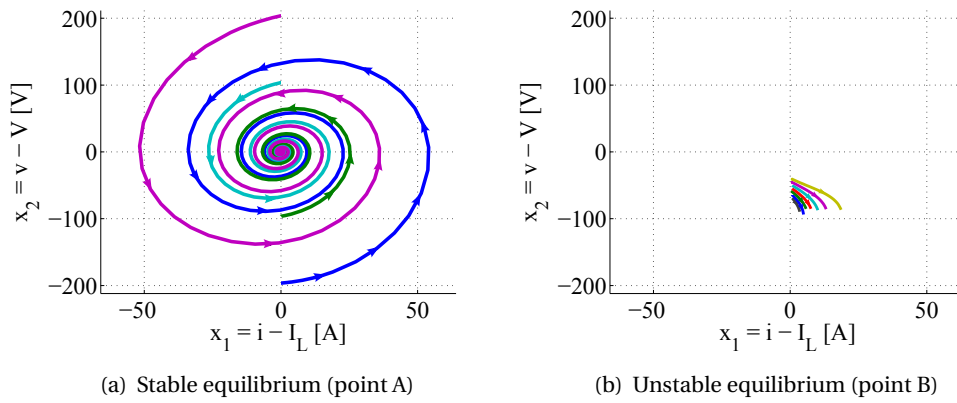


FIGURE 3.8: Stability of equilibria

The (in)stability of the equilibrium points A and B in fig. 3.7 also appears from the phase-plane in fig. 3.8. A phase-plane plot displays the trajectory that the two state variables  $x_1$  and  $x_2$  follow, starting from an initial condition. Figure 3.8 shows different trajectories that start from different initial conditions. Figure 3.8(a) shows that the trajectories converge to the steady-state equilibrium ( $x_1 = 0$  and  $x_2 = 0$ ), while the trajectories diverge from the equilibrium in Figure 3.8(b).

Quantity	Symbol	Value
Source voltage	$v_s$	300V
Inductance	L	1 mH
Capacitance	C	0.1 mF
CPL power	P	2 kW
Load resistor	R	10 $\Omega$
Source resistor	$R_s$	0.01 $\Omega$

TABLE 3.1: The circuit parameters for fig. 3.6

### 3.2.3 Stability of nonlinear systems

Lyapunov studied the stability of *autonomous systems*, i.e. systems without inputs that are described by  $\frac{dx}{dt} = \mathbf{f}(\mathbf{x})$ . From a system-theoretic point of view, an equilibrium point is stable when all trajectories that start at nearby points, stay nearby [40].

This “working definition” translates into following definition of stability:

The autonomous system is stable if:  $\forall \epsilon > 0, t : \exists \delta = \delta(\epsilon) > 0 : \|x(t_0)\| < \delta \Rightarrow \|x(t)\|$

This definition is intuitively understandable when considering the 2-variable phase-plane in 3.8. For an equilibrium point to be stable, every initial condition that is bounded, should remain bounded as in fig. 3.8(a). On the contrary, in fig. 3.8(b) such a bounded set does not exist.

Lyapunov approached the stability of mathematical systems from an energy perspective. He argued that when the stored energy in an autonomous system no longer changes, the system should be at rest. Furthermore, the stored energy should decrease up to the equilibrium point. This reasoning lead to the definition of a Lyapunov function, that resembles an energy function that describes the total energy that is stored in a system, but is more general. In mathematical terms, a Lyapunov function  $V(\mathbf{x})$  satisfies following criteria [25]:

1.  $V(\mathbf{0}) = 0$
2.  $V(\mathbf{x}) > 0$  when  $\|x\| \neq 0$
3.  $V(\mathbf{x})$  is continuous and has continuous derivatives with respect to all components of  $\mathbf{x}$
4. The total derivative  $\dot{V}(\mathbf{x}) \leq 0$  along the trajectories of the equation

Lyapunov stated that if a Lyapunov function can be found for a system, then the equilibrium point is stable and, furthermore, if condition 4 is restricted to  $\dot{V}(\mathbf{x}) < 0 \forall \mathbf{x} \neq \mathbf{0}$ , the equilibrium point is *asymptotically stable*, which means that any trajectory that starts nearby will end up in the equilibrium point itself:

The autonomous system is asymptotically stable around  $\mathbf{0}$  if:  $t \rightarrow \infty \Rightarrow \|\mathbf{x}(t)\| \rightarrow 0$

Lyapunov's theorem allows to investigate the stability of systems using the Lyapunov function  $V(\mathbf{x})$ . The main difficulty in applying Lyapunov's theorem to an arbitrary system, is finding a suitable Lyapunov function  $V(\mathbf{x})$ .

### 3.2.4 Stability of linear system

For a linear system, a Lyapunov function can be found:

Consider a linear time-invariant system:  $\frac{d\mathbf{x}}{dt} = \mathbf{F}\mathbf{x}$ . Lyapunov showed that the equilibrium point  $\mathbf{x} = \mathbf{0}$  is asymptotically stable, if and only if all eigenvalues  $\lambda_i$  of the system matrix  $\mathbf{F}$  satisfy  $\text{Re}(\lambda_i) < 0$ . For linear systems that satisfy this requirement, a Lyapunov function can be found [40].

The next chapter will show that power electronic converters are nonlinear systems. Moreover, a Lyapunov function cannot always be found, especially for larger DC networks that are considered in this work. However, following theorem exists, that allows to assess the stability of a nonlinear system around an equilibrium point, based upon a linearized version of the nonlinear system.

The theorem states that if  $\mathbf{x} = \mathbf{0}$  is an equilibrium point of the nonlinear system  $\frac{d\mathbf{x}}{dt} = \mathbf{f}(\mathbf{x})$  and  $\mathbf{f}(\mathbf{x})$  is continuously differentiable, then the system can be locally approximated around the origin by:

$$\frac{d\mathbf{x}}{dt} = \mathbf{f}(\mathbf{x}) \approx \nabla \mathbf{f}(\mathbf{x} = \mathbf{0})^T \mathbf{x} = \mathbf{F}\mathbf{x} \quad (3.3)$$

where  $\mathbf{F} = \nabla \mathbf{f}(\mathbf{x} = \mathbf{0})^T$  is the Jacobian of  $\mathbf{f}$  (i.e. the transpose of the gradient  $\nabla f(\mathbf{x})$  of  $\mathbf{f}$ ). Then, regarding stability of the origin:

1. The origin is asymptotically stable if  $\text{Re}(\lambda_i) < 0$  for all eigenvalues of  $\mathbf{F}$
2. The origin is unstable if  $\text{Re}(\lambda_i) > 0$  for one or more of the eigenvalues of  $\mathbf{F}$

This theorem is known as *Lyapunov's indirect method*, which can be summarized as follows [25]:

1. Find the linear approximation and compute the eigenvalues of  $\mathbf{F}$
2. If all the eigenvalues have strictly negative real parts (are in the left-half complex plane), then there is a region of stability about the origin
3. If at least one of the eigenvalues has a strictly positive real part (i.e. a right-half plane pole), then the origin is unstable
4. If the system has eigenvalues on the imaginary axis, no conclusion on stability can be drawn based on this method

It is important to note that a linearized approximation of the original unstable system is applied. Therefore, the statements on stability are only valid when the linear approximation is valid, which is mostly valid for small variations around the equilibrium point. Therefore, this type of analysis is termed *small-signal analysis*. On the contrary, *large-signal analysis* assesses the stability for large excursions around the equilibrium point. To guarantee large-signal stability, other tools that are less generally applicable are necessary, which is out of the scope of this work. The interested reader is referred to [50].

This work will draw conclusions on the stability of equilibria based upon small-signal analysis, since this is a method that is generally applicable. The drawback of this method is that it is only valid within a limited range around the equilibrium point.

Retake the example CPL circuit (Figure 3.6), which is nonlinear due to the power term in the second equation of eq. (3.2). Linearizing around the equilibrium point  $x_1 = 0$  and  $x_2 = 0$  gives:

$$\begin{cases} \frac{dx_1}{dt} = \frac{1}{L} f_1(x_1, x_2) = V_s - x_2 - V - R_s x_1 - R_s I_L \approx -\frac{R_s}{L} x_1 - \frac{1}{L} x_2 \\ \frac{dx_2}{dt} = \frac{1}{C} f_2(x_1, x_2) = x_1 + I_L - \frac{P}{x_2 + V} - \frac{x_2 + V}{R} \approx \frac{1}{C} x_1 + \left[ \frac{P}{CV^2} - \frac{1}{RC} \right] x_2 \end{cases} \quad (3.4)$$

The characteristic equation of eq. (3.4) is:

$$\lambda^2 + \left[ \frac{R_s}{L} - \frac{P}{CV^2} + \frac{1}{RC} \right] \lambda + \frac{1}{LC} - \frac{R_s P}{LC V^2} = 0 \quad (3.5)$$

To check whether the eigenvalues  $\lambda$  that satisfy eq. (3.5) have negative real parts, the Routh-Hurwitz criterion is applied [25], that requires all coefficients of  $\lambda$  in eq. (3.5) to be positive. This avoids a cumbersome calculation of the eigenvalues and leads to the same results, since we are only interested in the stability criteria that apply to the component parameters:

$$P < \frac{V^2}{R} + \frac{CV^2R_s}{L} \quad P < \frac{V^2}{R_s} \quad (3.6)$$

This limits are visualized in fig. 3.9. Since  $R_s$  is small, the term  $\frac{CV^2R_s}{L}$  in eq. (3.6) is negligible. Also since  $R_s$  is small, the second inequality will be automatically satisfied for moderate power values  $P$ . This stability criterion is the same as was developed in section 3.2.2: the power of the CPL should be smaller than the resistive load power, in order for the system to be stable.

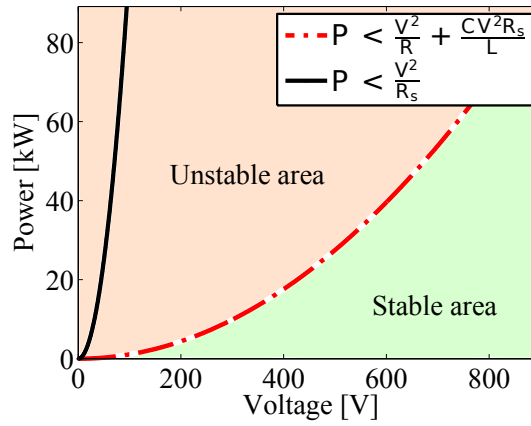


FIGURE 3.9: Stability limits for the CPL example network fig. 3.6

### 3.2.5 Minor-loop gain criteria

To study the system interaction between source and load subsystems, several stability criteria that are based on the minor-loop gain for DC systems are proposed [57]. These stability criteria specify input and output impedance requirements by breaking down the DC network into source and load subsystems. The minor-loop gain  $T_{MLG}$  is the ratio of the source subsystem output impedance  $Z_{s,out}$  and the load subsystem input impedance  $Z_{l,in}$ :

$$T_{MLG} = \frac{Z_{s,out}}{Z_{l,in}} \quad (3.7)$$

To obtain the output and input impedances, a transfer function of the linearized DC system is necessary. Therefore, all minor-loop gain criteria are only applicable in the range where the linearized system is valid (i.e. small-signal stability).

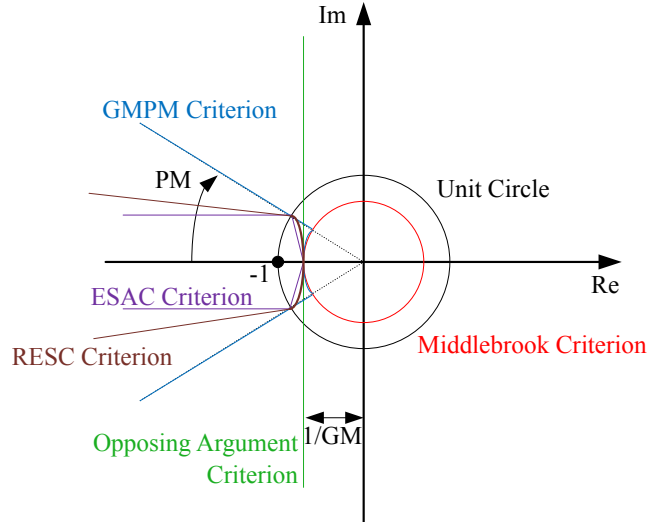


FIGURE 3.10: Minor loop gain criteria [57]

The use of the minor-loop gain  $T_{MLG}$  is justified by Middlebrook's *Extra Element Theorem*, that was originally intended for designing input filters of power converters in 1976 [52]. Consider the subsystems in fig. 3.11 and assume that the individual subsystem closed-loop transfer functions  $G_s$  and  $G_l$  are stable. Upon interconnecting the subsystems, the total input-to-output transfer function  $G_{sl}$  becomes:

$$G_{sl} = \frac{V_{l,out}}{V_{s,in}} = G_s G_l \cdot \frac{Z_{l,in}}{Z_{l,in} + Z_{s,out}} = G_s G_l \cdot \frac{1}{1 + T_{MLG}} \quad (3.8)$$

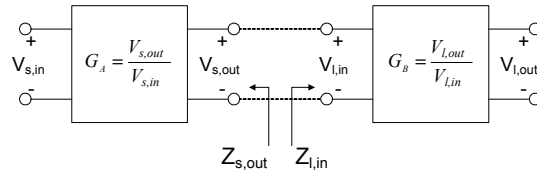
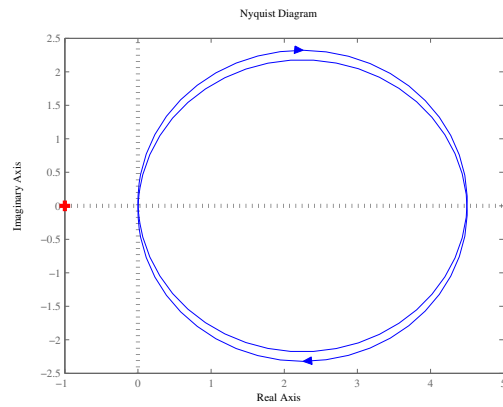


FIGURE 3.11: Subsystem interconnection [57]

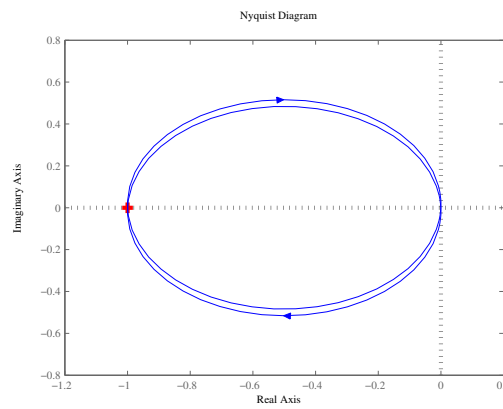
The last equality in eq. (3.8) is equivalent to the transfer function of a closed-loop system of which the loop-gain equals  $T_{MLG}$ . Therefore, the Nyquist criterion can be applied to  $T_{MLG}$  to ensure the stability of the interconnected system. The Nyquist criterion requires that the Nyquist contour of  $T_{MLG}$  does not encircle  $(-1, 0)$  [25]. This illustrated in fig. 3.10 and the Nyquist contour for the minor-loop gain of the CPL example is shown in fig. 3.12.

The Nyquist criterion is a *necessary and sufficient* condition for the stability of an operating point, but does not ensure *acceptability*. Therefore several DC stability criteria are developed that define forbidden areas in the Nyquist plot, that are more restrictive than the Nyquist criterion (Figure 3.10) [57]. These criteria are *sufficient* conditions, but not necessary. The drawbacks of these criteria is that they are only applicable for unidirectional power flow and depend on the component grouping of source and load subsystems. Therefore, these criteria are not applicable to DC systems with bi-directional power flow.

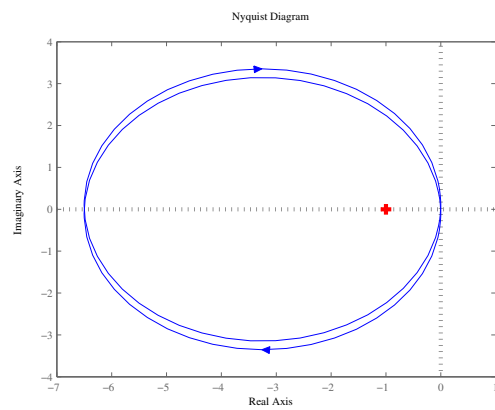
### 3.2. System-theoretical framework for stability



(a) Stable



(b) Stability boundary



(c) Unstable

FIGURE 3.12: Stability assessment of the CPL example by the minor-loop gain Nyquist plot

### 3.3 Control of the DC voltage

#### 3.3.1 AC and DC power system balance

The bus voltage in DC networks is an indicator of the power balance in the network, similar to the frequency in AC networks [7]. Although the AC frequency and DC voltage play a similar role, their dynamics are governed by similar, but physically different equations.

The frequency in AC power systems is governed by the *swing equation* that relates the rate of change of the *rotational kinetic energy* to the power balance in the network [42]:

$$\frac{d}{dt} \left( \frac{1}{2} J \omega^2 \right) = P_g - P_d - P_l \quad (3.9)$$

where  $J$  is the equivalent rotational inertia of the AC power system,  $\omega = 2\pi f$  is the grid angular frequency,  $P_g$  is the power generated,  $P_d$  is the power demand and  $P_l$  are the system losses.

The swing equation shows that the grid frequency will increase when the power generation exceeds the power demand and the losses. Consequently, the grid frequency will decrease when the power generation cannot meet the power demand and losses. The swing equation represents the mechanical dynamics of the (synchronous) generators that generate AC power: when the mechanical torque of the prime mover differs from the electrical counter-torque, that is provided by the electrical generator, the rotational speed will start to deviate.

On the other hand, the bus voltage  $v$  in DC distribution systems is governed by:

$$\frac{d}{dt} \left( \frac{1}{2} C v^2 \right) = P_g - P_d - P_l \quad (3.10)$$

This equation shows that the rate of change of the electrostatic energy that is stored in the equivalent capacitance  $C$  of the system is determined by the power generated  $P_g$ , power demand  $P_d$  and the system losses  $P_l$ . When the generated power exceeds the power demand, the DC bus voltage will start to rise. Consequently, the DC bus voltage will decrease when the power demand exceeds the generated power.

Although eq. (3.10) resembles eq. (3.9), the dynamics of the AC frequency and DC voltage represent different physical phenomena: the AC frequency is related to the rotational kinetic energy, while the DC voltage is determined by the electrostatic energy.

The converters that control the voltage will determine the steady-state bus voltages. This work refers to this type of control as *static control*. Dynamic control on the contrary, will control system variables during transient phenomena (e.g. to provide damping or improve the transient response).

### 3.3.2 Centralized and decentralized voltage control

To achieve power balance in DC networks, *centralized* and *decentralized* control schemes exist [39]. In a centralized master-slave control scheme (Figure 3.13(a)), all system data is collected in the master that sends out the power set points of the converters that are responsible for voltage control (the slaves). The master itself serves as a slack bus, that is the only device that controls the voltage and supplies the losses in the network. On the contrary, in a decentralized droop control scheme (Figure 3.13(b)), the local measurement of the voltage determines the power set-point of the converter. The advantage of a decentralized scheme is that a centralized master controller, that is a single-point-of-failure, is avoided.

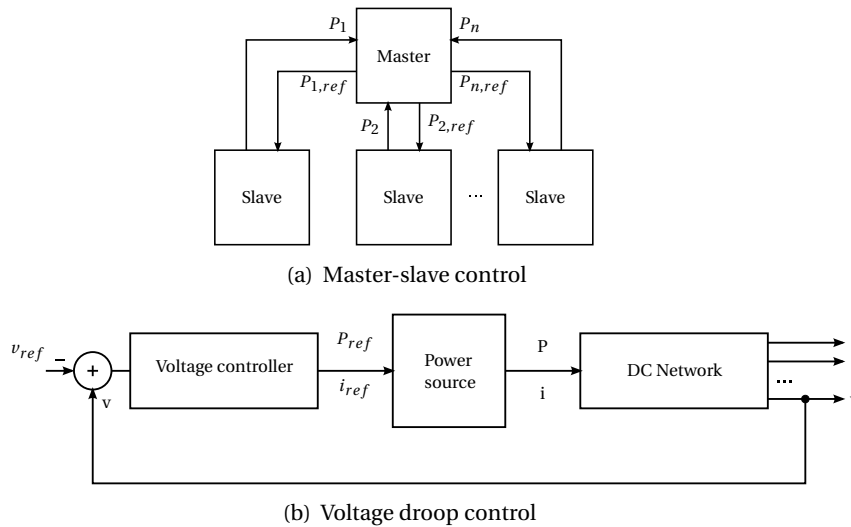


FIGURE 3.13: DC voltage control possibilities

With voltage droop control, each converter that participates in voltage control has a control scheme similar to fig. 3.13(b). The voltage controller sets the output power reference signal of the power source. Alternatively, a current reference signal can serve the same purpose, which reflects the linear control behavior of the DC network [7]. Working with current reference signals, will retain the linear system dynamics, while power reference signals will automatically introduce nonlinear control behavior.

The principle of droop control is illustrated in fig. 3.14. Every voltage controller will increase or decrease its power or current reference signal ( $\Delta P_{ref}$  or  $\Delta i_{ref}$ ) proportional to the voltage deviation ( $\Delta v$ ), that is measured relative to the nominal voltage. The slope  $K$  of the characteristic is referred to as the *droop setting* and determines the power or current reference signal:  $\Delta P_{ref} = -K\Delta v$  or  $\Delta i_{ref} = -K\Delta v$ . The larger the droop setting, the higher the power or current reference signal.

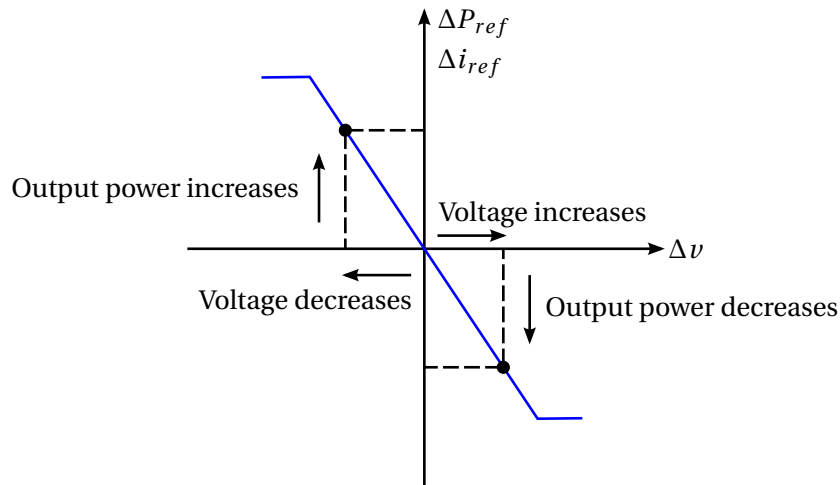


FIGURE 3.14: DC voltage droop control characteristic

The generators that participate in droop control should be able to regulate their power output. The generators that can be considered for droop control are battery energy storage systems (BESS), microturbines and fuel cells. Droop control with renewable energy sources that have an intermittent power output, is not feasible.

In practice, droop control schemes will also have to take the power limits into account, as is elaborated more in detail in [7]. Furthermore, when battery energy storage systems participate in voltage control, the state-of-charge should be monitored, since a BESS cannot supply power indefinitely. Therefore a control scheme using fuzzy control and gain scheduling is proposed in [38].

### 3.4 Conclusion

This chapter introduced a definition for *DC voltage stability*, where *acceptability* is a key concept. Acceptability means that the system variables remain within their operating limits. The definition was discussed and the importance of DC voltage stability was stressed.

A necessary condition to remain within the operating limits is stability from a system-theoretical point-of-view. An equilibrium point is stable when, starting from an initial condition and after a disturbance has occurred, the system state returns to the equilibrium point. The concepts and theorems of Lyapunov were reviewed in the second section.

Lyapunov also proved that, when the linear approximation of a nonlinear system is stable around the equilibrium point, then a stable region exists around that equilibrium point. Consequently, no stable region exists when the linearized system is unstable. This justifies the approach used in this work to assess the stability of DC networks using linearized subsystems.

To study the interaction between DC subsystems, minor-loop gain criteria were proposed, that assess stability based on source and load impedance representations. Minor-loop gain criteria can be considered a subclass of linear system analysis, since the impedance representations are obtained for the linearized DC system. However, minor-loop gain criteria cannot be applied for bi-directional power flow and are sensitive to the component grouping in source and load subsystems.

This chapter ended with a discussion on voltage control. The converters that participate in static voltage control govern the DC bus voltage in the network. Two control schemes were discussed: centralized master-slave control and decentralized droop control.



# Chapter 4

## Time-domain models of DC systems

Chapter 3 introduced a definition for DC voltage stability and mentioned the available techniques to analyze DC voltage stability. This thesis will rely upon small-signal analysis, complemented with time-domain simulations, to assess the stability of operating points before and after a disturbance has occurred.

This chapter will focus on the mathematical formulation of time-domain models of *DC systems*. Figure 4.1 gives an overview of the subsystems that constitute a DC system. In general, a DC system consists of a DC network, power electronic converters (PEC) and source/load subsystems. The *DC network* includes all busses, where components can be connected to, and all branches representing lines that transfer electrical power between the busses. The *source/load subsystems* can range from classical resistive loads to distributed energy resources (DER) like solar photovoltaic generation (PV). The *PEC* is the interface between the source/load subsystems and the DC network, that allows to condition the electrical power flow. Therefore a controller will provide the control inputs of the PEC, based upon (local) current and voltage measurements. The combination of a source/load subsystem, a PEC and it's control circuitry is referred to as a *component*.

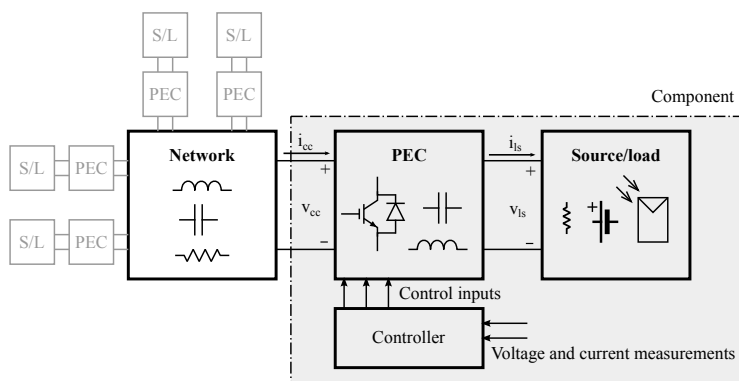


FIGURE 4.1: Overview of a DC system

The goal of this chapter is to provide a set of first-order ordinary differential equations (i.e. a state-space representation) that describes the time-domain dynamic behavior of all the subsystems that constitute a DC system. These state-space models are used in the subsequent chapters to simulate the time response of a DC system and to analyze the stability via small-signal analysis.

This chapter is organized as follows: the first section will discuss the modelling techniques for PEC. The second section will list available models for DER, that are validated in the technical literature. The third section shows the results of a time-domain simulation of a small DC system that allows to compare the accuracy between averaged and switched PEC models to study DC voltage transient phenomena.

### 4.1 Models of power electronic converters

Power electronic converters (PEC) are electrical devices that convert and process electrical energy by supplying voltages and currents in a form that is optimally suited for the application [54]. In essence, a PEC consists of:

- Power semiconductor devices (IGBTs, MOSFETS, bipolar transistors, diodes) to control the voltage, current or power.
- Passive elements (inductors, capacitors, resistors) to filter the switching harmonics
- Snubber circuits to reduce power semiconductor stresses and handle the reverse recovery current of diodes [54]
- Measurement and control circuitry to drive the gate of the power semiconductor switches

The power semiconductor devices operate in switching-mode to obtain a high power conversion efficiency in order to minimize losses. Minimizing losses is important because of the cost of wasted energy and the difficulty in removing heat [54].

DC systems are characterized by a high number of *controllable* PEC. This in contrast to AC systems that also include PEC like diode rectifiers, but those are not *controllable*. The most common converters in DC systems are DC/DC step-up (boost) and step-down (buck) converters. Furthermore AC/DC inverters allow to interconnect DC and AC systems.

Time-domain simulations of DC systems require models of PEC to verify the correct operation and study the system stability. The goal of the model is to approximate the behavior of the physical circuit with sufficient accuracy, without requiring excessive computational resources. A model is therefore always a trade-off between accuracy and computational resources. The required accuracy in turn depends on the needs of the designer. E.g. when designing snubber circuits, the designer is interested in the intra-cycle switching transients, typically considering time constants smaller than the switching period. For this application, detailed power semiconductor models are regularly provided by the manufacturers. On the contrary, in this work, the models are used to assess the stability of multi-component systems. Applying detailed models of the power semiconductors would require excessive computational resources and therefore simplifications are essential.

This section will introduce 4 modelling techniques for PEC, that are summarized in fig. 4.2. The figure shows the accuracy versus the required computational resources for the different modelling techniques qualitatively. On one hand, switched models (SWM) offer a detailed model of the PEC switching behavior, but require extensive computational resources. On the other hand standard averaged models (SAM) and sampled-data models (SDM) are less computationally intensive, but the behavior within one switching period is blurred. Generalized averaged models (GAM) are an extension to SAM that provide a better accuracy, while still requiring less computational resources than SWM.

Throughout this section, a bi-directional DC/DC converter is modeled to apply and compare the different modeling techniques. Figure 4.3 shows the circuit topology of the converter, where only components essential to the power processing functionality are shown. The purpose of the DC/DC converter is to step down the source voltage  $v_{cc}$  to the voltage level  $v_C$  that is suitable for the resistive load  $R$ . A gate signal is applied to the power semiconductors 1 and 2 to turn 1 and 2 on or off and by varying the time that the switches are on or off, the power flow is regulated. Note that 1 and 2 are never on simultaneously, to avoid a short-circuit at the source side of the converter. Figure 4.3(b) shows the two operating modes of the DC/DC converter, depending on the state of the power semiconductors. While 1 is on, the inductance  $L$  is charged. While 1 is off, the load resistor is powered by the energy that is stored in the inductor. The capacitor will dampen the load voltage fluctuations. The diodes allow the inductor current to flow in both directions. The inductor current and voltage waveforms are shown in fig. 4.4.

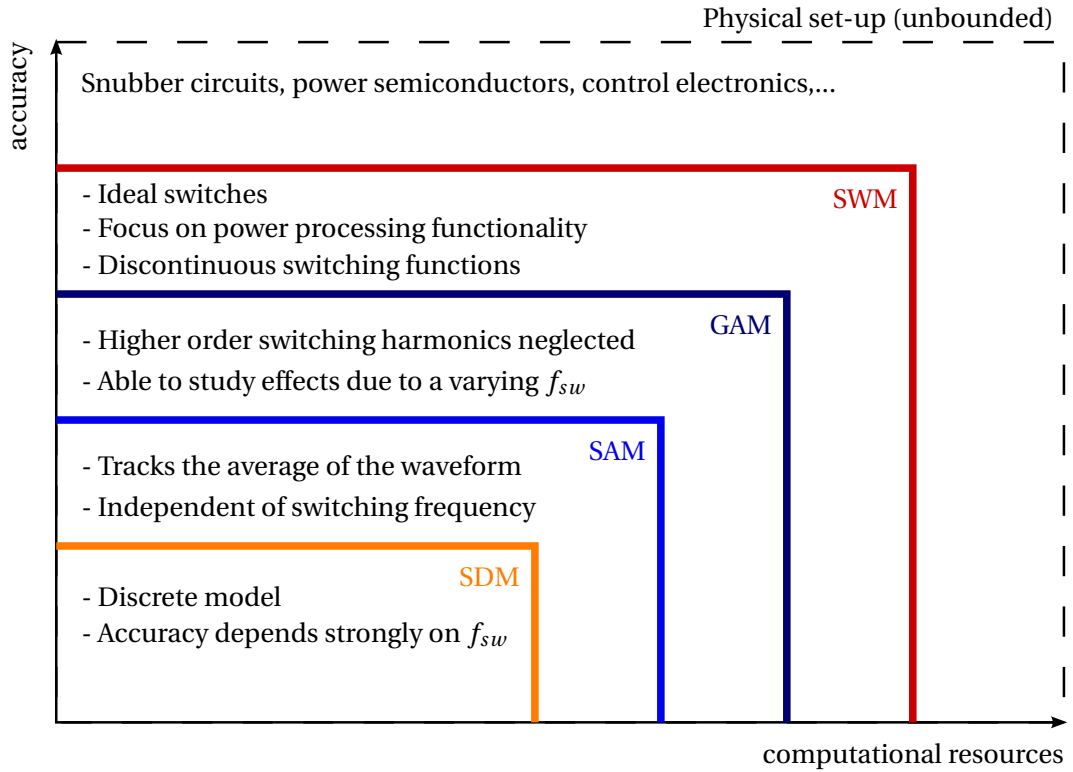


FIGURE 4.2: Overview of the modeling techniques for power electronic converters

#### 4.1.1 Switched models

Switched models (SWM) focus on the components central to the power processing function and therefore neglect snubber circuits and parasitics [46] [48]. Regularly, power semiconductor switches are represented by ideal switches, having a zero on-resistance and an infinite resistance when turned off. Elementary circuit analysis leads to detailed, continuous-time, nonlinear, time-varying models in state-space form:

$$\frac{d\mathbf{x}(t)}{dt} = [q(t)\mathbf{A}_1 + (1 - q(t))\mathbf{A}_0]\mathbf{x}(t) + [q(t)\mathbf{B}_1 + (1 - q(t))\mathbf{B}_0]\mathbf{u}(t) \quad (4.1)$$

where

- $q(t)$  is a switching signal, which is related to the voltage applied to the gate of power semiconductor switch. By convention  $q(t) = 1$  when the switch is on and  $q(t) = 0$  when it is off.
- $(A_0, B_0)$  and  $(A_1, B_1)$  are the system matrices when the switch is off and on respectively.

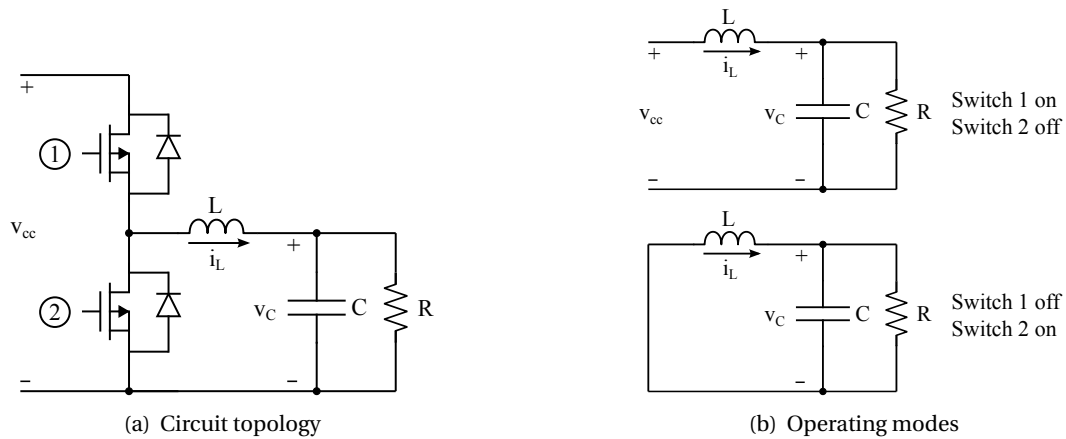


FIGURE 4.3: DC/DC converter

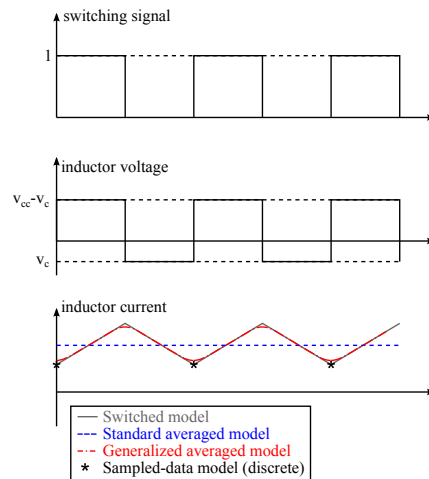


FIGURE 4.4: DC/DC converter inductor voltage and current waveforms

The approach thus comprises following steps:

1. Construct the system state matrices  $(A_0, B_0)$  and  $(A_1, B_1)$  for the system when the power semiconductor switch is open and closed respectively.
2. Apply eq. (4.1) to obtain the switched model

This approach can be automated, starting from state-space representations or a circuit schematic. E.g. PLECS is a Matlab/Simulink toolbox that can simulate switched circuits.

Consider the example of a switched circuit model for a bidirectional DC-DC converter (fig. 4.3). 1 and 2 are complementary on: when 1 is on, 2 is off and when 2 is on, 1 is off. In practice, there is a short *deadtime* during which both 1 and 2 are off; this deadtime is neglected in a switched model.

$\mathbf{x} = [i_L(t) v_C(t)]^T$  and  $\mathbf{u}(t) = v_{cc}(t)$  are the state and input vector. When 1 conducts (index 1) or 2 conducts (index 0), following state-space matrices govern the circuit dynamics:

$$A_0 = \begin{bmatrix} 0 & -1/L \\ 1/C & -1/RC \end{bmatrix} \quad B_0 = \begin{bmatrix} 0 \\ 0 \end{bmatrix} \quad (4.2)$$

$$A_1 = \begin{bmatrix} 0 & -1/L \\ 1/C & -1/RC \end{bmatrix} \quad B_1 = \begin{bmatrix} 1/L \\ 0 \end{bmatrix} \quad (4.3)$$

From eq. (4.1), the switched model equations become:

$$\frac{di_L}{dt} = \frac{1}{L} [-v_C(t) + q(t)v_{cc}(t)] \quad (4.4)$$

$$\frac{dv_C}{dt} = \frac{1}{C} \left[ i_L(t) - \frac{v_C(t)}{R} \right] \quad (4.5)$$

#### 4.1.2 Averaged models

Averaged models are derived from switched models like eq. (4.5), but neglect part of the dynamics within one switching period. Initially, standard averaged models (SAM) were developed that consider average state variables that are averaged over one switching period [48]. Later, generalized averaged models (GAM) were developed, that improve the accuracy of SAM; GAM approximate the switching waveform by a truncated Fourier series within one switching period. SAM only track the 0-th order Fourier coefficient (the DC average value of a waveform), and are thus a subclass of GAM.

##### Standard averaged models

SAM track the *average state variable* over one switching period  $T_s$ :

$$\bar{x}(t) \equiv \frac{1}{T_s} \int_{t-T_s}^t x(\tau) d\tau \quad (4.6)$$

The average state variables represent the average of the switching waveform within one switching period and neglect the waveform ripple. This approximation is justified when the waveform ripple (i.e. the higher order harmonics) can be neglected and the waveform is sufficiently approximated by its switching period average [48]. A first justification for this approximation is that converter components are selected to limit the waveform ripple, since this can lead to intolerable component stresses. Moreover, at higher switching frequencies, the waveform ripple diminishes and the accuracy of SAM improves. A second justification is that the details of the switching ripple are not of interest when designing feedback compensation, since the objective is to control the average quantity.

The SAM of the DC/DC converter (Figure 4.3) is readily obtained by averaging both sides of the switched model (Equation (4.1)):

$$\frac{d\bar{\mathbf{x}}(t)}{dt} = [d(t)\mathbf{A}_1 + (1 - d(t))\mathbf{A}_0]\mathbf{x}(t) + [d(t)\mathbf{B}_1 + (1 - d(t))\mathbf{B}_0]\mathbf{u}(t) \quad (4.7)$$

Where  $\mathbf{x}(t)$  and  $\mathbf{u}(t)$  now represent the average value of the state-variables, and  $d(t) = \bar{q}(t)$ . This equation implicitly assumes that  $\overline{q(t)v_{cc}(t)} \approx \bar{q}(t)\bar{v}_{cc}(t)$ , which is acceptable when the voltage ripple is small as compared to the average value of the voltage waveform.

Applying eq. (4.7) leads to the SAM of the buck converter:

$$\frac{d\bar{i}_L}{dt} = \frac{1}{L} [-\bar{v}_C(t) + d(t)\bar{v}_{cc}(t)] \quad (4.8)$$

$$\frac{d\bar{v}_C}{dt} = \frac{1}{C} \left[ \bar{i}_L(t) - \frac{\bar{v}_C(t)}{R} \right] \quad (4.9)$$

### Generalized averaged models

The main idea of generalized averaged models is to approximate waveforms within one switching period by a truncated Fourier series [12, 47]. The SAM is a special case of generalized averaged models, where only the zero-th order Fourier coefficient is considered and the higher order terms are neglected.

For the mathematical elaboration, consider a portion of the waveform (which can be for instance the inductor current or capacitor voltage of the buck converter) in a timeframe  $\tau \in [t - T; t]$  and the Fourier representation of the signal in the specified time interval:

$$x(\tau) = \sum_{l=-\infty}^{\infty} \langle x \rangle_l(t) e^{jl\omega_s\tau} \quad (4.10)$$

where  $\omega_s = 2\pi f_{sw}$ ,  $T = \frac{1}{f_{sw}}$  and  $\langle x \rangle_l(t)$  is the *index-k coefficient* in the Fourier series, which is also referred to as the *k-phasor*. The k-phasor is in general a *complex* quantity given by:

$$\langle x \rangle_l(t) = \frac{1}{T} \int_{t-T}^t x(\tau) e^{-jk\omega_s\tau} d\tau \quad (4.11)$$

Equation (4.11) explicitly denotes the dependency of the complex k-phasor on the time t. This means that the k-phasor will vary as the window  $[t - T; t]$  slides along the waveform as t advances.

Only retaining the first-order Fourier coefficients  $\langle x \rangle_{-1}(t)$ ,  $\langle x \rangle_0(t)$  and  $\langle x \rangle_1(t)$  already leads to acceptable results, as will be shown in the last subsection. Note that  $\langle x \rangle_0(t)$  corresponds to the averaged quantity as in the SAM:

$$\langle x \rangle_0(t) = \frac{1}{T} \int_{t-T}^t x(\tau) d\tau \quad (4.12)$$

The procedure for obtaining a generalized averaged model is [60, 48]:

1. Apply the averaging operator on both sides of the switched model
2. Apply the following properties to simplify the equations:
  - Property 1. Derivative of the k-phasor:  $\frac{d\langle x \rangle_k(t)}{dt} = \left\langle \frac{dx}{dt} \right\rangle(t) - jk\omega_s \langle x \rangle_k(t)$
  - Property 2. Average of a product:  $\langle q(t)x(t) \rangle = \sum_{i=-\infty}^{\infty} \langle q \rangle_{k-i} \langle x \rangle_i$
  - Property 3. Negative k-phasors:  $\langle x \rangle_{-k} = \langle x \rangle_k^*$ , where  $\cdot^*$  denotes the complex conjugate
3. When necessary, apply assumptions (such as slow variations of  $\langle x \rangle_k(t)$ ) to obtain a state-space representation.

Applying this procedure to obtain a GAM of the the buck converter inductor current 0-phasor:

$$\frac{d\langle i_L \rangle_0}{dt} = \frac{1}{L} [-\langle v \rangle_0 + \langle q v_{cc} \rangle_0] \quad (4.13)$$

$$= \frac{1}{L} [-\langle v \rangle_0 + \langle q \rangle_1 \langle v_{cc} \rangle_{-1} + \langle q \rangle_0 \langle v_{cc} \rangle_0 + \langle q \rangle_{-1} \langle v_{cc} \rangle_1] \quad (4.14)$$

The other phasors can be obtained in a similar way, leading to following GAM state-space representation [17]:

$$\frac{d}{dt} \begin{bmatrix} \langle i_L \rangle_1^R \\ \langle i_L \rangle_1^I \\ \langle v_C \rangle_1^R \\ \langle v_C \rangle_1^I \\ \langle i_L \rangle_0 \\ \langle v_C \rangle_0 \end{bmatrix} = \begin{bmatrix} 0 & \omega_s & \frac{-1}{L} & 0 & 0 & 0 \\ -\omega_s & 0 & 0 & \frac{-1}{L} & 0 & 0 \\ \frac{1}{C} & 0 & \frac{-1}{RC} & \omega_s & 0 & 0 \\ 0 & 0 & 0 & 0 & 0 & \frac{-1}{L} \\ 0 & 0 & 0 & 0 & \frac{1}{C} & \frac{-1}{RC} \end{bmatrix} \begin{bmatrix} \langle i_L \rangle_1^R \\ \langle i_L \rangle_1^I \\ \langle v_C \rangle_1^R \\ \langle v_C \rangle_1^I \\ \langle i_L \rangle_0 \\ \langle v_C \rangle_0 \end{bmatrix} + \begin{bmatrix} \frac{d}{L} & 0 & \frac{1}{2\pi L} \sin(2\pi d) \\ 0 & \frac{d}{L} & -\frac{1}{2\pi L} (1 - \cos(2\pi d)) \\ 0 & 0 & 0 \\ 0 & 0 & 0 \\ \frac{1}{\pi L} \sin(2\pi d) & \frac{-1}{\pi L} (1 - \cos(2\pi d)) & \frac{d}{L} \\ 0 & 0 & 0 \end{bmatrix} \begin{bmatrix} \langle v_{cc} \rangle_1^R \\ \langle v_{cc} \rangle_1^I \\ \langle v_{cc} \rangle_0 \end{bmatrix} \quad (4.15)$$

where the real and imaginary state variables are denoted by  $\langle \cdot \rangle^R$  and  $\langle \cdot \rangle^I$  respectively.

$d = d(t)$  denotes the *averaged* switching waveform, which is introduced by the quantities:

$$\langle q \rangle_0 = \frac{1}{T} \int_{t-T}^t q(\tau) d\tau \equiv d(t) \quad (4.16)$$

$$\langle q \rangle_1 = \frac{j}{2\pi} \left( e^{-j2\pi d} - 1 \right) \quad (4.17)$$

Equation (4.15) clearly shows that the state-space representation of the GAM depends upon the switching frequency via  $\omega_s = 2\pi f_{sw}$ . This is a useful feature to study the influence of the switching frequency on the stability of the system, which is not possible when applying SAM or SDM. Moreover, GAM are suited to model resonant converters applied for soft-switching [60].

### 4.1.3 Sampled-data models

Sampled-data models (SDM) are *discrete* time models that are similar to averaged models in the sense that the behavior of the waveform within a switching period is blurred [64].

SDM obtain the values of a waveform at discrete instants. Starting from an initial value, the switched model is solved using matrix exponentials [46]. While the switch is on, during the first part of the switching period  $[t - T; t - T + d[k]T]$ , the circuit dynamics are given by:

$$x(t) = e^{\mathbf{A}_1(t-t_0)}\mathbf{x}(t_0) + \int_{t_0}^t e^{\mathbf{A}_1(t-\tau)}\mathbf{B}_1\mathbf{u}(\tau)d\tau \quad (4.18)$$

where  $t_1$  denotes the time  $t - T + d[k]T$  that the switch operates,  $\mathbf{x}(t_0)$  is the initial condition of the state-vector  $\mathbf{x}(t)$ , and  $\mathbf{u}(t)$  is the input vector.

At the end of the period  $[t_0, t_1]$  the state is given by evaluating eq. (4.18) at  $t = t_1$ , which is the initial condition for the equation governing the parts in the second part  $[t_1, t]$  of the switching period when the switch is off:

$$\begin{aligned} x(t) &= e^{\mathbf{A}_0(t-t_1)}\mathbf{x}(t_1) + \int_{t_1}^t e^{\mathbf{A}_0(t-\tau)}\mathbf{B}_0\mathbf{u}(\tau)d\tau \\ &= e^{\mathbf{A}_0(t-t_1)} \left[ e^{\mathbf{A}_1(t_1-t_0)}\mathbf{x}(t_0) + \int_{t_0}^{t_1} e^{\mathbf{A}_1(t_1-\tau)}\mathbf{B}_1\mathbf{u}(\tau)d\tau \right] + \int_{t_1}^t e^{\mathbf{A}_0(t-\tau)}\mathbf{B}_0\mathbf{u}(\tau)d\tau \\ &= e^{\mathbf{A}_0(1-d[k])T} \left[ e^{\mathbf{A}_1 d[k]T}\mathbf{x}(t-T) + \int_{t-T}^{t-T+d[k]T} e^{\mathbf{A}_1(t-T+d[k]T-\tau)}\mathbf{B}_1\mathbf{u}(\tau)d\tau \right] \\ &\quad + \int_{t-T+d[k]T}^t e^{\mathbf{A}_0(t-\tau)}\mathbf{B}_0\mathbf{u}(\tau)d\tau \end{aligned} \quad (4.19)$$

Using following simplifications and assumptions, eq. (4.19) is reduced to a discrete model eq. (4.20):

- $e^{\mathbf{A}T} \approx \mathbf{I} + \mathbf{A}T$
- Assume  $u(t) \approx u(t_0)$  is constant during one switching period [23]
- Neglect terms in  $T^2$

$$\mathbf{x}[k+1] = \mathbf{x}[k] + T \left[ (d[k]\mathbf{A}_1 + d'[k]\mathbf{A}_0)\mathbf{x}[k] + (d[k]\mathbf{B}_1 + d'[k]\mathbf{B}_0)\mathbf{u}[k] \right] \quad (4.20)$$

where  $d'[k] \equiv 1 - d[k]$ .

A discrete model facilitates the design procedure of digital controllers, that rely upon discrete-time control techniques [25]. SDM enable fast time-domain simulations, since only a discrete, linear set of difference equations needs to be solved. The drawback of SDM is that the accuracy is poor at low switching frequencies, as will be illustrated in the next paragraph.

#### 4.1.4 Comparison between the models

Figure 4.2 (repeated in fig. 4.5) gives an overview of the modelling techniques for power converters, with respect to the required computation time and the accuracy. As is mentioned in the introduction, a model intends to approximate the real behavior of a power converter. The physical system, per definition, has an infinite accuracy and requires an infinite computation time as is shown in the figure. The figure furthermore shows the approximations that are at the base of these models.

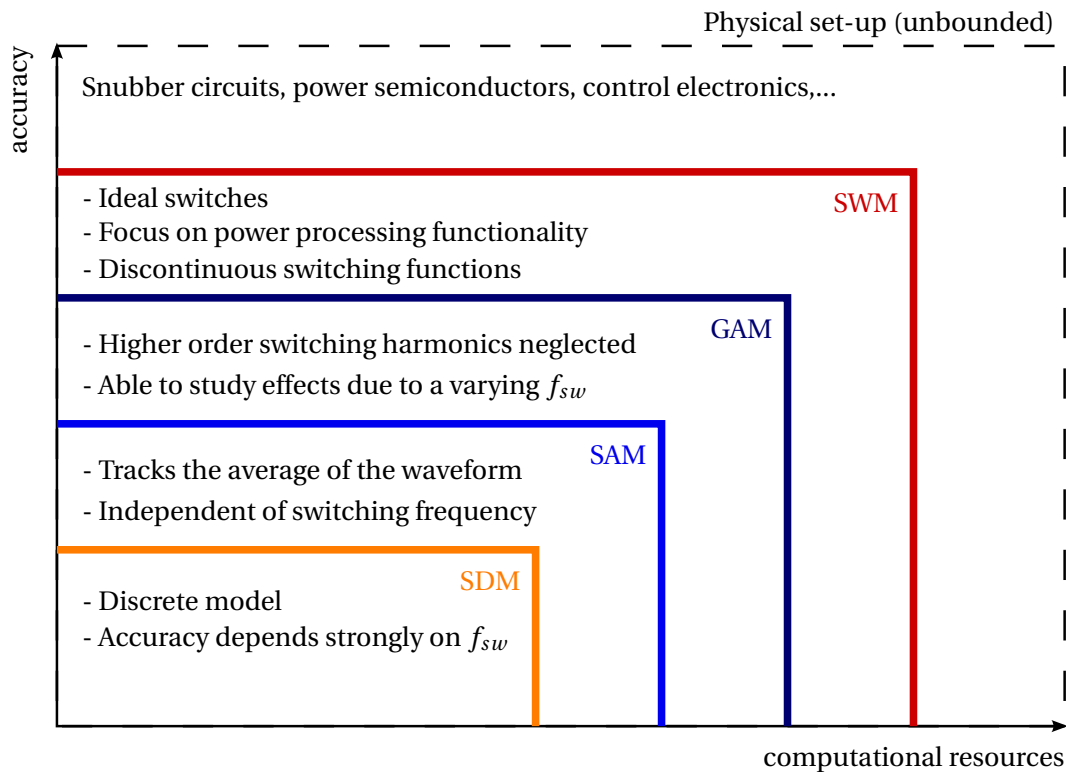


FIGURE 4.5: Overview of the modeling techniques for power electronic converters

The switched model generally focuses on the components essential for the power processing function of the circuit. The power semiconductors are modeled as ideal switches, which lead to discontinuous, square wave switching functions like  $q(t)$  in section 4.1.1. Applying this switching function results in current and voltage waveforms as shown in fig. 4.4. The GAM approximates these waveforms by a truncated Fourier series (within one switching period), thereby neglecting higher order switching harmonics. Only retaining the zero-th order Fourier coefficient, leads to the SAM, which is independent from the switching frequency. The SAM is a good approximation when the waveform ripple is negligible. The SDM differs from the SAM and GAM in the sense that it is a discrete model and only samples at multiples of the switching period are used. Therefore the accuracy of the SDM depends strongly on the switching frequency. For developing digital controllers, the discrete SDM model can be applied when the switching frequency is sufficiently high.

The overview in fig. 4.2 is only *qualitative* and therefore this paragraph shows the modeling results for a buck converter (the equations were derived in sections 4.1.1 to 4.1.3) to obtain a *quantitative* comparison. The model of the buck converter is simulated in Matlab/Simulink/PLECS using the different techniques. Moreover, these simulations are carried out for different parameter variations. This comparison will show that the GAM gives good results with respect to computation time and accuracy. The switched model serves as a reference for the model accuracy.

### Methodology

To compare the accuracy of each model to the detailed SWM, the error is defined by:

$$E = \frac{1}{n} \sqrt{\sum_{t=1}^n (x^{(t)} - x_{sw}^{(t)})^2} \quad (4.21)$$

where

$n$  is the number of data points that are calculated numerically

$x^{(t)} - x_{sw}^{(t)}$  is the error at time  $t$  between the SAM, GAM or SDM and the SWM

$x^{(t)}$  is a general notation that refers to the current or voltage respectively

This error measure comes down to calculating the 2-norm of the error vector containing  $n$  error values. The error is normalized per data point through dividing by  $n$ , since the number of data points differs between the models. The detailed SWM contains the most data points, but these points do not necessarily coincide in time with the SAM, GAM or SDM. Therefore the points of the SWM are linearly interpolated to coincide with the SAM, GAM or SDM.

The absolute error is taken as a measure to quantify the accuracy of the models, since the relative error would lead to large numbers when the reference value is low.

Apart from the error, the computation time is measured to compare the computational speed between the models. This computation time is obtained by repeating the simulations 50 times and computing the average computation time to eliminate random effects that slow down or speed up the computation temporarily, like other processes running on the computer.

Parameter description	Symbol	Value
Inductance	L	10 mH
Capacitance	C	20 $\mu$ F
Resistance	R	2 $\Omega$
Switching frequency	$f_{sw}$	5 kHz
Duty cycle	D	0.5
Source voltage	$v_{CC}$	400V
Load voltage	$v_c$	200V
Load power	P	2kW

TABLE 4.1: Model parameters

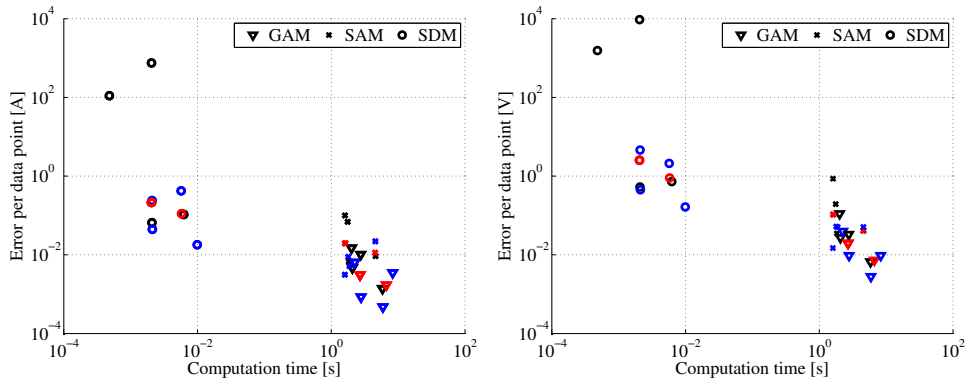


FIGURE 4.6: A comparison between the different models w.r.t. computation time and error for the inductor current (left) and capacitor voltage (right)

## Results

Figures 4.7 to 4.10 shows the results for the comparison between the different models, where the DC/DC converter is modeled. The model parameter values are given in section 4.1.4. Four parameters are subsequently varied to see the effect on the model accuracy:

- Case 1. Variation of the switching frequency
- Case 2. Variation of the inductance value L
- Case 3. Variation of the capacitance value C
- Case 4. Variation of the duty cycle D

The error versus computation time for both the current and voltage waveforms is given in figs. 4.7 to 4.10. Figure 4.6 combines all results for the different cases and shows that the GAM gives the most accurate results.

#### 4. TIME-DOMAIN MODELS OF DC SYSTEMS

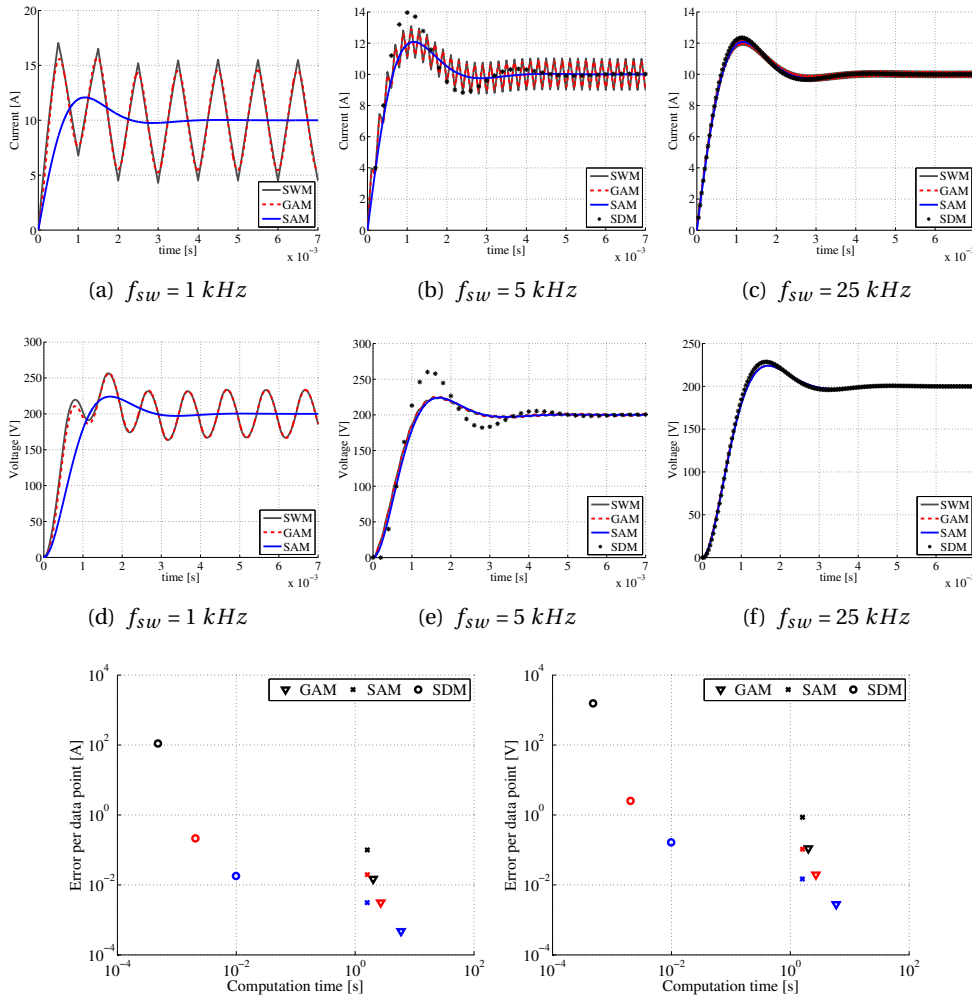


FIGURE 4.7: Case 1 — Variation of the switching frequency

Following conclusions can be drawn:

- At *high switching frequencies*, the current and voltage ripple due to the switching waveforms will diminish. Therefore the accuracy of the average models, both SAM and GAM, improves. Although the results for the SAM remain the same, the error will decrease since the SWM will match the averaged waveform more closely. The SDM proves only to be accurate when the switching frequency is sufficiently high (25 kHz).
- The GAM includes the influence of the switching frequency. This is the only model presented here that models the quantities within a switching cycle.

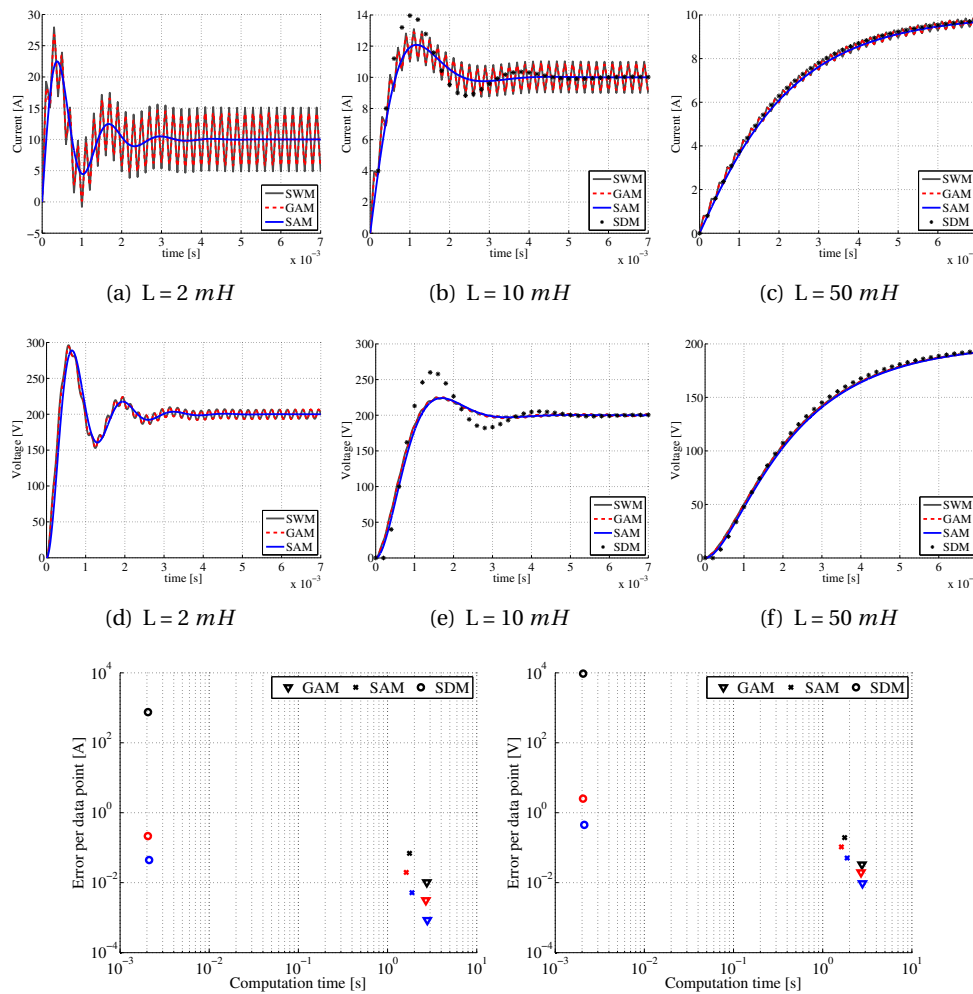


FIGURE 4.8: Case 2 — Variation of the inductance

- The voltage waveform ripple is lower than the current waveform ripple. Reducing the capacitance, will increase the voltage ripple, but the results show that even decreasing or increasing the capacitance by a factor 3, does not alter the results appreciably. When focusing on voltage stability, SAM are sufficiently accurate.
- The GAM fails to approximate the sharp peaks of the SWM (fig. 4.7), as this involves higher harmonic order Fourier coefficients that are not modeled in the GAM. This is also pointed out in [12].
- The SDM model requires substantially less computation time, but suffers from poor accuracy.

#### 4. TIME-DOMAIN MODELS OF DC SYSTEMS

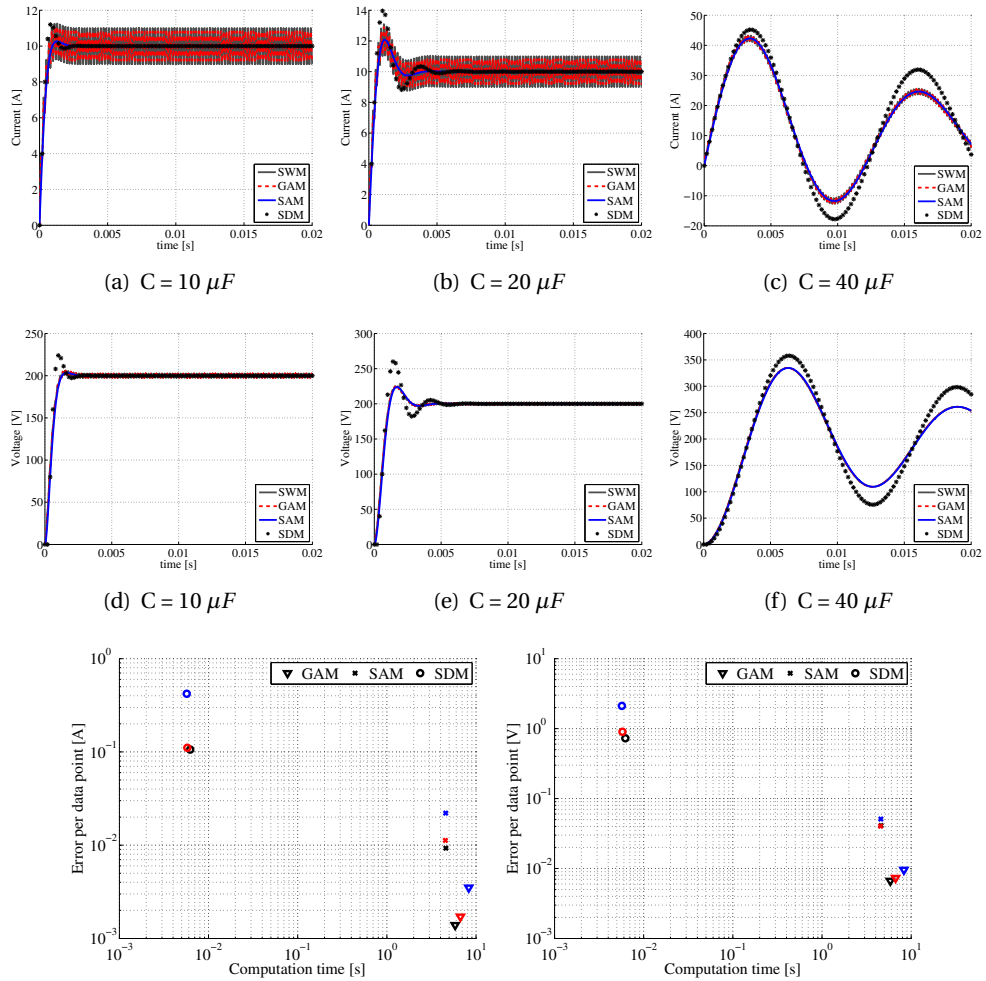


FIGURE 4.9: Case 3 — Variation of the capacitance

- The SAM gives good results, when the switching ripple can be neglected. For stability analysis, the SAM gives the average of the switching waveform, which may be sufficient to determine the stability of the network. However, when power quality requirements require the voltage to remain within restrictive bounds, not taking into account the switching ripple, may result in violating these constraints.
- The GAM gives the best accuracy as compared to the switched model, at the expense of more computation time.

Although the GAM improves the model accuracy, it is less suited to study DC *systems* because the k-phaser state variables of different converters can only be related when they share the same switching frequency [17]. Moreover, the converter controllers regulate the average waveform value (0-phaser) and not the higher-order k-phasers.

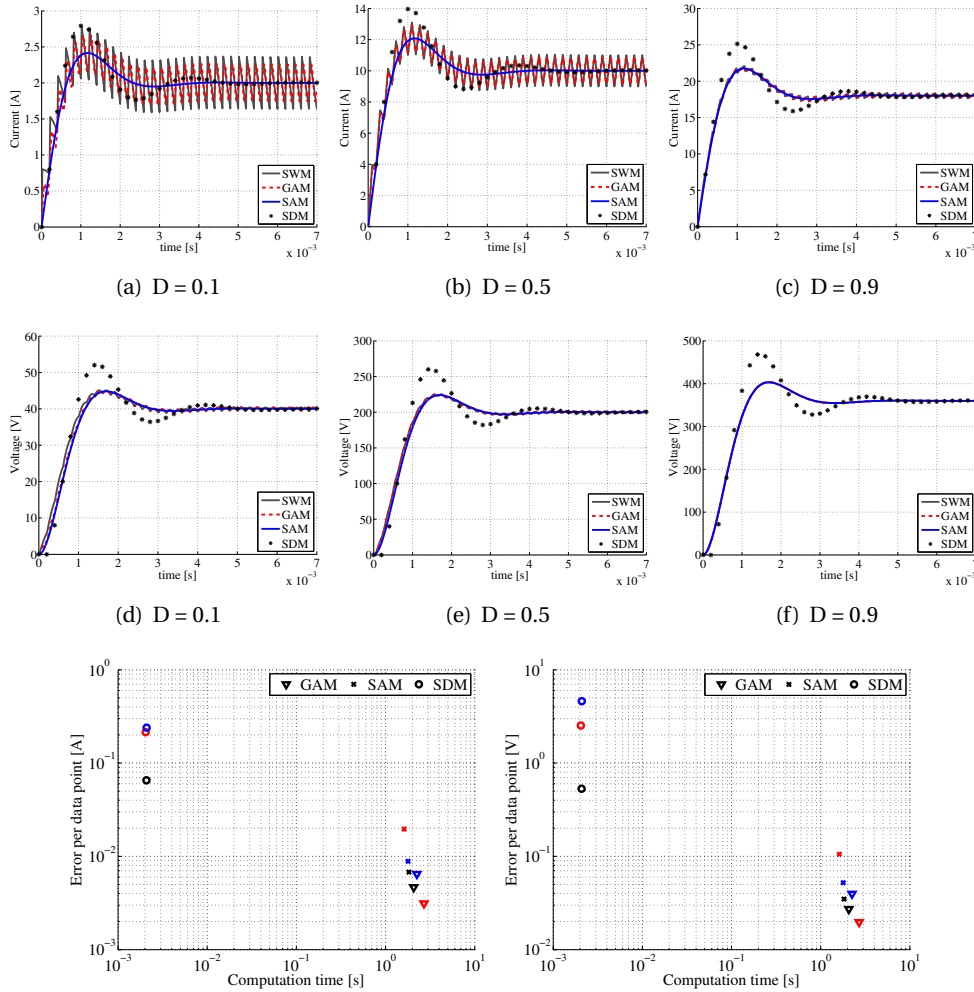


FIGURE 4.10: Case 4 — Variation of the duty cycle

### 4.1.5 Model of an AC/DC converter

This subsection will present a model of an AC/DC voltage-source inverter (VSI), that allows to interconnect AC and DC networks [67]. In contrast to thyristor-based current-source inverters (CSI), the inverter current flow (and hence the power flow) can be controlled in both directions.

The AC side is modelled as an infinite bus, connected via an RL filter to the converter. To facilitate the controller operation and design, AC quantities are expressed in the dq reference frame. This approach allows to simplify the controller equations and hence increase the controller performance. The dq frame control requires a synchronization mechanism that is usually achieved through the phase-locked loop (PLL).

The model of the AC/DC interface converter can either control the AC active power injection or the DC bus voltage. The latter case can be considered an extension to the first: controlling the DC bus voltage requires an additional control loop that determines the active power setpoint of the power controller.

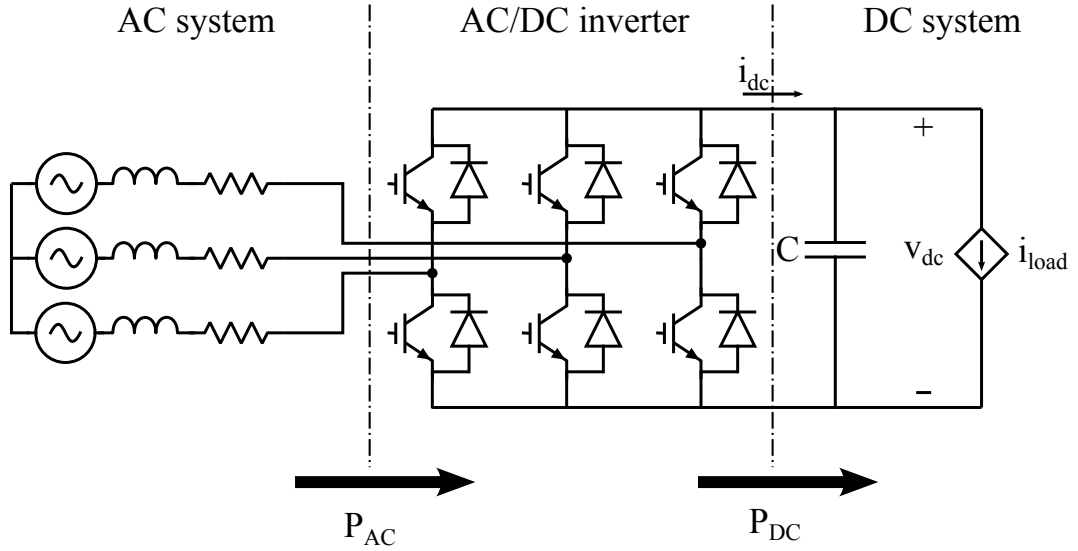


FIGURE 4.11: AC/DC interface converter

Following assumptions are introduced to simplify the analysis of the AC/DC inverters:

1. The AC grid is modelled as an infinite bus system, arbitrarily assuming the AC grid voltage to be aligned with the d-axis.
2. The effect of the phase-locked loop is neglected. This corresponds to setting the quadrature component of the AC grid voltage to zero ( $V_{sq} = 0$ ).
3. The interface converter operates at unity power factor in steady-state. This assumption comes down to setting  $i_q^* = 0$ .
4. The AC frequency is assumed to be constant at  $\omega_0 = 2\pi \cdot 50 \text{ rad/s}$
5. Switching and resistive losses in the interface converter are neglected

The equations of the AC side, expressed in dq quantities are:

$$\frac{di_d}{dt} = \frac{1}{L}(-Ri_d + u_d) \quad (4.22)$$

$$\frac{di_q}{dt} = \frac{1}{L}(-Ri_q + u_q) \quad (4.23)$$

$R$  is the AC resistance,  $i_d$  and  $i_q$  are the direct and indirect line current components.  $u_d$  and  $u_q$  are defined by:

$$m_d(t) \equiv \frac{2}{v_{dc}(t)} (u_d(t) + V_{sd} - L\omega_0 i_q(t)) \quad (4.24)$$

$$m_q(t) \equiv \frac{2}{v_{dc}(t)} (u_q(t) + V_{sq} + L\omega_0 i_d(t)) \quad (4.25)$$

$m_d$  and  $m_q$  refer to the modulation index,  $V_{dc}$  is the DC bus voltage,  $V_{sd}$  and  $V_{sq}$  represent the AC grid voltage,  $L$  is the AC inductance,  $\omega_0$  is the steady-state frequency.

Two PI controllers control  $i_d(t)$  and  $i_q(t)$  to their respective reference values.  $i_q^*(t)$  is set to zero, regulating the reactive power flow to zero in steady-state.  $i_d$  in this case determines the active power flow. The presence of an integrator in the PI controller, requires the introduction of an additional state variable per controller ( $x_d$  and  $x_q$  respectively). The controller equations become:

$$u_d(t) = x_d(t) + K_{pd} (i_d^*(t) - i_d(t)) \quad (4.26)$$

$$u_q(t) = x_q(t) + K_{pq} (i_q^*(t) - i_q(t)) \quad (4.27)$$

$$\frac{dx_d(t)}{dt} = K_{id} (i_d^*(t) - i_d(t)) \quad (4.28)$$

$$\frac{dx_q(t)}{dt} = K_{iq} (i_q^*(t) - i_q(t)) \quad (4.29)$$

$x_d$  and  $x_q$  are the internal states of the PI controllers,  $K_{pd}$  and  $K_{pq}$  are the proportional control gains,  $K_{id}$  and  $K_{iq}$  are the integral controller parameters. Since the dynamics of both  $i_d$  and  $i_q$  are similar, the two PI controllers can have the same parameters (i.e.  $K_{pd} = K_{pq}$  and  $K_{id} = K_{iq}$ ).

The dc side consists of a capacitor. The capacitor current equals the difference between the output dc current of the interface converter and the dc grid load current. Both are equal in steady-state. When neglecting converter losses, the AC power and DC power should be equal. That allows to relate DC to AC quantities, without describing the power electronic switching dynamics in detail:

$$P_{dc} = P_{ac} \Rightarrow v_{dc}(t) i_{dc}(t) = \frac{3}{2} (V_{sd} i_d(t) + V_{sq} i_q(t)) \quad (4.30)$$

The dynamics of the capacitor are governed by:

$$\frac{dv_{dc}}{dt} = \frac{1}{C} \left[ \frac{\frac{3}{2} [V_{sd} i_d(t) + V_{sq} i_q(t)]}{v_{dc}} - i_{load}(t) \right] \quad (4.31)$$

The first term represents the interface converter output current. The DC load current  $i_{load}(t)$  is determined by the DC grid input impedance, which relates  $i_{load}(t)$  to  $v_{dc}(t)$ .

By applying an additional outer control loop to regulate the DC bus voltage  $v_{dc}(t)$  to  $v_{dc}^*$ , the voltage controller equations become:

$$i_d^* = x_v(t) + K_{pv}(v_{dc}^* - v_{dc}(t)) \quad (4.32)$$

$$\frac{dx_v(t)}{dt} = K_{iv}(v_{dc}^* - v_{dc}(t)) \quad (4.33)$$

Equations (4.23), (4.29), (4.31) and (4.33) constitute the state-space representation of an AC/DC inverter. The six state variables are  $i_d, i_q, x_d, x_q, v_{dc}, x_v$ .

## 4.2 Models of distributed energy resources

The technical literature has presented innumerable models of distributed energy resources. The models that are applied in this thesis are listed in table 4.2. This section will review the model of a PV generator that is current-controlled, which differs from the model that is proposed in [66], where a power controller is applied. The models of the other distributed energy resources are available in the references.

Model	Reference
Models of DER	
PV generation	[66] (modified in this section)
Microturbine	[24]
Battery Energy Storage System	[28]
Models of power converters	
AC/DC inverter	[67] (included in previous section)
Voltage balancer	[35][44]
Current balancer	[45]

TABLE 4.2: References to the models of distributed energy resources and power converters that are applied in this thesis

### 4.3 Model of a photovoltaic system

This section develops a model for a photovoltaic (PV) system (Figure 4.12). The model consists of a boost DC/DC converter and a PV source, comprising  $n_p$  strings that each have  $n_s$  PV modules connected in series. The boost converter is included to regulate the PV DC voltage  $v_{pv}(t)$ , in order to operate at the PV maximum power point (MPP), and maximize the power output [20].

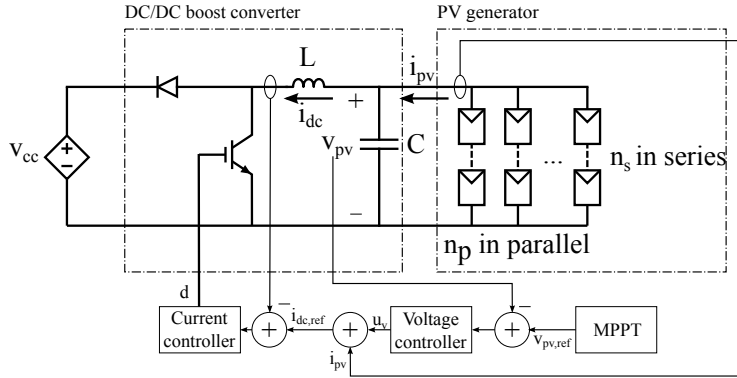


FIGURE 4.12: Control scheme of a PV generator interfaced via a DC/DC boost converter

The PV array is modelled as follows [66]:

$$i_{pv}(t) = n_p I_{ph} - n_p I_s \left[ \exp\left(\frac{q}{k\theta A} \frac{v_{pv}(t)}{n_s}\right) - 1 \right] \quad (4.34)$$

where  $n_p$  denotes the number of PV strings in parallel,  $n_s$  equals the number of PV modules connected in series per string,  $I_s$  denotes the reverse saturation current,  $q = 1.0622 \cdot 10^{-19} C$  is the electron charge,  $k = 1.38 \cdot 10^{-23} J/K$  is the Boltzmann constant,  $\theta$  is the temperature in Kelvin,  $A$  is the ideality factor and  $v_{pv}(t)$  is the voltage at the PV terminals as defined in fig. 4.12.

$I_{ph}$  is the photo-current, which in turn depends linearly upon the incoming solar radiation  $S[\%]$ <sup>1</sup> and the cell temperature  $\theta[K]$ :

$$I_{ph} = [I_{scr} + k_\theta (\theta - \theta_{ref})] \frac{S}{100} \quad (4.35)$$

where  $I_{scr}$  denotes the short-circuit current of one PV module at the reference temperature  $\theta_{ref}$ ,  $k_\theta$  is the temperature coefficient.

<sup>1</sup>  $S = 100\%$  corresponds to  $1 \text{ kW/m}^2$  solar irradiation

The dynamics of the coupling capacitor  $C$  (Figure 4.12) are governed by:

$$C \frac{dv_{pv}(t)}{dt} = i_{pv}(v_{pv}, S, \theta) - i_{dc}(t) \quad (4.36)$$

in which  $i_{dc}(t)$  denotes the current flowing into the boost converter. An inner control loop in the boost converter regulates the current to the reference dc current  $i_{dc}^*$ , which can be controlled by varying the duty cycle of the boost converter. The reference current  $i_{dc}^*$  is in turn set by the outer loop voltage controller, that controls  $v_{pv}(t)$ .

The dynamics of the boost converter are governed by:

$$L \frac{di_{dc}}{dt} = v_{pv} - d v_{cc} \quad (4.37)$$

where  $d$  denotes the duty cycle and  $L$  the value of the boost converter inductor.

Now consider the outer-loop voltage controller that regulates  $v_{pv}$  (Figure 4.12). The dynamics of  $v_{pv}$  were given by eq. (4.36). Note that eq. (4.36) is nonlinear, since the PV output current  $i_{pv}$  is related to  $v_{pv}$  via eq. (4.34). Feedback linearization [40] is applied to eliminate this nonlinearity.  $u_v$  is defined by eq. (4.38) as the output of the voltage controller. This way, the dynamics of  $v_{dc}$  reduce to eq. (4.39).

$$u_v \equiv i_{dc,ref} - i_{pv} \quad (4.38)$$

$$C \frac{dv_{pv}(t)}{dt} = -u_v \quad (4.39)$$

The voltage and current controller equations are:

$$\begin{cases} d = K_{pi}(i_{dc,ref} - i_{dc}) + x_i \\ \frac{dx_i}{dt} = K_{ii}(i_{dc,ref} - i_{dc}) \end{cases} \quad (4.40)$$

where  $K_{pi}$  and  $K_{ii}$  are the current controller proportional and integral gain and  $x_i$  is the current controller state variable.

$$\begin{cases} u_v = K_{pv}(v_{pv,ref} - v_{pv}) + x_v \\ \frac{dx_v}{dt} = K_{iv}(v_{pv,ref} - v_{pv}) \end{cases} \quad (4.41)$$

where  $K_{pv}$  and  $K_{iv}$  are the voltage controller proportional and integral gain and  $x_v$  is the voltage controller state variable.

## 4.4 Switched simulation of a small LVDC system

The previous sections in this chapter focussed on the individual components in DC systems. This section presents a time-domain simulation of a small LVDC network, that allows to compare the results of averaged and switched PEC models. The results that are presented in this section were accepted for publication on the Young Researchers Symposium 2014 [27]. The publication is included in appendix C.

The DC system that is investigated (fig. 4.13) consists of 2 power sources and two loads that are interconnected via 3 distribution lines. Source 1 is an AC/DC inverter interfaced with the utility grid that controls the DC bus voltage in the network and hence is responsible for the power balance in the system. Source 2 is a PV generator, that is interfaced via a DC/DC boost converter to the distribution network. The DC system also includes a battery energy storage system (BESS), that is connected via a DC/DC boost converter at bus 3. Load 1 and 2 are modelled as constant-power loads, that are interfaced via a buck DC/DC converter to the distribution network. For a detailed explanation on the models, the reader is referred to appendix C.

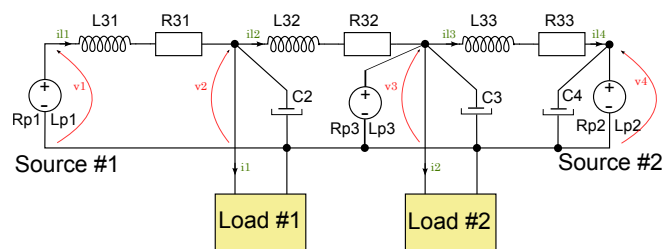


FIGURE 4.13: Circuit diagram of the investigated DC system

Three simulation scenarios are considered to compare the time-domain responses between switched and averaged converter models:

**Test case 1** Decrease of the PV solar irradiation from 100% to 75%, corresponding to a decrease of 1750W of PV generation

**Test case 2** Variation of the battery operating mode from discharging  $-5A$  to charging  $5A$

**Test case 3** Variation of the AC/DC inverter DC bus voltage reference from 400V to 380V.

In all three cases, the switched and averaged DC bus voltage waveforms at bus 3 are compared. The results in fig. 4.14, indicate that the averaged model is a good approximation of the switched voltage waveform to study DC voltage stability. It is moreover argued and demonstrated by the simulations in 4.1 that averaged models will become more accurate with increasing switching frequencies and harmonic filtering. Therefore it is concluded that averaged models of PEC in *DC systems* are applicable to study DC voltage stability in DC power systems that include distributed energy resources and feedback controllers.

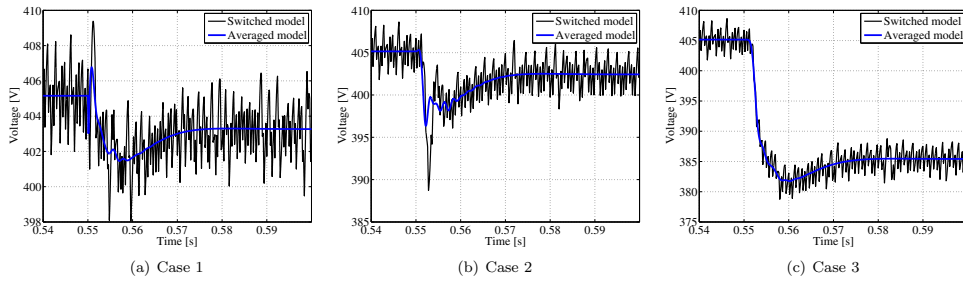


FIGURE 4.14: Comparison between averaged and switched DC bus voltage waveforms at bus 3

## 4.5 Conclusion

This chapter presented the existing modelling techniques for power electronic converters and models of distributed energy resources. These models are required to assess the stability of DC power systems and are applied in the subsequent chapters.

In a design environment where the designer wants to verify the influence of design decisions, simulation time is a concern. Therefore, much attention has been drawn to the modelling of power electronic converters in this chapter. It is concluded that averaged models are advised, since they significantly speed up simulations as compared to switched models. This conclusion is based on the time-domain simulation of a DC/DC buck converter in the first section, and a time-domain simulation of a DC power system in the third section. The time-domain simulation of a DC power system demonstrated that averaged models are also applicable to DC power systems that include distributed energy resources and feedback controllers.

## Chapter 5

# MatLVDC

MatLVDC is a Matlab® toolbox, developed to analyze DC networks (including power electronic converters and distributed energy resources) via time-domain simulations and small-signal stability analysis. The MatLVDC input format is similar to MatPower [68] and therefore facilitates the simulation setup of unipolar and bipolar DC networks. MatLVDC has a component library, including power electronic converters and distributed energy resources (Chapter 4). Users are able to define custom components in an obvious manner.

This chapter provides an overview of MatLVDC, that will be applied in chapter 6 to analyze a medium-sized LVDC network. The first section will introduce the capabilities of MatLVDC, the second section will explain the structure of the toolbox and the last section provides an application example to make the reader comfortable with the input data format of MatLVDC and its functionalities. A user guide is included in appendix B.

### 5.1 Capabilities of MatLVDC

MatLVDC analyzes DC voltage stability via time-domain simulations and small-signal analysis. This tool has more capabilities than the DC Stability Toolbox [63] that has been published in the past. That toolbox assesses the small-signal stability of DC systems by using minor-loop gain criteria. As was outlined in chapter 3, minor-loop gain criteria are only applicable for unidirectional power flow and may lead to conservative design decisions [57].

The capabilities of MatLVDC are:

- Perform time-domain simulations of DC networks
  - Including loads and generation that are interfaced via power electronic converters
  - Simulate bipolar and unipolar network configurations
  - Simulate radial, ring and meshed network topologies
  - Calculate time-domain transients for varying parameter values
- Determine the steady-state operating point
- Perform small-signal stability analysis
  - Calculate a linearized system state-space representation
  - Calculate the poles of the linearized system
  - Plot a root locus for varying parameter values

**Perform time-domain simulations of DC networks** MatLVDC facilitates setting up the dynamic equations of the networks and components to perform a time-domain simulation subsequently. The network can contain unipolar and bipolar connections (or feasible combinations of both). MatLVDC can also handle various network topologies: from radial topologies to meshed topologies (Figure 5.1). The input data format is provided in the user guide (Appendix B).

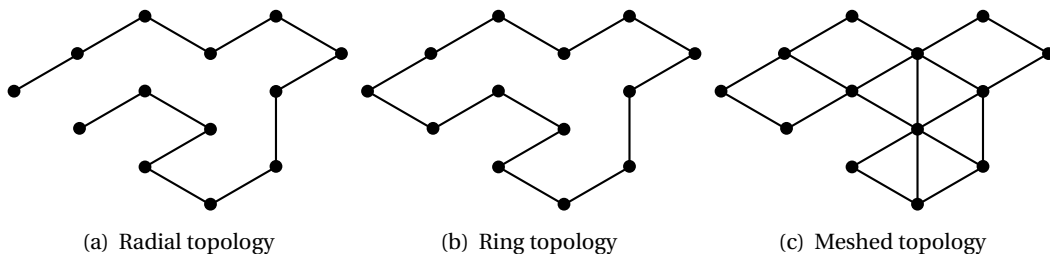


FIGURE 5.1: Possible network topologies

MatLVDC will subsequently construct a (nonlinear) state-space representation of the network in a format that is compatible with Matlab® built-in ordinary differential equation (ODE) solvers.

**Determine the steady-state operating point** The state-space representation of the network can be solved using a nonlinear equation solver like `fsolve`. This allows to determine the steady-state equilibrium solution.

**Perform small-signal stability analysis** The state-space representation that is constructed can subsequently be linearized around a specific operating point. This allows to calculate the system poles and apply conventional linear analysis techniques.

## 5.2 Structure of the toolbox

MatLVDC uses the object-oriented capabilities of Matlab to obtain a structured program code. An overview of the classes is shown in fig. 5.2. DC System is the main class of MatLVDC that works together with the subclasses *Network*, *Bus* and *Component* to setup the model equations:

**Network** The network class will handle the state-space representation of the electrical network.

**Component** The components represent the devices (load and generation) that are present in the network.

**Bus** The bus class represents the physical busses in the network, where components can be connected to.

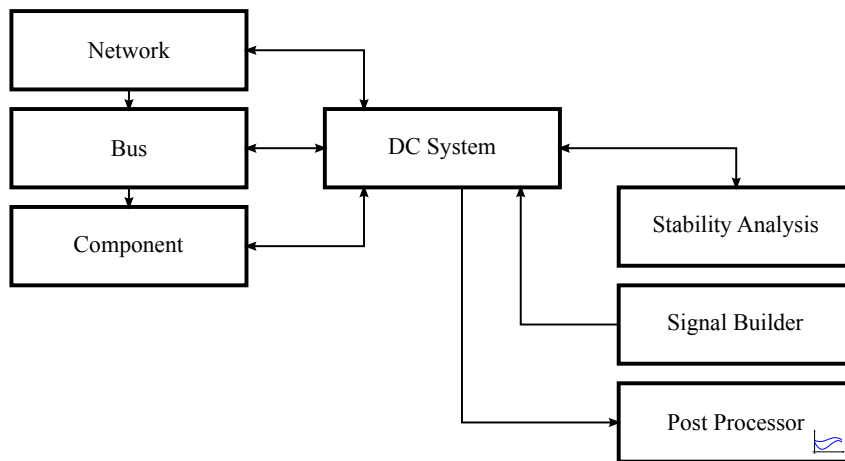


FIGURE 5.2: Class overview of MatLVDC

The class structure thus strongly relates to the real DC system, that includes the electrical network and components that represent subsystems. MatLVDC will provide the state-space representation of the DC system, which incorporates the interconnections between different components in the system. An interconnection connects the output of one subsystem, which can be a Network object or a Component object, to the input of another subsystem (Figure 5.3). MatLVDC furthermore distinguishes internal inputs and external inputs. *Internal inputs* are inputs that are determined by the interconnection of subsystems. Examples are terminal voltages or load currents. On the other hand, *external inputs* are inputs that need to be provided to the DC system externally. Examples are solar irradiation and reference set-points.

Figure 5.3 also shows that the Component objects and the Network object have parameters. MatLVDC is constructed in a way that Component parameters can be modified externally between simulations. This allows to study the effect of parameter variations on the system response, steady-state equilibrium and pole locations.

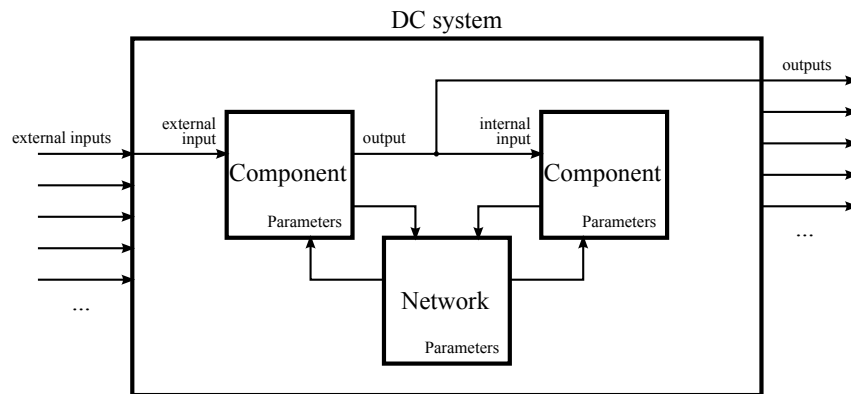


FIGURE 5.3: Overview of a DC system

DC systems include a method to execute a time-domain simulation. The *Signal Builder* class is used to create the external input signals as a function of time. MatLVDC includes step signals and constant signals, but users can also define other input signals. The results of a time-domain simulation can subsequently be plotted using the *Post Processor* class.

The DC system object can also calculate the steady-state operating point. The steady-state solution can serve as a starting point for the time-domain simulation, or as an operating point around which the DC system is linearized.

### 5.3 Application Example: circuit including a constant-power load

This section uses MatLVDC to assess the stability of a small DC system that is depicted in fig. 5.4. The circuit consists of two busses that are connected by a branch. At bus 1 a voltage source (COMP 1) is connected; at bus 2, an RL load (COMP 3), a capacitor (COMP 2) and a DC/DC converter supplying an R load are connected. The DC/DC converter component (COMP 4) includes an inner loop current controller and an outer loop voltage controller. The reference voltage  $v_{ref}$  is regulated at a constant value (100V). Consequently, COMP 4 operates at constant power and it has been demonstrated in chapter 3 that this can cause voltage instability.

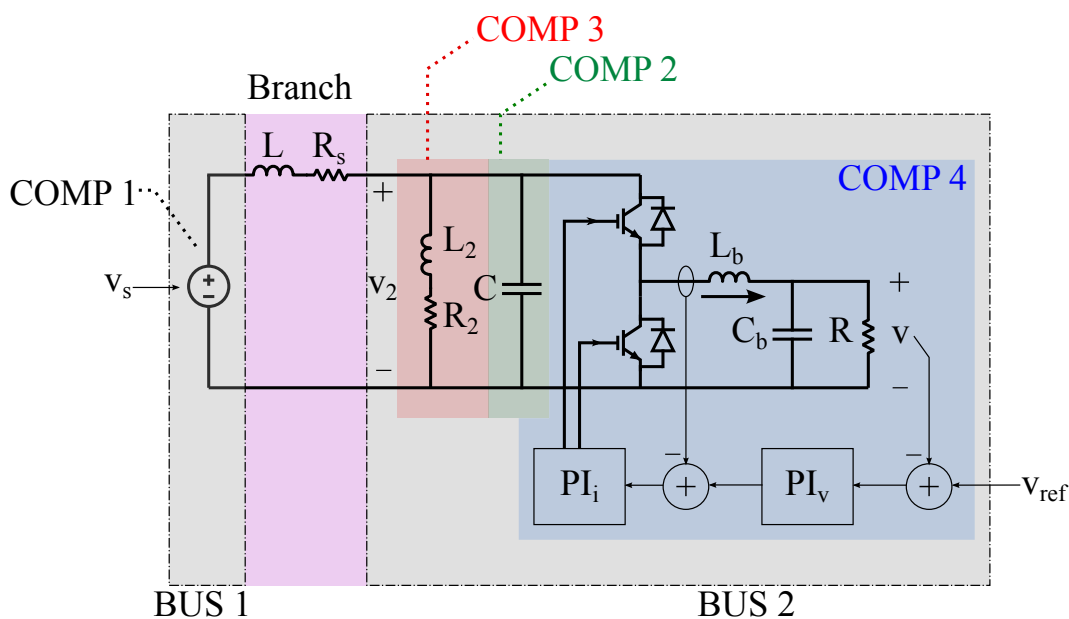


FIGURE 5.4: Application example to demonstrate MatLVDC

#### Goal

MatLVDC is used to determine the load resistor values  $R$  for which the DC system becomes unstable.

Following steps will be taken to demonstrate the use of MatLVDC:

1. Provide the input data for MatLVDC
2. Determine the system poles of the linearized DC system for varying  $R$  values
3. Plot the time-domain response for varying  $R$  values to verify the results from the linear system analysis

### 1. Input data for MatLVDC

The input data for the example circuit is entered using the MatLVDC input data format (Figure 5.5). Once the bus matrix, branch matrix and component matrix are created, a new DCSystem object is setup. Subsequently the method steadyState is applied to calculate the steady state of the DCSystem.

### 2. System poles of the linearized DC system

Since the output voltage of the buck converter is regulated at a constant value, the power will remain constant for a constant  $R$  value. The goal is to determine for which values of  $R$  the system is stable. Therefore the poles of the linearized DCSystem are determined, using the function `dc_system_cpl.linearSys(X,u_ext)` where  $X$  is the steady-state operating point for the linearization and  $u\_ext$  is a vector containing the external inputs to the DCSystem (i.e. the voltage source value  $v_s$  (COMP 1) and the voltage setting  $v_{ref}$  (COMP 4)).

This procedure is repeated for various values of  $R$ , that lead to the root locus plot in fig. 5.6(a). The root locus plot displays the poles of the DC system, that should be located in the left-half plane in order to be stable.

The stability is concluded based upon the location of the system poles. The results are shown in table 5.1. One pole is located in the right-half plane for  $R = 0.0005\Omega$ . Since this value is very small, stability of the DC system can be concluded for realistic values of  $R$ .

<b>R [<math>\Omega</math>]</b>	<b>Stable/Unstable</b>
0.0005	Unstable
0.278	Stable
0.556	Stable
0.833	Stable
1.11	Stable
1.38	Stable
1.67	Stable
1.94	Stable
2.23	Stable
2.5	Stable

TABLE 5.1: Stable and unstable values of  $R$

### 3. Time-domain response

The results of the stability analysis in the previous paragraph are verified via a time-domain simulation. The voltage transients at bus 2 for varying values of  $R$  are shown in fig. 5.6(b). The power waveforms in this case are depicted in fig. 5.6(c).

```

% Bus data
BUSDC_I      BUSDC_CONFIG
1            1;
2            1];

% Branch data
F_BUS T_BUS BR_CONFIG BR_R1 BR_R2 BR_Rn BR_L1 BR_L2 BR_Ln BR_C1 BR_C2

branch_data = [ 1 2 1 0.01 0 0 0.5e-3 0 0.5e-3 0 0];

% Component data
COMP_I COMP_BUS COMP_TYPE COMP_CONFIG COMP_CONN C1 C2 C12

component_data = [ 1 1 6 2 1 0 0 0; % BUS 1 V source
                  2 2 10 2 1 0.1e-3 0 0; % BUS 2 C
                  3 2 18 1 1 0 0 0; % BUS 2 RL
                  4 2 8 1 1 0 0 0; % BUS 2 Buck converter R load
];

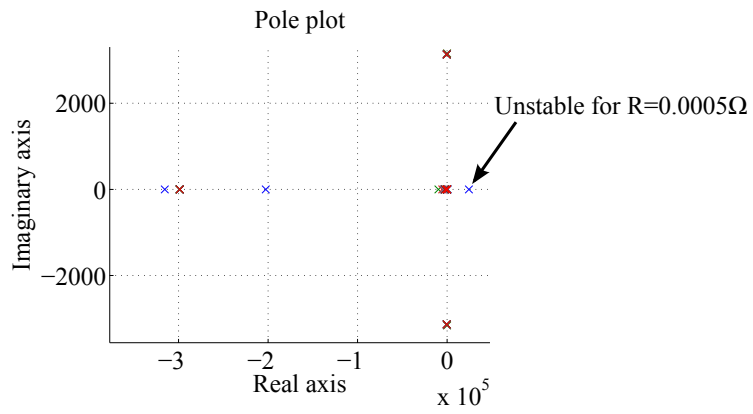
% Create a DCSystem object
dc_system_cpl = DCSystem(bus_data, branch_data, component_data);

% Set parameters
dc_system_cpl.setComponentParameters(2, dc_system_cpl.getBusCapacitances(2)); % BUS 2 C
dc_system_cpl.setComponentParameters(3, [10 1e-6]); % BUS 2 RL
dc_system_cpl.setComponentParameters(4, [5 1e-4 1e-3 1 100 0.1 10]); % BUS 2 Buck converter supplying R load

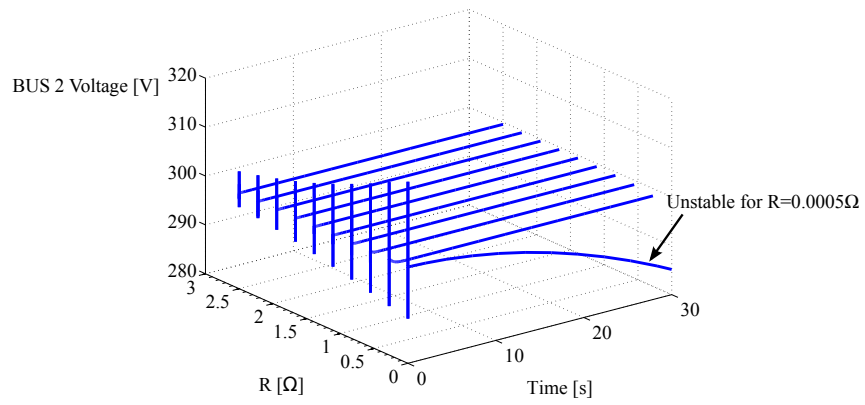
% Steady state
u_ext = [300 100]';
opts = optimset('Display','iter','TolFun',1e-3,'MaxFunEvals',1e4,'MaxIter',1e4,'Algorithm','trust-region-reflective');
STST = dc_system_cpl.steadyState(u_ext, [1 300 1 1 100 0.1 0.1]', 300, opts);

```

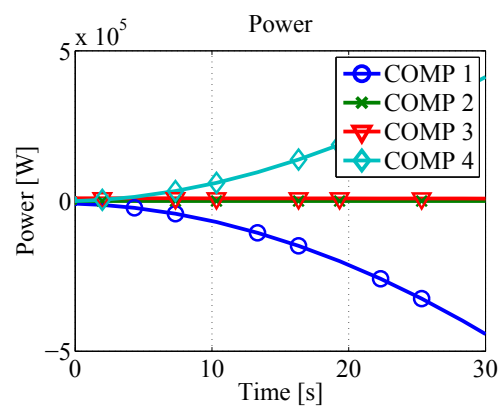
FIGURE 5.5: Input data for MatLVDC



(a) System poles for varying  $R$



(b) Bus voltages for varying  $R$



(c) Power waveforms for  $R = 0.0005\Omega$

## 5.4 Conclusion

This chapter introduced the capabilities and structure of MatLVDC. MatLVDC is a Matlab® toolbox that allows to perform steady-state calculations, time-domain simulations and small-signal analysis of DC systems. This functionality is not included in the DC System Stability Toolbox that was published in the past and relies on minor-loop gain criteria that are only applicable for unidirectional power flow.

MatLVDC facilitates the simulation of DC systems, via a straightforward input data format. This allows to setup a simulation easily and fast. MatLVDC will construct a nonlinear set of ordinary differential equations (ODE), that can be solved using Matlab built-in ODE solvers. MatLVDC can simulate both bipolar and unipolar networks and different network topologies, including meshed topologies. Users can furthermore extend the available component library with custom components.

The structure of the program code is object-oriented and matches the physical structure of DC networks. By applying object-oriented programming, the program code remains structured.

The use of MatLVDC was illustrated in the last section using a small LVDC network that includes a DC/DC converter that operates at constant-power and therefore may cause instability. Using MatLVDC, instability of certain operating points was investigated via small-signal analysis and subsequently confirmed by time-domain simulations.



## Chapter 6

# DC voltage stability of a LVDC network

The previous chapter introduced MatLVDC, a Matlab toolbox to assess the DC voltage stability of LVDC networks with the presence of distributed energy resources. This chapter will use this toolbox to analyze the stability of two LVDC networks that resemble the reference microgrid proposed by [56]. The first network has a unipolar configuration, while the second network has a bipolar configuration.

The first section will describe the unipolar and bipolar networks that will be subsequently analyzed. The second section will demonstrate the effect of power variations on the bus voltages in the network.

### 6.1 Description of the network

The unipolar and bipolar networks, that are analyzed in this chapter, are shown in fig. 6.1 and fig. 6.2 respectively. The unipolar network operates at 380V across the positive  $L+$  and negative  $L-$  conductor; the bipolar network operates at  $\pm 380V$  across the positive  $L+$ , neutral  $L0$  and negative  $L-$  conductors.

To compare the performance of the unipolar and bipolar configuration, the unipolar and bipolar network have the same network topology and serve the same loads and generators. The network topology contains a main feeder and 4 side branches. The main feeder connects bus 1, 2, 3, 4, 6 and 8. Bus 10 is connected to bus 3; bus 5 is connected to bus 4; bus 7 is connected to bus 6 and bus 9 is connected to bus 8.

Following load and generator components are present in the network:

- 1 AC/DC inverter that interfaces the DC network to the AC bus. The AC/DC inverter controls the DC voltage and adjusts the power transfer between the AC and DC network accordingly to balance load and demand. In the bipolar network configuration (Figure 6.2), a voltage balancer is connected at the DC output of the AC/DC inverter to generate +380V, 0V and -380V.
- 2 Battery energy storage systems that are connected via a bi-directional DC/DC converter. The battery current is controlled.
- 6 Resistive loads are connected via a DC/DC buck converter to step down the load supply voltage. The resistor output voltage is regulated at 100V, and therefore the load power is constant ( $P = V^2/R$ ).
- 3 PV generators that are connected via a DC/DC boost converter. The boost converter steps up the PV voltage to 380V and regulates the PV voltage to operate at the maximum power point.
- 1 Microturbine generator that is connected via an AC/DC inverter to the DC network. The rotational speed of the generator is regulated at a constant value.

Table 6.1 lists the main parameters of the components. For a detailed mathematical description of the models that are applied in this chapter, the reader is referred to chapter 4.

Component	Parameter	Symbol	Value [Unit]
PV generator	Rated power	P	6 kW
	PV voltage	$v_{pv}$	200V
Microturbine generator	Rated power	P	30 kW
	Nominal rpm	$n$	55854 rpm
BESS	Rated power	P	3 kW
	Nominal voltage	$v$	60V
Resistive load	Rated power	P	1 kW
	Nominal voltage	$v$	100V
	Resistance	$R$	10 $\Omega$
AC/DC inverter	Rated power	P	30 kW
	AC rms line-line voltage	$v$	300V

TABLE 6.1: Main component parameters



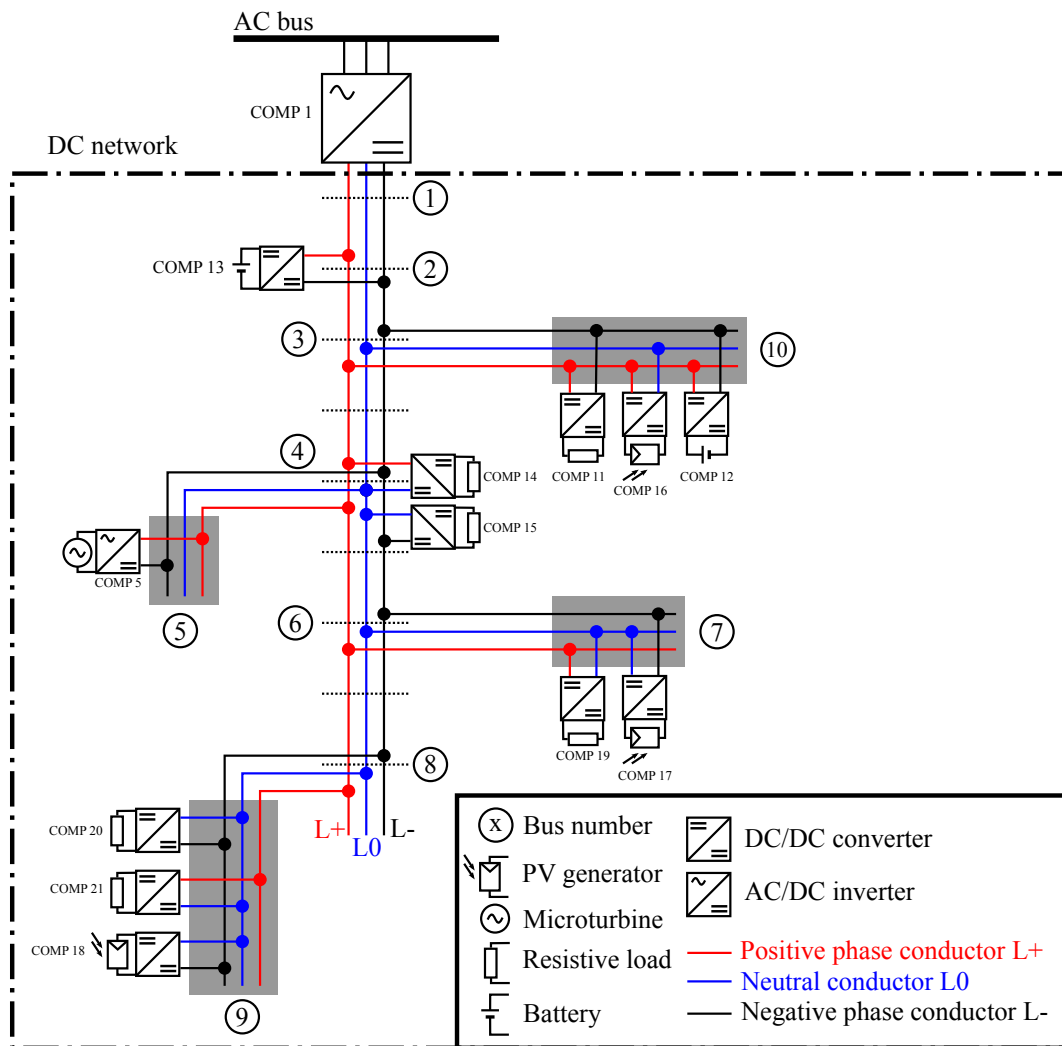


FIGURE 6.2: Bipolar DC network

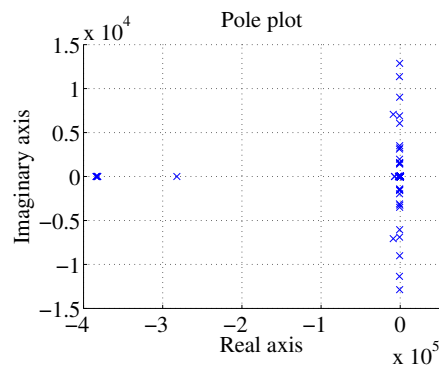
## 6.2 Influence of power variations

This section will analyze the influence of power variations on the bus voltages in the DC network using MatLVDC. Three simulation scenarios are considered:

- Variation of the generated PV power, connected at BUS 7, 9 and 10
- Variation of the microturbine power, connected at BUS 5
- Variation of the resistive load power, connected at the positive phase of BUS 4

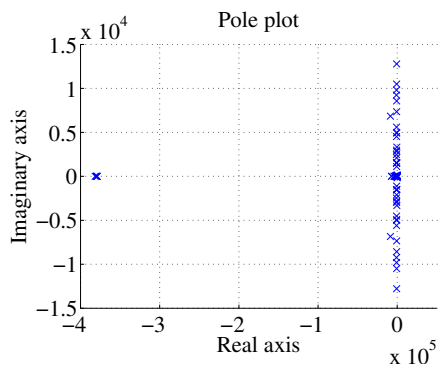
### 6.2.1 Stability of the initial operating point

The unipolar and bipolar DC system are linearized around the initial operating point. This allows to determine the poles of the overall system and assess the stability of the initial operating point (fig. 6.3). The poles are located in the left-half plane, indicating that the initial equilibrium is stable.



(a) Poles of the unipolar network

FIGURE 6.3: Linearized system poles



(a) Poles of the bipolar network

### 6.2.2 Variation of the generated PV power

The influence of a variation in generated PV power is studied. The generated PV power depends on the incoming solar irradiance, that is converted to electricity by the PV array. The PV array is interfaced to the DC network via a DC/DC boost converter that regulates the PV voltage to operate at the maximum power point: following a variation in solar irradiance, the maximum power point will move and the PV voltage is regulated accordingly.

In the unipolar and bipolar DC network, three PV generators are present that each initially deliver 5 kW when the solar irradiance is  $1 \text{ kW/m}^2$ . Subsequently, at  $t = 0.01 \text{ s}$  a step change in solar irradiance occurs and the PV output power of all converters changes. The influence on the main feeder bus voltages (positive to negative terminal) with respect to time is shown in fig. 6.5 for the unipolar configuration and in fig. 6.6 for the bipolar configuration for varying magnitudes of the step change.

The simulation results of the power generation and demand and the system losses are shown in fig. 6.4. This figure clearly shows that the bipolar configuration has less losses than the unipolar configuration, as expected since the voltage level is doubled ( $\pm 380 \text{ V}$ ).

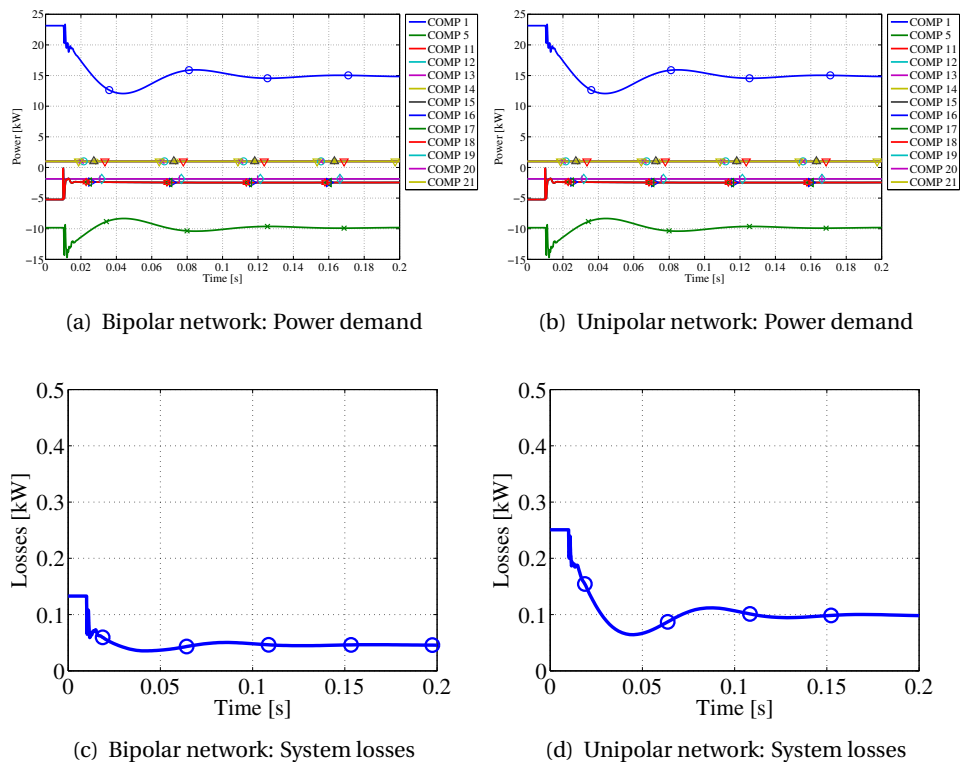


FIGURE 6.4: Simulation results for a PV input power 50% step change

The voltage transients at the bipolar network busses show a larger variation, since less losses (Figure 6.4) occur in the bipolar network and therefore the variation is less damped. Note that the bus voltages are measured between the positive and negative phase conductor, both for the unipolar network and the bipolar network.

Figure 6.7 shows a bode diagram that represents the frequency response of the main feeder bus voltages to variations in the PV input irradiances  $S$ . A resonance peak is observed for both the unipolar and bipolar network at 13.2 Hz, that matches the period that is observed in the bus voltage transients (fig. 6.5; fig. 6.6).

### 6.2.3 Variation of the microturbine generation

Similar to the simulation scenario that is elaborated in the previous section, the microturbine power generation at bus 5 is varied and the effects on the bus voltages are simulated for the unipolar (Figure 6.8) and bipolar network (Figure 6.9).

The voltage transient in this scenario is less pronounced than in the PV scenario, since the initial operating power is lower (15 kW initially for PV, while 10 kW initially for the microturbine).

The bode diagram resembles the bode diagram for the PV scenario (Figure 6.7) and is therefore omitted.

### 6.2.4 Variation of the load power

Similar to the previous simulation scenarios, the load power at bus 4 (1 kW) is varied in this scenario. The bus voltage transients for the unipolar and bipolar topology are presented in fig. 6.10 and fig. 6.11. The influence on the bus voltage of a load change is marginal, since the load power is relatively low as compared to the other simulation scenarios.

## 6. DC VOLTAGE STABILITY OF A LVDC NETWORK

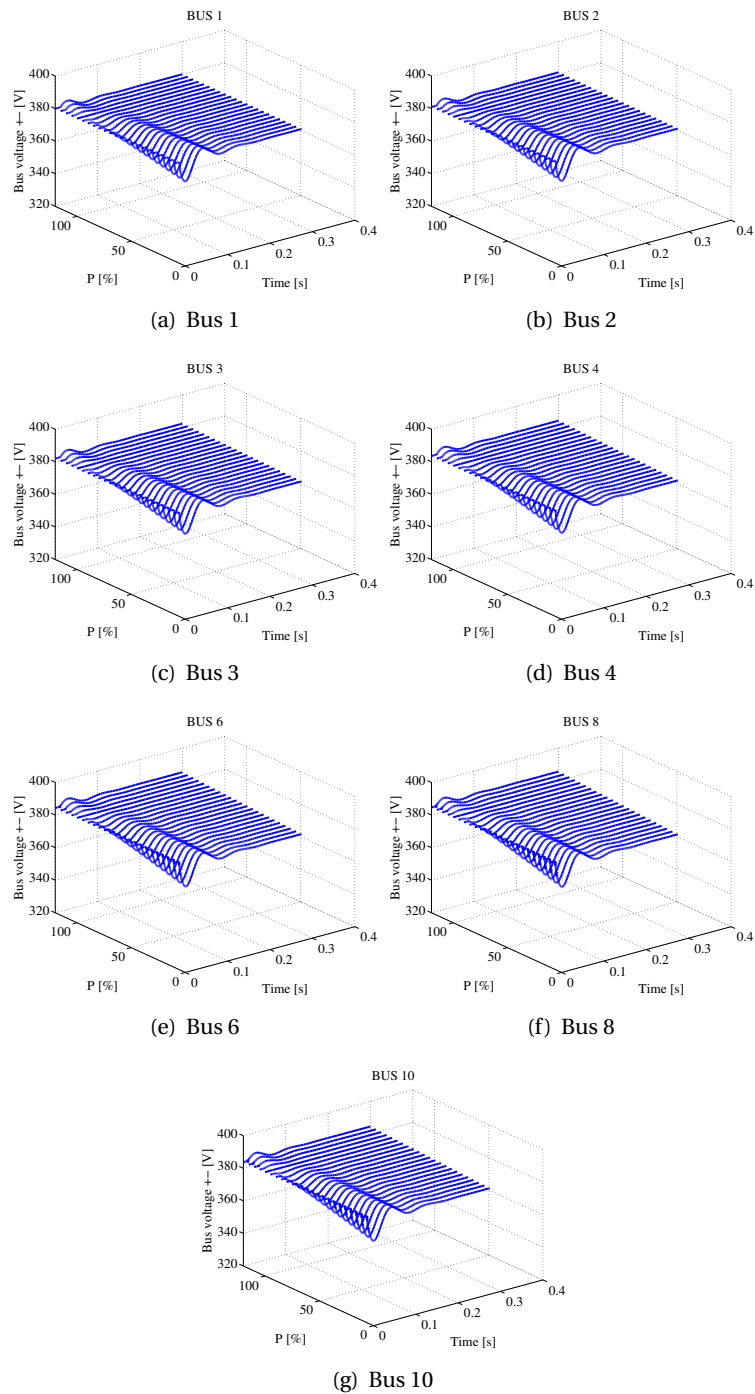


FIGURE 6.5: Unipolar bus voltage transients for varying PV power generation

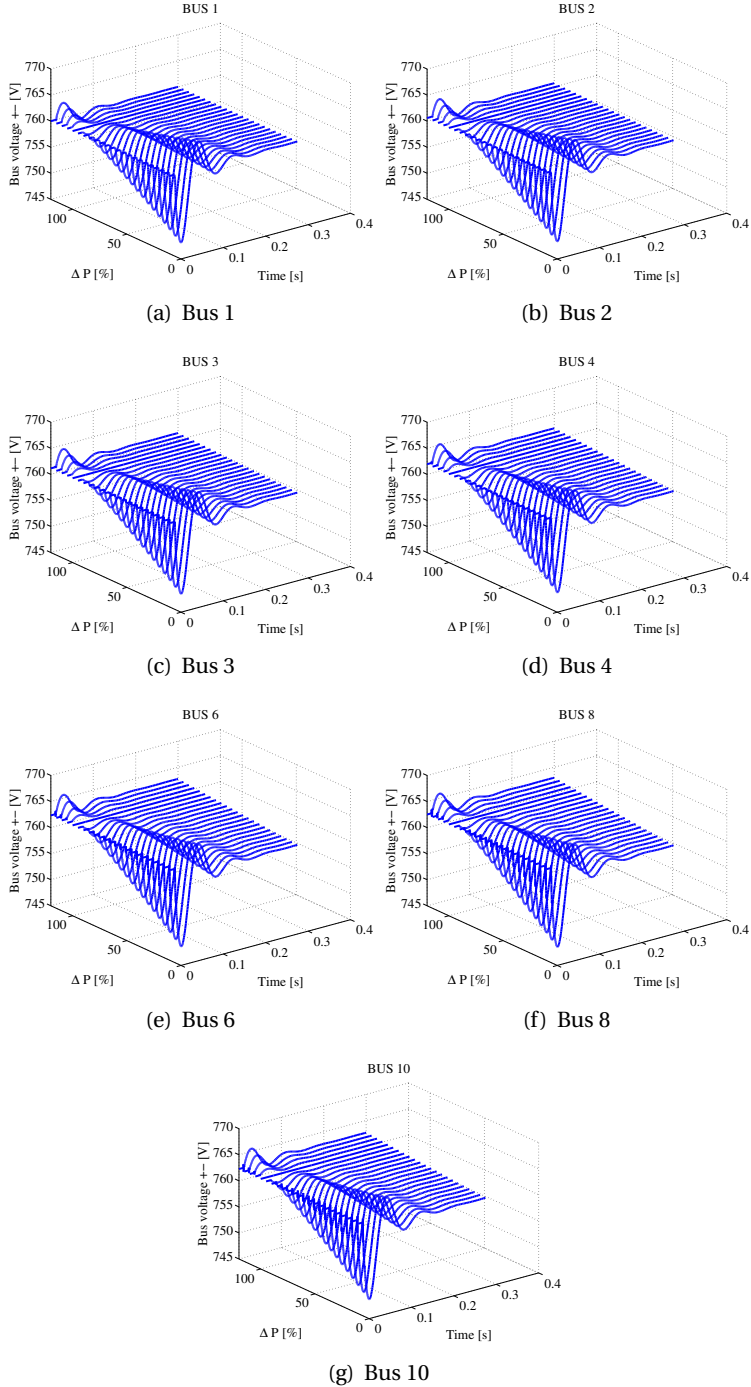


FIGURE 6.6: Bipolar bus voltage transients for varying PV generation

## 6. DC VOLTAGE STABILITY OF A LVDC NETWORK

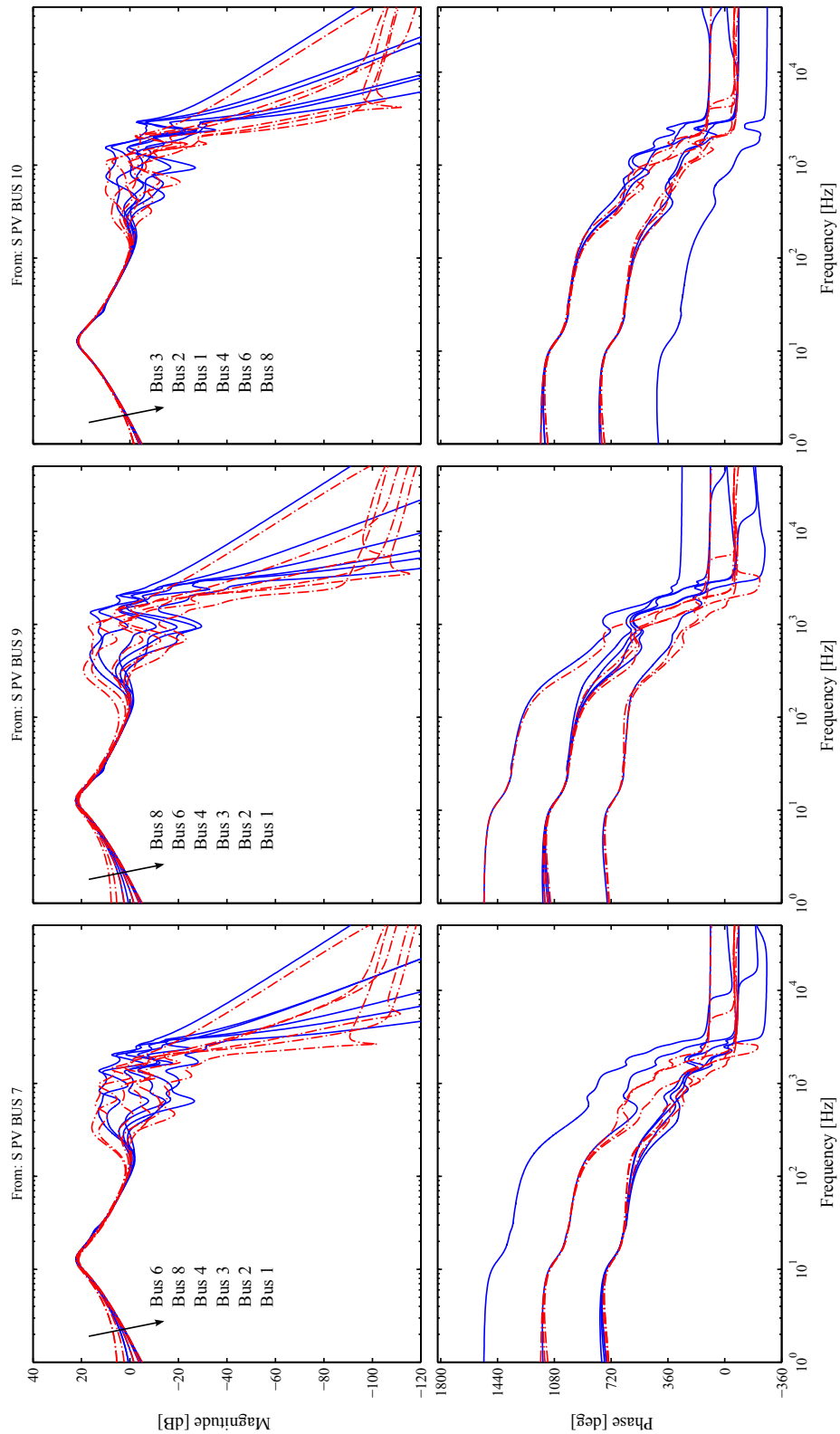


FIGURE 6.7: Bode plot for the linearized DC system around the initial operating point w.r.t. the PV irradiance inputs (dashed line for unipolar network; solid line for bipolar network)

## 6.2. Influence of power variations

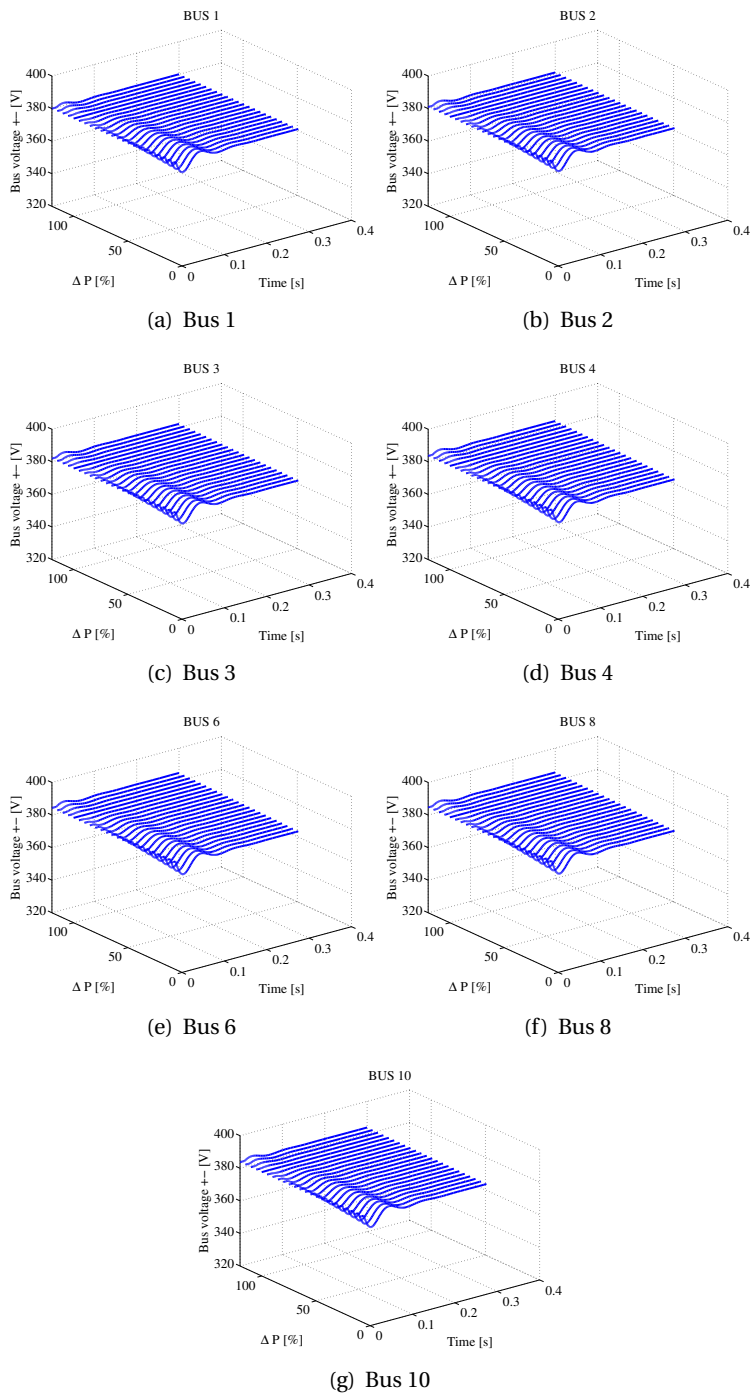


FIGURE 6.8: Unipolar bus voltage transients for varying microturbine power generation

## 6. DC VOLTAGE STABILITY OF A LVDC NETWORK

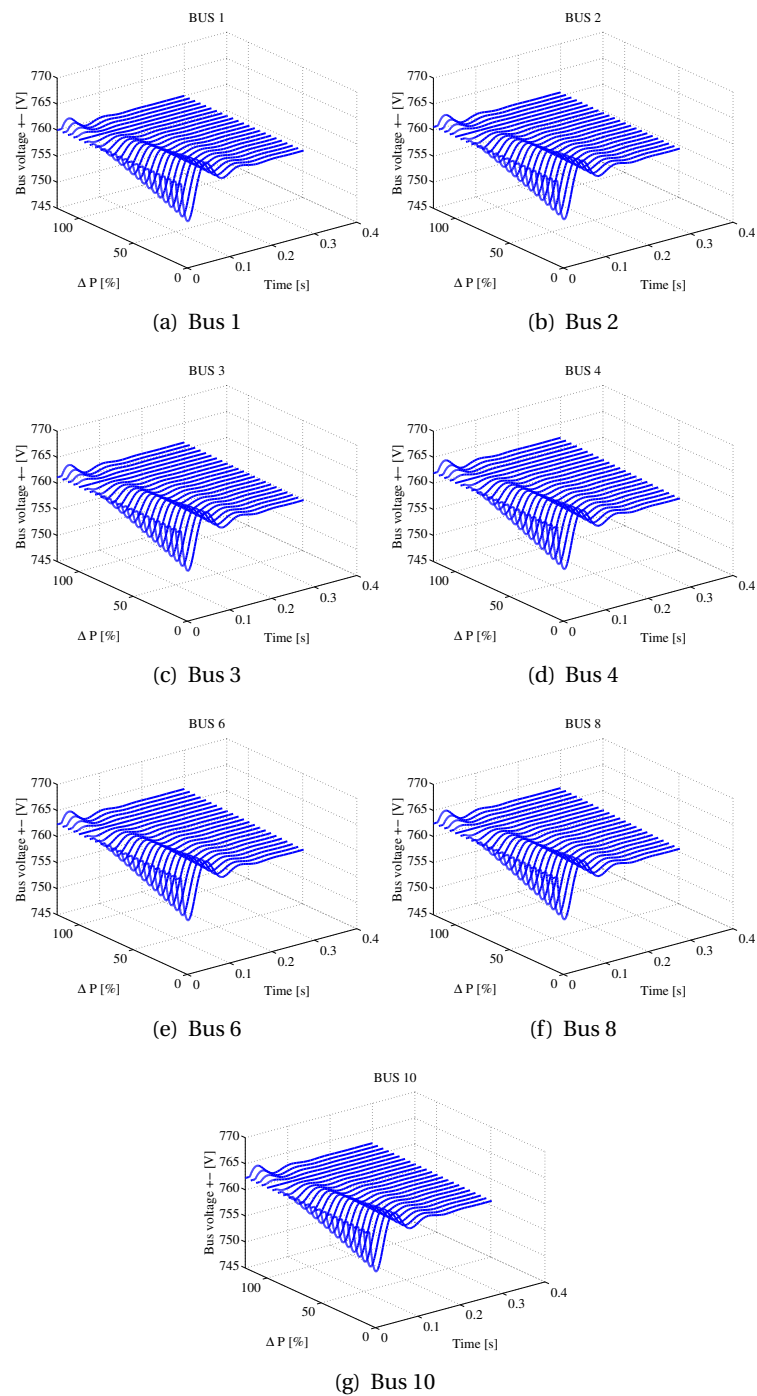


FIGURE 6.9: Bipolar bus voltage transients for varying microturbine power generation

## 6.2. Influence of power variations

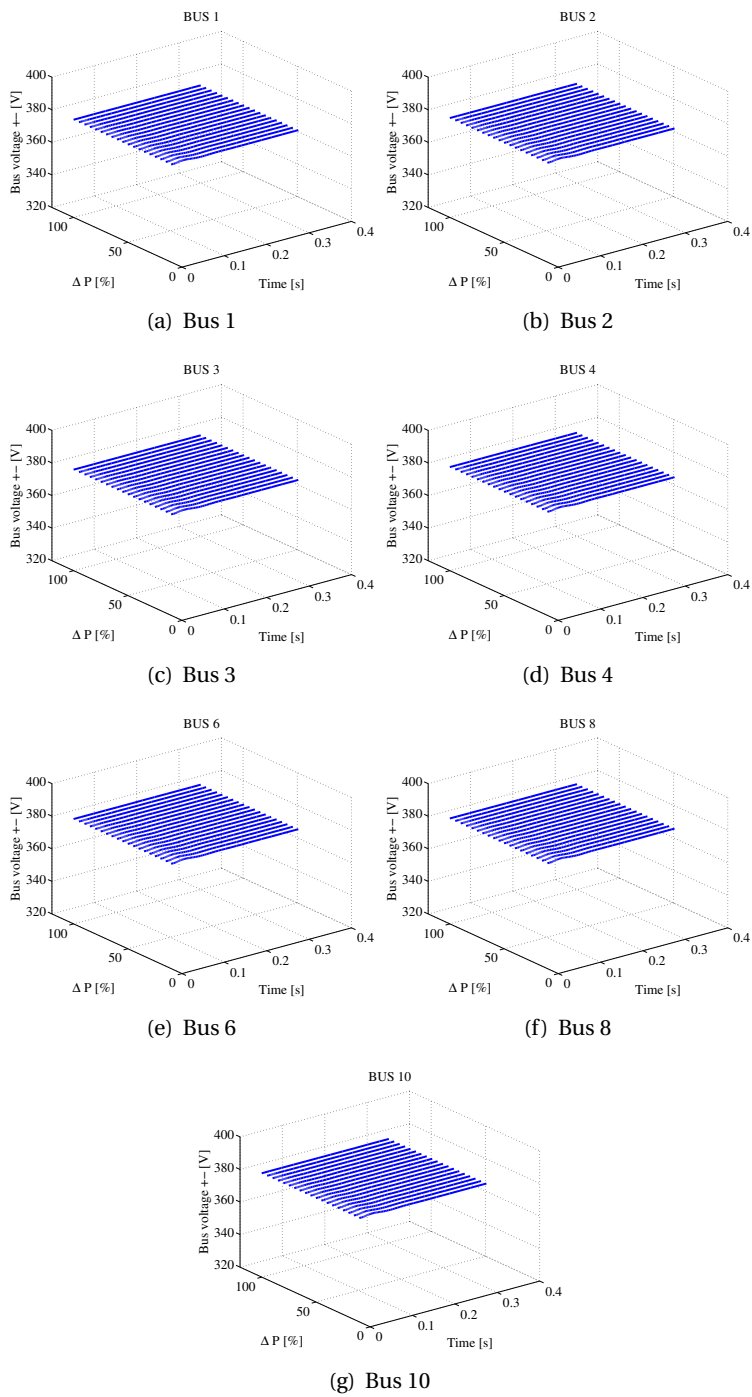


FIGURE 6.10: Unipolar bus voltage transients for varying resistive load (BUS 4) power demand

## 6. DC VOLTAGE STABILITY OF A LVDC NETWORK

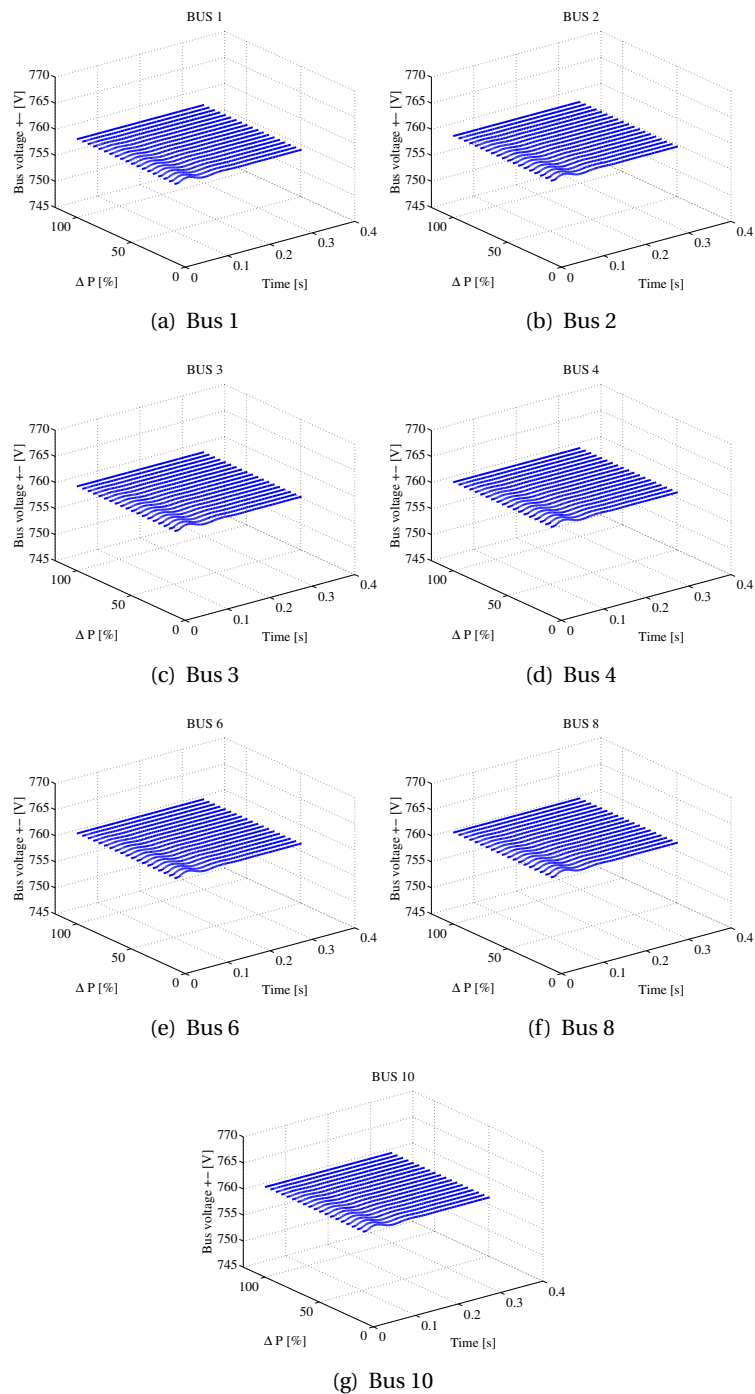


FIGURE 6.11: Bipolar bus voltage transients for varying resistive load (BUS 4) power demand

## 6.3 Conclusion

This chapter used the toolbox MatLVDC to study the influence of power input variations on the bus voltages in a DC network. A unipolar and bipolar network, that supply the same loads and have the same topology, were presented and the results were subsequently compared.

The bipolar configuration shows higher voltage fluctuations when a power variation occurs, in comparison to unipolar networks. Meanwhile it was observed that the conduction losses in the bipolar network are lower. Therefore less damping is present in bipolar networks, which is an explanation for the higher voltage transients.

The results are also given for variations of the microturbine generated power and load power. Similar transients are observed with the same period, that can also be derived from a bode diagram of the linearized network.

While this chapter considered some specific power variations to demonstrate the use of MatLVDC, future work should investigate the influence of short-circuits and grounding schemes on the voltage stability. Furthermore, the DC systems that were studied in this chapter are AC grid-connected. In the context of DC microgrids, voltage stability in islanding-mode should also be investigated. The toolbox MatLVDC can contribute to investigate these phenomena.



## Chapter 7

# Conclusion and future work

The increasing number of distributed energy resources that require DC power, in particular renewable energy sources, and the increasing number of DC loads, offer opportunities to apply DC power instead of AC power in distribution networks.

DC power systems have furthermore strengths, weaknesses and threats in comparison to AC power systems. The increased power transfer capability and increased power quality are identified as the main strengths. The main weakness of DC power systems is the unproven reliability, in contrast to AC power systems. The lack of standardization presents today the main threat to DC power systems. In particular, no nominal voltage level has been standardized, but several nominal voltage levels are proposed in the technical literature (an overview was provided in table 2.1).

To ensure the safe and reliable operation of DC networks, stability of the DC voltage is of utmost importance. Since no definition for DC voltage stability is available, this thesis proposed one that is based upon the accepted definition of power system stability.

The destabilizing influence of constant-power loads on the DC voltage is demonstrated from different perspectives and they all lead to the same result: the maximum power that can be drawn by the constant-power load depends quadratically on the nominal voltage level.

Multiple stability criteria for DC networks were proposed in the past, but have some inherent drawbacks. All these are restricted versions of the Nyquist criterion for linear systems applied to the minor-loop gain at the point of interconnection between source and load subsystems. Therefore, these criteria only apply for unidirectional power flow. Consequently, these criteria are not valid when bidirectional power flow occurs in DC networks that contain distributed generators. Moreover, these criteria only provide sufficient conditions for stability that can lead to conservative design decisions.

To overcome these drawbacks, this thesis addresses voltage stability using small-signal analysis and time-domain simulations. Small-signal analysis can only be applied for small disturbances around a specific operating point, but can prove instability of an operating point when poles are located in the right-half plane. To study large disturbances, time-domain simulations for specific scenarios are considered.

Both the time-domain simulations and the small-signal analysis require a dynamic model of DC power systems. This model should include the network equations, and models of the loads, power sources and the power electronic converters. The equations can subsequently be linearized to analyze small-signal stability or solved to study time-domain responses.

Time-domain simulations are always a trade-off between the required accuracy and the available computational resources. Time-domain simulations that take too long will not facilitate the design process, where the designer wants to verify the stability and check the influence of design decisions on the safety and reliability of DC networks. Switched models of power electronic converters exist that are very accurate, but require substantial simulation times, especially when larger networks need to be analyzed. On the contrary, simulations have proven that averaged models of power electronic converters require significantly less computational resources, while still providing sufficiently accurate results to assess voltage stability.

To analyze the stability of DC power systems, the author has developed MatLVDC, a Matlab® toolbox that is capable of setting up a model of a DC power system fast and easy using a user-friendly input data format. MatLVDC includes functions to execute time-domain simulations, compute linearized system poles and study the influence of parameter variations. MatLVDC can also be used to determine source and load impedance specifications for existing stability criteria.

This thesis uses MatLVDC to assess the stability of a DC network and to compare the voltage transients between the unipolar and bipolar configuration for different simulation scenarios. The simulations show that power fluctuations in the bipolar network configuration result in larger voltage deviations compared to the unipolar network configuration.

Further research should focus on causes for instability and solutions to improve the stability of DC networks. The application of active damping techniques, that for instance can be provided by energy storage systems in DC microgrids, should be considered. Also the influence of grounding and protection schemes on the voltage stability should be investigated. When a short-circuit occurs in the network, this may result in unstable behavior. Therefore the fault-ride through capability of the power generators in the network should be defined based upon large-signal stability assessment. DC voltage stability should also be ascertained when DC microgrids operate in islanding-mode. MatLVDC can contribute to analyze these phenomena.

# **Appendices**



## Appendix A

# Maximum power through a line

The maximum power through a line is calculated for three-phase AC, unipolar DC and bipolar DC distribution networks. The formulas that are derived in this appendix, apply to a line that connects between a source and a load. This facilitates the comparison between possible configurations for distribution networks, and shows that more power can be transmitted through the same line when DC is applied [9, 4].

### A.1 Assumptions

- The maximum line-line voltage between the conductors  $\hat{V}$  equals the peak voltage of the cable insulation. The source voltage in every case that is studied is assumed to deliver the peak voltage:

$$V_{AC,src} = \frac{\hat{V}}{\sqrt{2}} \text{ (three-phase AC)}, V_{DC2,src} = \hat{V} \text{ (unipolar DC)} \text{ and } V_{DC3,src} = \frac{\hat{V}}{2}.$$

- The maximum line current ( $I$ ) through a conductor equals the maximum rms current
- The maximum voltage drop across a line equals 10% of the source voltage
- The load is assumed to be balanced in case of the three-phase AC and the bipolar DC distribution network
- Following line elements are taken into account in the calculation:
  - AC: line resistance  $r$  and inductance  $x$  per unit length<sup>1</sup>
  - Unipolar DC: line resistance  $r$  and neutral resistance  $r_n$  per unit length
  - Bipolar DC: line resistance  $r$  per unit length

---

<sup>1</sup>Since the three-phase AC distribution line is balanced, no current flows through the neutral conductor and consequently, the resistance and inductance of the neutral conductor do not have to be taken into account.

## A.2 Maximum power through a line

In the subsequent paragraphs, the expressions will be derived for the maximum transmissible power at the load end of the distribution line. The maximum rms current through and maximum voltage drop across the line limits the transmissible power. For short lengths, the maximum rms current will limit the maximum transmissible power, while for long lengths the voltage drop will be the limiting factor. There thus will be a cross-over between both limits at a certain line length.

### Three-phase AC distribution

When the maximum rms current flows through the distribution line, the maximum three-phase transmissible power at the load end equals:

$$P_{AC,i} = \sqrt{3}V_{load}I \cos \phi = \sqrt{3} \sqrt{\left(\frac{\hat{V}}{\sqrt{2}} - L \cdot r \cdot I\right)^2 + (L \cdot x \cdot I)^2} I \cos \phi \quad (\text{A.1})$$

where  $V_{load}$  is the rms load line voltage and  $\cos \phi$  is the power factor of the load.  $r$  and  $x$  are the line resistance and inductance per unit length respectively.  $L$  is the line length. In the last step,  $V_{load}$  is substituted and it is assumed that the peak voltage at the source end equals the maximum peak current of the conductor.

When the maximum voltage drop  $\Delta V_{max} = 10\% \frac{\hat{V}}{\sqrt{2}}$  appears across the distribution lines, the maximum three-phase transmissible power at the load end equals:

$$P_{AC,\Delta v} = \sqrt{3} \sqrt{\frac{\hat{V}}{\sqrt{2}} + 0.1 \frac{\hat{V}}{\sqrt{2}}} \frac{0.1 \frac{\hat{V}}{\sqrt{2}}}{\sqrt{(L \cdot r)^2 + (L \cdot x)^2}} \cos \phi \quad (\text{A.2})$$

### Unipolar DC distribution

When the maximum rms current flows through the unipolar DC distribution line, the maximum transmissible power at the load end equals:

$$P_{DC2,i} = (\hat{V} - L \cdot (r + r_n) \cdot I) I \quad (\text{A.3})$$

where  $r_n$  denotes the neutral conductor resistance value per unit length.

When the maximum voltage drop  $\Delta V_{max} = 10\% \hat{V}$  appears across the unipolar DC distribution line, the maximum three-phase transmissible power at the load end equals:

$$P_{DC2,\Delta v} = (\hat{V} - 0.1 \hat{V}) \frac{0.1 \hat{V}}{L \cdot (r + r_n)} \quad (\text{A.4})$$

**Bipolar DC distribution**

When the maximum rms current flows through the bipolar DC distribution line, the maximum transmissible power at the load end equals:

$$P_{DC3,i} = \left(2 \cdot \frac{\hat{V}}{2} - 2 \cdot L \cdot r \cdot I\right) I \quad (\text{A.5})$$

When the maximum voltage drop  $\Delta V_{max} = 10\% \hat{V}$  appears across the bipolar DC distribution line, the maximum three-phase transmissible power at the load end equals:

$$P_{DC3,\Delta V} = \left(2 \cdot \frac{\hat{V}}{2} - 0.1 \frac{\hat{V}}{2}\right) \frac{0.1 \frac{\hat{V}}{2}}{2 \cdot L \cdot r} \quad (\text{A.6})$$



## **Appendix B**

# **MatLVDC User Guide**

# MatLVDC<sub>v1.0</sub> User Guide

Giel Van den Broeck

MatLVDC is a Matlab® toolbox to analyze the stability of low-voltage direct current (LVDC) networks (including power electronic converters and distributed energy resources) via time-domain simulations and small-signal stability analysis. The toolbox is intended for students and researchers that are investigating DC networks and to facilitate the design process.

## 1 Capabilities

MatLVDC includes following capabilities:

- Time-domain simulation of DC networks
  - Including loads and generation that are interfaced via power-electronic converters
  - Unipolar and bipolar network configurations
  - Radial, ring and meshed network topologies (Figure 1).
- Analyze the DC network stability
  - Perform small-signal analysis
  - Determine system pole locations
  - Analyze the frequency response

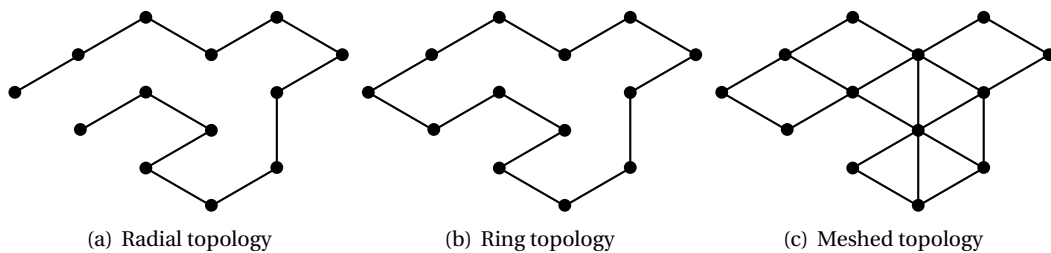


Figure 1: Possible network topologies

## 2 Installation

MathWorks Matlab® is required to use MatLVDC

1. Unpack the MatLVDC zip-file
2. Open Matlab®
3. Add the unzipped folder MatLVDC and its subfolders to the Matlab® path

## 3 Terminology and input data

The *DC system* (fig. 2) refers to the overall system that includes all elements and control loops that are present in the DC network. MatLVDC distinguishes three types of elements that constitute a DC system:

**Bus** A bus is a connection point in a network where loads and generation can be connected to (fig. 3).

**Branch** A branch is an electrical connection between two busses. The branch model is shown in Figure 5.

**Component** A component refers to a load or generation subsystem that is part of the DC network. Examples of a component are: photovoltaic generation, battery energy storage system, AC/DC voltage-source inverters.

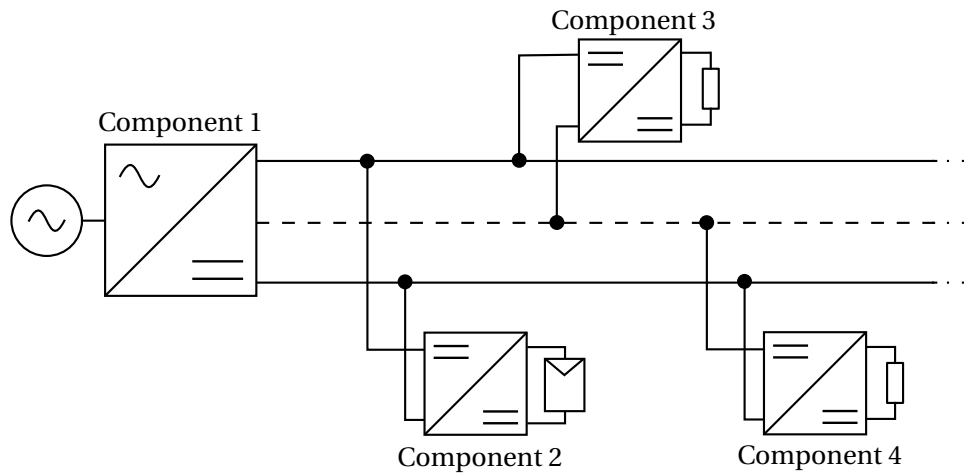


Figure 2: DC system

To setup a DC system, the busses, branches and components need to be defined as input data in a matrix format that resembles the input data format of MatPower and MatACDC (see Table 1, 2 and 3).

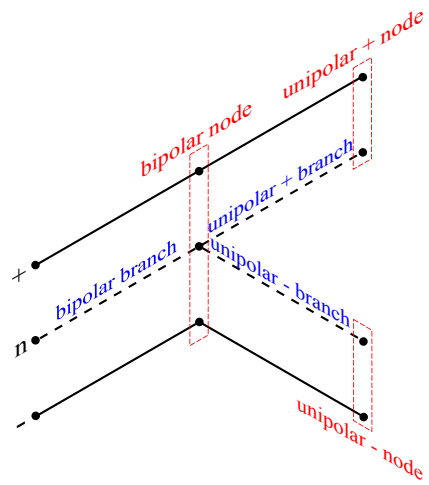


Figure 3: Possible branch and bus configurations

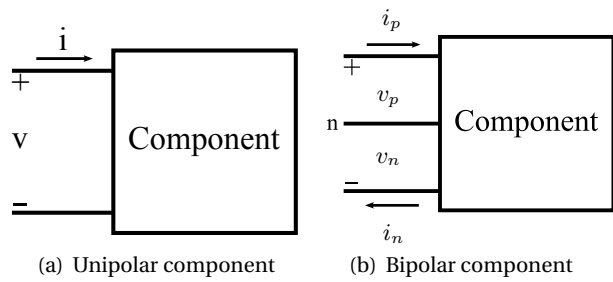


Figure 4: Possible component configurations

The branches, busses have a *configuration* and components have a *connection* parameter that can take 3 values (see Fig. 3):

1. **Unipolar positive** In case of a bus, the bus has a positive and a neutral terminal. In case of a branch, the branch has a positive and neutral conductor and in case of a component, the component is connected between the positive and neutral terminal of a bus.
2. **Unipolar negative** In case of a bus, the bus has a negative and a neutral terminal. In case of a branch, the branch has a negative and neutral conductor and in case of a component, the component is connected between the neutral and negative terminal of a bus.
3. **Bipolar** In case of a bus, the bus has a positive, negative and a neutral terminal. In case of a branch, the branch has a positive, negative and neutral conductor and in case of a component, the component is connected to the positive, negative and neutral terminal of a bus.

*Components* are considered as (multi)port subsystems, that can take the terminal voltage as an input and take the input current that flows into the component as an output. Be careful not to confuse input currents and voltages with *system* in and outputs: the input current can be a subsystem output.

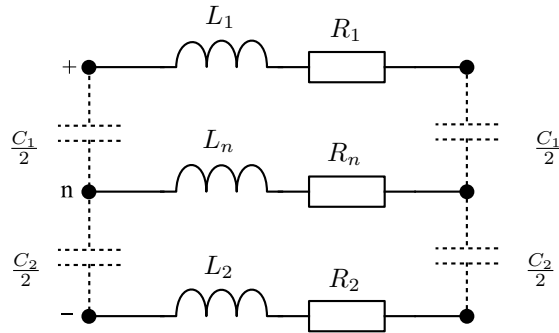


Figure 5: Branch model

1	BUSDC_I	Bus number
2	BUSDC_CONFIG	The bus configuration: <ol style="list-style-type: none"> <li>1. Unipolar + to n</li> <li>2. Unipolar n to -</li> <li>3. Bipolar p to n</li> </ol>

Table 1: Bus input data

Two component configurations exist:

1. *Current controlled components* control the input current that flows into the component. The input voltage is taken as a system input and the input current is the system output.
2. *Voltage controlled components* control the input voltage across the component terminals. The input current is taken as a system input and the input voltage is the system output.

Because of the internal structure of the software, *every bus needs to have just one voltage controlled component* connected to every terminal (between positive and neutral and negative and neutral). In most of the cases<sup>1</sup>, this will be a capacitor component. This capacitor component should also include the branch shunt capacitances. The resulting capacitance at a bus can be calculated using the function `getBusCapacitances(busNumbers)`.

## 4 Component library

MatLVDC contains a component library that includes common models for DC networks. The available components are listed in table 3.

<sup>1</sup>Other cases are when the bus is used to regulate the network voltage. E.g. an AC/DC converter or a battery energy storage system that regulate the DC voltage.

1	F_BUS	The number of the bus where the branch departs
2	T_BUS	The number of the bus where the branch arrives
3	BR_CONFIG	The configuration of the branch: 1. Unipolar + to n 2. Unipolar n to - 3. Bipolar p to n
4	BR.R1	Series resistance of the positive conductor (Figure 5)
5	BR.R2	Series resistance of the negative conductor (Figure 5)
6	BR.Rn	Series resistance of the neutral conductor (Figure 5)
7	BR.L1	Series inductance of the positive conductor (Figure 5)
8	BR.L2	Series inductance of the negative conductor (Figure 5)
9	BR.Ln	Series inductance of the neutral conductor (Figure 5)
10	BR.C1	Shunt capacitance between positive and neutral conductor (Figure 5)
11	BR.C2	Shunt capacitance between the neutral and negative conductor (Figure 5)

Table 2: Branch input data

## 5 Using MatLVDC

### How to run a time-domain simulation

1. Create the bus matrix, branch matrix and component matrix
2. Create a new DC System object via `DCSystem`
3. Determine an initial condition. Use the steady-state method of the DC System class via `steadyState` to determine the steady-state solution. Provide a nonlinear equation solver (e.g. `fsolve`) to the method.
4. Create a `SignalBuilder` object and define the external input signals to the DC system.
5. Run `simulate`, provide an initial condition and a time frame to simulate

`simulate` allows to specify a ordinary differential equation (ode) solver. The Matlab built-in variable step ode solver `ode23tb` is recommended. Users can specify error tolerances according to the required accuracy.

### How to perform a small-signal stability analysis

1. Determine an equilibrium point for the small-signal analysis
2. Run `linearSys` to calculate the linearized system. `linearSys` also returns the linearized system poles.
3. Process the results
  - Use `PostProcessor.polePlot()` to plot the system poles
  - Use `PostProcessor.rootLocus()` to plot the system poles for varying system parameters
  - Use `PostProcessor.time3dplot()` to study the influence of a parameter variation on the time-domain transient in a xyz axis representation

1	COMP_I	Component number
2	COMP_BUS	The bus number of the bus where the component is connected to
3	COMP_TYPE	The type of the component: 1. Photovoltaic array interfaced via a boost DC/DC converter 2. Battery energy storage system interfaced via a DC/DC boost converter 3. Three-phase AC/DC inverter 4. Current source 5. (No component defined) 6. Voltage source 7. (No component defined) 8. Resistive load interfaced via a DC-DC converter 9. Bipolar capacitors 10. Unipolar capacitors 11. Voltage balancer 12. AC/DC converter interfaced via a voltage balancer 13. Permanent-magnet synchronous generator 14. Microturbine
4	COMP_CONFIG	The component configuration: 1. Current controlled 2. Voltage controlled
5	COMP_CONN	The component connection: 1. Unipolar + to n 2. Unipolar n to - 3. Bipolar p to n
6	C1	Input capacitor connected between + and n
7	C2	Input capacitor connected between n and -

Table 3: Component input data

## 6 Troubleshooting

### Errors

MatLVDC verifies the input data that is entered by the user. Following errors can occur and subsequently be resolved by adapting the input data:

**Component x has an invalid connection specified** Check the connection of component x

**Invalid input data: multiple voltage controlling components connected at positive/negative terminal of BUS x** Check the number of voltage controlling components at BUS x. Only one voltage controlling component per bus terminal (positive/negative) is allowed.

**Invalid input data: no voltage controlling component is connected at the positive/negative terminal of BUS x** Make sure that just one voltage controlling component is connected at BUS x. Regularly, this can be a capacitor component (COMP 9 for bipolar busses or COMP 10 for unipolar busses)

**Branch x is a bipolar branch and cannot be connected between unipolar busses** Check the branch and bus configuration

**Branch x is a positive/negative branch and cannot be connected between unipolar negative/positive busses** Check the branch and bus configuration

**Component x cannot be connected to a unipolar positive/negative bus** Check the bus connection

Following *warnings* may occur:

**The component numbering has been updated** The user can assign random component numbers in the component matrix. However, MatLVDC requires the numbers to be in ascending order, starting from 1. If the component matrix numbering does not follow this rule, the component numbers are updated by MatLVDC.

**The bus numbering has been updated** The user can assign random component numbers in the bus matrix. However, MatLVDC requires the numbers to be in ascending order, starting from 1. If the bus matrix numbering does not follow this rule, the bus numbers are updated by MatLVDC. MatLVDC will transfer the bus numbers in the component matrix to the updated versions.

### Difficulties with steady-state convergence

To determine the steady-state, MatLVDC allows to specify a nonlinear equation solver. Matlab built-in nonlinear equation solver `fsolve` is recommended, but can have difficulties to converge to the steady-state solution.

This difficulty can be overcome by providing a good initial estimate of the DC system state. Therefore the `steadyState` method in the `DCSystem` class initializes the bus voltage to the nominal voltage level.

Alternatively, the user can provide an initial estimate. A good initial estimate can be obtained by running a short time-domain simulation of the DC system until steady-state. The last solution in the time-domain simulation can then serve as an initial point for the nonlinear equation solver.

## 7 For developers

### How to define custom component definitions?

1. Determine the configuration of component x: unipolar (2 terminals) or bipolar (3 terminals)
2. Create 3 Matlab functions, starting from the template scripts:
  - x\_deqn** contains the state-space representation of the custom component. Replace 'x' by a custom component name.
  - x\_oeqn** contains the outputs of the custom component. The first outputs are predetermined according to table xxx.
  - x\_labels** contains the state, input, output and parameter labels of the component. This allows to automatically create legend entries for plots.

Component configuration	Type	Required internal inputs	Required outputs
Unipolar	Voltage-controlled	$i$	$v$
	Current-controlled	$v$	$i$
Bipolar	Voltage-controlled	$[i_p i_n]$	$[v_p v_n]$
	Current-controlled	$[v_p v_n]$	$[i_p i_n]$

Table 4: Component inputs and outputs

## 8 Function reference

The Matlab code is documented, including all input and output specifications of the functions of MatLVDC. This function reference gives an overview of the main functions of MatLVDC

**DCSystem** is the main class of MatLVDC

`DCSystem(bus_matrix, branch_matrix, component_matrix)` Create a new DC system object  
`steadyState(extInputs, x0, nominalVoltage, solverOptions)` Calculate the steady state using `fsolve`, for the given set of external inputs to the DC system

`simulate(odesolver, solverOptions, t_span, signalBuilder, x0)` Simulate the DC system response for a given set of external input signals specified by a Signal Builder object.

`linearSys(X, extInputs)` return the linearized system matrices for the DC system around an operating point X for a given set of external inputs.

`setComponentParameters(COMP_ID, parameters)` Set the component parameters of the component specified by the COMP\_ID. The parameters is an input vector.

`displayStates, displayInputs, displayOutputs` Display the states/inputs/outputs of a DC System. The index of the state/input/output is returned, the component it belongs to and the label. This function allows to track the system variables.

**PostProcessor** presents the simulation results graphically

`polePlot(poles, markerSize)` plot the poles that are specified in the poles array.

`statePlot(time, results, labels)` Create a plot with the results with respect to time. The results array has the same structure as the array that is returned by Matlab built-in ode solvers. The labels are the legend entries for the results.

`time3dplot` Create a xyz plot of the time response for a specified quantity and a specified range of a parameter that is altered. To be used in conjunction with `StabilityAnalysis.multiTimeSim`.

**StabilityAnalysis** includes the functions to analyze the stability and effect of parameter variations on the DC system stability

`rootLocus` Create a root locus pole plot for a specified range of a parameter

`multiTimeSim` Run multiple time-domain response simulations for a specified range of a parameter

**SignalBuilder** creates the input signals for time-domain simulations

`newSignal(externalInputNumber, signalFcn, SignalParameters)` Adds a signal to the SignalBuilder that will be applied at the external input that is specified by externalInputNumber. signalFcn allows to specify a type of signal. Built-in signals are `@ constant` (1 parameter being the constant signal value) and `@step` signal (3 parameters: the instant when the step occurs, the initial value and the final value).

## **Appendix C**

# **Modeling Dynamics of Electric and Electronic Components in DC Distribution Grids**

Published in the transactions of the Young Researchers Symposium 2014 [27].

# Modeling Dynamics of Electric and Electronic Components in DC Distribution Grids

Giel Van den Broeck, Mai Tuan Dat, *Graduate Student Member, IEEE* and Johan Driesen, *Senior Member, IEEE*

**Abstract**—DC power has recently become a potential option to contribute to future power systems. While the steady state analysis of DC distribution networks becomes more and more mature, dynamic analysis of DC grids is under-investigated. On the other hand, transient of DC network is different from AC networks' due to a greater participation of electronics converters at generator sides and consumption sides. This paper describes a model of a DC network comprising several components to produce a general formulation which is subsequently simulated and validated.

**Index Terms**—DC power system, DC grids, distribution networks, Renewable Energy Sources (RESs), converters, dynamic analysis, transient.

## I. INTRODUCTION

The continuous power demand at distribution grids drives distribution systems to operate more efficiently. Nevertheless, quick development of Distributed Energy Resources (DERs) introduces a technical stress on the existing AC power networks because of unpredictable production of Renewable Energy Sources (RESs) particularly low-power top-roof PVs and wind turbines.

In order to overcome this issue, DC grid is proposed as an alternative solution at distribution power networks to integrate completely RESs, electronically based loads, and electric vehicles into DC power. DC technology is already widespread in several applications such as telecommunication systems, data centers and mobility applications. DC power at power distribution levels currently has technical-economical advantages over traditional AC power. One of distinguishing features of DC grids is the requirement of electronic converters at both generator sides and load sides to regulate power as well as voltage in the networks.

While the analysis of DC distribution networks becomes more and more mature in steady states, the dynamic analysis is under-investigated to assess the reliability during transient [1]. Firstly, independent controllers of each converter should be taken into account in the analysis. Secondly, non-linearity of constant power loads causes incorrect results if the linearisation does not coordinate all of sub-models of the system. Thirdly, grouping different sub-models, which yield an overall system, need to be defined for stability analysis. However, this task has not been straightforward.

G. Van den Broeck, T-D. Mai and J. Driesen are with group Electa, the Department of Electrical and Electronics Engineering at Katholieke Universiteit Leuven (KU Leuven) and Energy Ville, Belgium. This work was supported in part by FWO Project of DC grids G037312N Dynamische Efficacite Analyse van Midden-en Laagspanning DC Distributie Netwerken

This paper proposes a general methodology to formulate a DC grid network. A generalized formulation of the network is manipulated by sub-models of electrical components in space-states matrix. The models of generators, distribution lines and loads are introduced in average mode equations. Different kinds of controlled-converters situated at generator side and loads side are taken into account. Large signal analysis and results of various test cases are employed to validate the proposed formulation method.

## II. SWITCHING-MODEL TYPE VERSUS AVERAGE-MODEL TYPE IN SIMULATION

Due to the switching operation of power converters, values of voltage and current quickly vary corresponding to the states of power switches. A simulation of DC grid in a switching model hence provides more detail results. However, the simulation in the switching model also requires more computational resources that becomes insufficient for a large scale simulation of DC grids. On the other hand, the simulation in average-model yields the same results as the switching-model approach and fully expresses the transients of values. A comparison of these two different approaches is introduced in Fig.1. Issues of harmonics is assumed not to be presented in this paper. Therefore the average-model approach is adequate for modeling large scale systems.

## III. DC MICRO-GRID MODELING

This paper introduces a simple model of a DC network, comprising an AC/DC interface converter at node 1, 2 constant power loads (CPLs) at node 2 and 3, a PV system (node 4) and a battery energy storage system (BESS) at node 3, which are interconnected by 3 distribution lines. This simple model shown in Fig.2 is suitable to emphasize the context of this paper. While Source #1 represents the AC/DC interface converter, which controls the DC bus voltage  $v_1$  by varying the amount of power exchanged between the DC and the AC grid. It therefore operates as a slack bus. Source #2 is considered as a PV array system interfaced via a DC-DC boost converter. Source #3 is a battery energy storage system (BESS) operating as a current controlled-source. Load #1 and #2 are both constant-power loads which behave as a negative incremental impedance that subsequently leads to instability. The nominal voltage level of the DC grid is assumed at 400V.

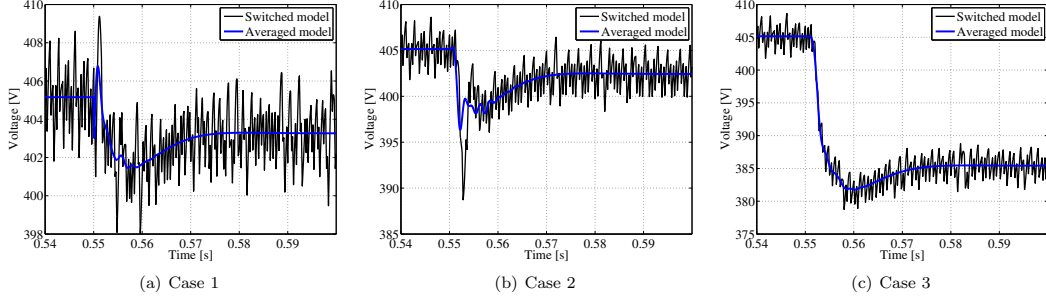


Fig. 1. Step responses of the voltage at different test cases simulated by the detail switching-model and the average-model approach

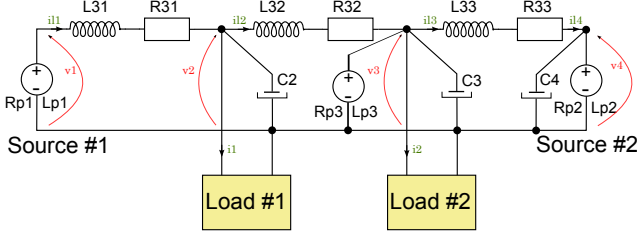


Fig. 2. Representation diagram of a simple DC network with 3 sources and 2 loads

#### IV. ELECTRICAL ELEMENTS OF THE DC MICRO-GRID

##### A. Distributed generators

Model of generators is divided into 3 groups depending on the hardware topology. They are categorized into three phase AC-DC rectifiers, single phase AC-DC rectifiers and DC-DC converters. Controller integrated at each converter regulates either voltage or current at bus. Due to the assumption in this paper, models of a single phase DC converter and an AC-DC converter are described as a demonstration. The alternative representative model of DC-DC converter is slightly different from [2] and suitable with the PV model in [3]. The model of AC-DC rectifier is formulated in an average-model approach with a DC voltage control.

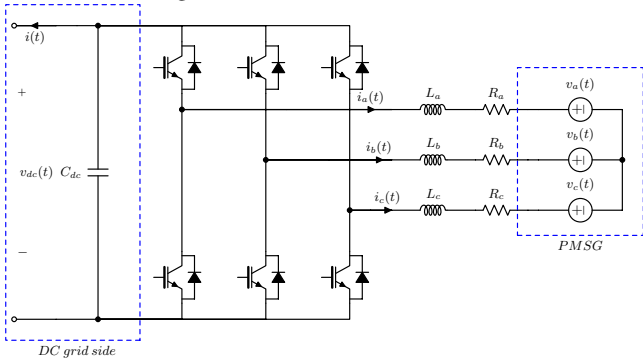


Fig. 3. Representation of a three-phase PMSG interfacing with a three phase converter

1) *Three phase AC-DC rectifier*: AC-DC PWM interface rectifier is a power converter that interconnects between a DC distribution grid and an AC grid. This device allows power to be delivered in a bidirectional flow. The AC side is modeled as an infinite bus, connected via an RL filter to the converter.

AC electrical components are expressed in the  $d-q$  rotating reference frame to facilitate the controller operation and design. This approach considerably simplifies the controller's equations and hence improves the controller performance. The  $d-q$  frame control requires a synchronization mechanism. It is usually achieved through the phase-locked loop (PLL) which is assumed to work properly in this scheme. The model of the AC-DC PWM rectifier controls not only the AC active power injection but also the DC bus voltage level. The proposed cascade structure controlling the DC bus voltage is an outer-loop control which determines the active power set-point of the inner-loop controller.

$$\begin{aligned} L_f \frac{di_d}{dt} &= -R_f i_d + \omega L_f i_q - V_{conv_d} + V_d \\ L_f \frac{di_q}{dt} &= -R_f i_q - \omega L_f i_d - V_{conv_q} + V_q \end{aligned} \quad (1)$$

By giving 2 control inputs  $V_{conv_d} = m_d \frac{v_{dc}}{2}$  and  $V_{conv_q} = m_q \frac{v_{dc}}{2}$

$$\begin{aligned} L_f \frac{di_d}{dt} &= -R_f i_d + \omega L_f i_q - \frac{v_{dc}}{2} m_d + V_d \\ L_f \frac{di_q}{dt} &= -R_f i_q - \omega L_f i_d - \frac{v_{dc}}{2} m_q + V_q \end{aligned} \quad (2)$$

Modulation index  $m_d$  and  $m_q$  are regulated by the control law:

$$\begin{aligned} m_d &= \frac{2}{v_{dc}} (-u_d + L_f \omega i_q + V_d), \\ m_q &= \frac{2}{v_{dc}} (-u_q - L_f \omega i_d + V_q) \end{aligned} \quad (3)$$

*Inner loop current controller*:

$$\begin{aligned} L_f \frac{di_d}{dt} &= -R_f i_d + u_d \\ L_f \frac{di_q}{dt} &= -R_f i_q + u_q \end{aligned} \quad (4)$$

By introducing two controller equations which are expressed as follows

$$\begin{aligned} u_d(t) &= x_d(t) + k_d(s) (i_d(t) - i_{dref}(t)) \\ u_q(t) &= x_q(t) + k_q(s) (i_q(t) - i_{qref}(t)) \end{aligned} \quad (5)$$

Two PI controllers  $k_p(s)$  and  $k_q(s)$  are employed to control  $i_d(t)$  and  $i_q(t)$  corresponding to their respective reference values and are described as follows

$$k_d(s) = k_q(s) = \frac{k_p s + k_i}{s} \quad (6)$$

where  $k_p = \frac{L_f}{\tau_i}$ ,  $k_i = \frac{R_f}{\tau_i}$

Current  $i_q(t)$  is set to zero to regulate the reactive power flow at zero in steady-state while  $i_d(t)$  determines the active

power flow. The participation of PI controllers for close loop control produces two additional state variables ( $x_d$  and  $x_q$  respectively) at each converter. Eq.4 yields

$$\frac{i_d(s)}{i_{dref}(s)} = \frac{i_q(s)}{i_{qref}(s)} = \frac{1}{\tau_i s + 1} \quad (7)$$

Therefore, the transfer function between the actual values and the set-point values of the system is composed as a low-pass filter when an inner loop feedback are implemented by the current loop controllers.

*Outer loop current controller:* DC voltage at the DC side is expressed as

$$\frac{C}{2} \frac{dv_s^2}{dt} = P_{convout} - P_{grid} = \frac{3}{2} v_d i_d - v_s i_s \quad (8)$$

where  $v_s, i$  are the grid connected DC side voltage and its current respectively.

By neglecting switching loss:

$$\begin{aligned} \frac{3}{2} v_d i_d &= P_{electric} - \frac{3}{2} R_f i_d^2 \\ \frac{C}{2} \frac{dv_s^2}{dt} &= P_{electric} - \frac{3}{2} R_f i_d^2 - v_s i_s \end{aligned} \quad (9)$$

where  $P_{electric} = P_{prime mover} - \frac{J}{2n_p} \frac{d\Omega^2}{dt}$  is the number of pole pairs.  $R_f$  is small and considered as a disturbance.

Introduce  $i_{ref} = u_v + \gamma \frac{P_{electric}}{v_s}$ ;  $e(t) = v_{sref}^2 - v_s^2$

DC-link equation yields

$$\begin{aligned} \frac{C}{2} \frac{dv_s^2}{dt} &= (1 - \gamma) P_{wind} - v_s u_v \\ U_v(s) &= k_v E_v(s) = \frac{\alpha_1 s + \alpha_2}{s(s + \alpha_3)} E_v(s) \end{aligned} \quad (10)$$

By combining Eq.7 and Eq.10, the space states yield

$$\frac{d}{dt} \begin{bmatrix} i_d \\ i_q \\ \zeta_1 \\ \zeta_2 \\ i_{dref} \end{bmatrix} = \underbrace{\begin{bmatrix} 0 & 0 & 0 & 0 & \frac{1}{\tau_i} \\ 0 & 0 & 0 & 0 & 0 \\ 0 & 0 & -\alpha_3 & 0 & 0 \\ 0 & 0 & 1 & 0 & 0 \\ 0 & 0 & \alpha_1 & \alpha_2 & 0 \end{bmatrix}}_A \underbrace{\begin{bmatrix} i_d \\ i_q \\ \zeta_1 \\ \zeta_2 \\ i_{dref} \end{bmatrix}}_x + \underbrace{\begin{bmatrix} 0 \\ 0 \\ 1 \\ 0 \\ 0 \end{bmatrix}}_B e(t) \quad (11)$$

The Eg.11 demonstrates that an AC-DC converter with cascade controllers in DC grid is feasible to be implemented as a slack bus and modeled in a states-space representation form.

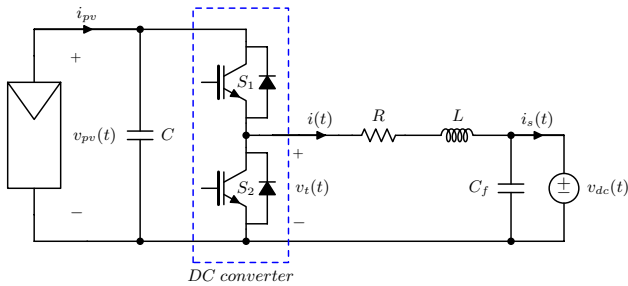


Fig. 4. Representation pf an PV array interfacing with a buck converter

2) *DC-DC converter:* Model of a PV array is described as a current function according to the PV output voltage and expressed as the following

$$i_{pv} = n_p I_{ph} - n_p I_{rs} \left[ \exp \left( \frac{q}{k\vartheta A} \frac{v_{dc}}{n_s} \right) - 1 \right] \quad (12)$$

where

$I_{rs}$  : reverse saturation current of  $p - n$  junction.

$q = 1.602 \times 10^{-19} C$  : unit electric charge.

$k = 1.38 \times 10^{-23} J/K$  : Boltzman 's constant.

$\vartheta$  :  $p - n$  junction temperature (in  $^{\circ}K$ ).

$A$  : ideality factor.  $I_{ph}$  : short-circuit current of one string of the PV panels, is the function of temperature, is a linear function of the solar irradiation level  $S$ , as

$$I_{ph} = [I_{scr} + k_{\vartheta}(\vartheta - \vartheta_r)] \frac{S}{100} \quad (13)$$

where

$\vartheta_r$ : cell reference temperature

$I_{scr}$ : short circuit current of one PV cell at the reference temperature irradiation level, and  $k_{\vartheta}$  is a temperature coefficient.

$$\begin{aligned} P_{pv} &= i_{pv} v_{dc} \\ P_{pv} &= f(v_{dc}, S, \vartheta) \\ &= n_p I_{ph} v_{dc} - n_p I_{rs} v_{dc} \left[ \exp \left( \frac{q}{k\vartheta A} \frac{v_{dc}}{n_s} \right) - 1 \right] \end{aligned} \quad (14)$$

The PV array is interfaced with the DC network through a DC-DC boost converter. Controller of the DC-DC converter regulates  $v_{pv}$  in order to operate the PV array at the maximum power point (MPP). The dynamics of  $v_{pv}$  are negatively affected by the capacitor  $C$  at the input of the DC-DC converter:

Dynamical equation of DC-link voltage is based on the principle of power balance, as

$$C \frac{dv_{pv}(t)}{dt} = i_{pv}(v_{pv}, S, \theta) - i(t) \quad (15)$$

where  $P_{dc}$  denotes the power delivered to the VSC DC side  $v_{pv}$  voltage across PV array.

A PV array interfaced via a DC buck converter is expressed as the following

$$\begin{aligned} P_{dc} &= v_s i + R i^2 + L \frac{di}{dt} \\ &= v_s i + R i^2 + \frac{1}{2} \frac{di^2}{dt} \end{aligned} \quad (16)$$

where  $i(t)$  : inductive current controlled by an inner current control loop via the control input  $d(t)$ .

The PV characteristic  $i_{pv}$  in 15 is a nonlinear expression. To facilitate the controller design, an alternative control input is proposed as follows

$$u_v \equiv i^* - i_{pv} \quad (17)$$

Thanks to the inner control loop control, output current is assumed to quickly fit with the reference current  $i(t) \approx i^*$ 's  $i(t)$ . In addition, response of the inner control is considerably faster than the outer voltage control loop. Therefore the transfer

function of current shown in Fig. 18 is approximated by a first-order low pass-filter.

$$\frac{I_{dc}(s)}{I_{dc}^*(s)} = \frac{1}{\tau s + 1} \quad (18)$$

A PI controller  $k_v(s) = K_p + \frac{K_i}{s}$  regulates  $v_{pv}$  to the desired reference value  $v_{pv}^*$ , corresponding to the MPP. The voltage controller parameters are tuned by matching the desired system poles to a second order closed-loop transfer function.

The system state-space description corresponding to Equation 19 yields

$$\frac{d}{dt} \begin{bmatrix} v_{pv} \\ \zeta \end{bmatrix} = \begin{bmatrix} -K_p/C & -1/C \\ K_i & 0 \end{bmatrix} \begin{bmatrix} v_{pv} \\ \zeta \end{bmatrix} + \begin{bmatrix} K_p/C \\ -K_i \end{bmatrix} v_{pv}^* \quad (19)$$

3) *General dynamic equation:* Both two models of generator are combined in one state-space matrix. The general form of this matrix is described as follows:

$$\begin{aligned} \frac{d}{dt} x_{gen} &= A_c \cdot x_{gen} + B_c \cdot i + S_c \cdot e_{source} \\ i_{gen} &= C_c \cdot x_{gen} \\ v_{gen} &= E_c \cdot x_{gen} \end{aligned} \quad (20)$$

A generator operates at one of two functions which are either a slack bus or a no-slack bus depending to the operational scheme of a multi-terminal DC grid [4], where

$$\begin{aligned} A_c &= \begin{bmatrix} A_c(\text{slack}) & 0 \\ 0 & A_c(\text{no slack}) \end{bmatrix}; \\ B_c &= \begin{bmatrix} 0 \\ 0 \end{bmatrix}; \\ S_c &= \begin{bmatrix} S_c(\text{slack}) \\ 0 \end{bmatrix}; \\ C_c &= \begin{bmatrix} C_c(\text{slack}) \\ 0 \end{bmatrix}; \\ E_c &= \begin{bmatrix} 0 \\ E_c(\text{no slack}) \end{bmatrix}; \end{aligned} \quad (21)$$

## B. Battery Energy storage system - BESS

The BESS is modeled as a constant voltage source and an internal resistance and neglected the dynamics of the state-of-charge of the battery. This assumption is valid since the state-of-charge will not show fast dynamics during the transients which are the topic of this paper. The BESS is interfaced via a bi-directional DC-DC converter with the DC network, which allows to control the battery current. Conversely, the BESS is modeled as a current constant load in charging mode. The NREL model of a Lead-acid battery shown in in Fig.5 is implemented in this paper.

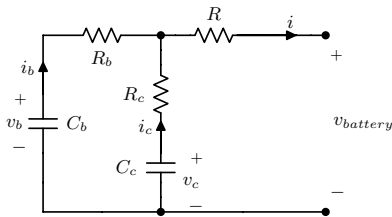


Fig. 5. NREL model of a lead-acid battery

## C. Distribution Lines

Distribution lines are modeled as components consisting of resistance and inductance values. Although the inductance value is rather smaller than the resistance values in distribution lines, it is not neglected in the simulation because of the voltage impact during transients. The dynamics of voltage and current in the distribution lines yields

$$\begin{aligned} \frac{d}{dt} x_{line} &= A_n \cdot x_{line} + B_n \cdot u_v + G_n \cdot u_c + L_n \cdot u_{load} \\ i_{line} &= C_n \cdot x_{line} \\ v_{conv_i} &= E_n \cdot x_{line} \\ v_{bus} &= H_n \cdot x_{line} \end{aligned} \quad (22)$$

where

$$x_{line} = [i_{lines}, v_{current\ source}];$$

$u_v$ : voltage at other buses ;

$u_c$ : current generated by current-source converters

$u_{load}$ : current required by loads

For instance, representative matrix of the distribution lines introduced in Section III. is formulated as follows:

$$\begin{aligned} A_n &= \begin{bmatrix} -\frac{R_{31}}{L_{31}} & 0 & 0 & \frac{1}{L_{31}} & 0 & 0 \\ 0 & -\frac{R_{32}}{L_{32}} & 0 & -\frac{1}{L_{31}} & -\frac{1}{L_{32}} & 0 \\ 0 & 0 & -\frac{R_{33}}{L_{33}} & 0 & -\frac{1}{L_{33}} & -\frac{1}{L_{33}} \\ \frac{1}{C_2} & -\frac{1}{C_2} & 0 & 0 & 0 & 0 \\ 0 & \frac{1}{C_3} & -\frac{1}{C_3} & 0 & 0 & 0 \\ 0 & 0 & \frac{1}{C_4} & 0 & 0 & 0 \end{bmatrix} \\ B_n &= \begin{bmatrix} \frac{1}{L_{31}} & 0 & 0 & 0 & 0 & 0 \\ 0 & 0 & 0 & -\frac{1}{C_2} & 0 & 0 \end{bmatrix} \\ C_n &= \begin{bmatrix} 0 & 0 & 0 & 0 & -\frac{1}{C_3} & 0 \end{bmatrix} \\ D_n &= \begin{bmatrix} 0 & 0 & 0 & 0 & 0 & -\frac{1}{C_4} \end{bmatrix} \end{aligned}$$

## D. Loads

1) *R-L Load:* is considered as a current depending load.

$$\begin{aligned} \frac{d}{dt} x_{load} &= A_l \cdot x_{load} + B_l \cdot u_l \\ x_{load} &= C_l \cdot x_{load} \end{aligned} \quad (23)$$

where  $x_{load} = i_L$  ;  $u_l$  is the voltage across load ;  $A_l = \frac{R_l}{L_l}$  ;  $B_l = \frac{1}{L_l}$  ;  $C_l = 1$  for one load.

2) *Constant power Load (CPL):* A CPL is interfaced through a power electronic stage which is either DC-DC or DC-AC converter [5]. A feedback loop is required to control load demand described in [6]. A formula in [7] expresses a strict relation of consumption demand and converter component values as the following

$$P_L < V_l^2 \left( \frac{C}{L_l} R_l + \frac{1}{R_0} \right) \quad (24)$$

where  $V_l$  is the steady voltage across load;  $C, R_0$  are capacitor and resistor connecting in parallel with CPL respectively;  $L_l, R_l$  are inductor and resistor connecting in series with the power converter stage.

TABLE I  
CIRCUIT PARAMETERS

Parameter description	Symbol	Value
Constant-power load power	$P_{cpl}$	3 kW
Rated PV power	$P_{pv}$	7 kW
Distribution line resistance	$R_{31} = R_{32} = R_{33}$	0.138 $\Omega$
Distribution line inductance	$L_{31} = L_{32} = L_{33}$	0.26 mH
Distribution line capacitance	$C_2 = C_3 = C_4$	1 mF
AC/DC interface converter capacitance	$C_1$	2.2 mF
Nominal DC grid voltage	$V_{dc}$	400 V

## V. GLOBAL LINEARIZED MODEL

Different elements of the DC micro grid introduced in the previous section are composed and formulated in the unique matrix. Thanks to the mutual interconnection of electrical values, outputs of one element are inputs of other elements. The general dynamic equation  $\dot{X}_{sys} = f(X_{sys}) + g(u)$  after linearization yields:

$$\frac{d}{dt} X_{sys} = \begin{bmatrix} A_c & B_c \times E_n & 0 \\ B_n \times C_c & A_n & L_n \times E_l \\ 0 & B_l \times H_n & A_l \end{bmatrix} \cdot X_{sys} + \begin{bmatrix} S_c & B_c(noslack) & 0 \\ 0 & 0 & 0 \\ 0 & 0 & B_l(CPL) \end{bmatrix} \cdot \begin{bmatrix} e_{source} \\ i_{ref} \\ P_{CPL} \end{bmatrix} \quad (25)$$

where  $X_{sys} = [x_{gen}; x_{line}; x_{load}]$

Dimension of matrices in Eq.25 depends on a number of components of components, including generators, loads and distribution lines so that the global linearized model matrix consists 2 sparse matrices  $A_{ov}$  and  $B_{ov}$ . The sparsity of the system matrices allows to exploit sparse matrix solvers, which are computationally less intensive.

## VI. VALIDATION

In order to validate the method of modeling DC grids with converters proposed in this paper, a simulation using PLECS and Matlab/Simulink is presented here. Electrical components are separately built as sub-models before being formulated in a global generalized model in Eq.25. Three test cases are deployed as follows to fully evaluate the formulation as well as the simulation results in average mode approach.

- 1) *Test case 1* - Shading PV showing the transient when the production on PV diminishes.
- 2) *Test case 2* - Transient caused by BESS when the battery switches from discharging to charging mode.
- 3) *Test case 3* - Voltage step-change at slack bus showing the transient when the output voltage level at the AC-DC converter is immediately regulated from 400V to 380V.

Results of the three test cases are evaluated at each bus in terms of the variation of voltage, current, power and losses. The simulation interval is examined from 0.54s to 0.6s. Initial condition of three test cases have the same values to emphasize the variation of each value during transient. Some assumptions are applied to simplify the simulation model which include the following

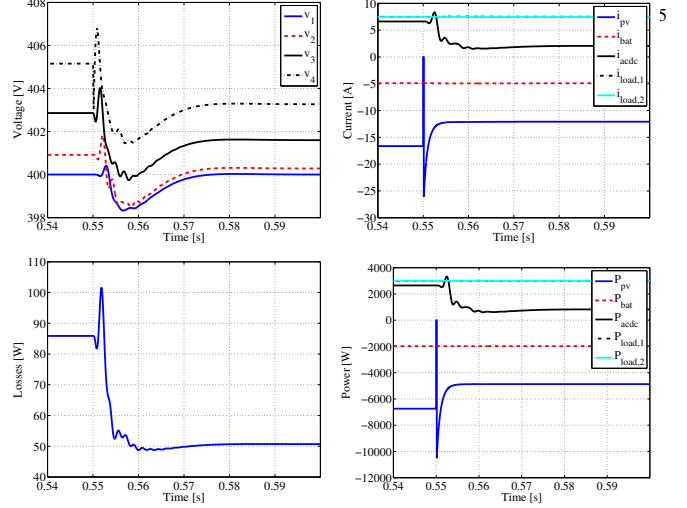


Fig. 6. Transient of voltage, current, load and power in Test case 1 in case of changing PV power

- The BESS is modeled as a constant voltage source and an internal resistance, interfaced via a DC-DC buck converter to the DC network.
- Averaged models are used for the converters by assuming that the switching ripple is negligible as compared to the time averages of the voltages and currents.
- The converter is a loss-less device in which no switching losses and conduction losses are taken into account.
- The MPP of the PV array is tracked instantaneously, thereby neglecting the MPPT algorithm dynamics.
- The PLL properly functions to keep  $V_q$  at 0V.
- The AC-DC interface converter drives as a slack bus. The AC grid is modeled as an infinite bus with a constant voltage amplitude.

A PV shading in Test case 1 assumes that the solar irradiation suddenly decreases from 100% to 75% corresponding to a decline of 1750W of PV production. The transients of values shown in Fig. 6 mainly affect the voltage level at each node. The voltage at node 4 where PV array is installed drops by nearly 2V while the voltage at other buses is less influenced by this PV power variation. The power sent back to AC grid side also decreases so that total losses in distribution lines also decreases.

Operation mode of the BESS is switched from discharging mode to charging mode in Test case 2 in which the output current is triggered from  $-5A$  to  $5A$ . The BESS behaves as a constant current source rather than a slack bus in this simulation. A DC converter is interfaced to boost voltage from 200V at battery's terminals to 400V at the DC side. Although the electrical oscillation appears and lasts during the transient, the voltage step change is unremarkable. However, the overshoot of line currents and bus power where the BESS is installed are twice higher than the deviation of two steady state values which is shown in the Fig. 7. So the losses are also overshoot of their values and ringed during transient.

The responses of electrical values when the set-point value of the slack bus declines to 380V are introduced in Fig. 8.

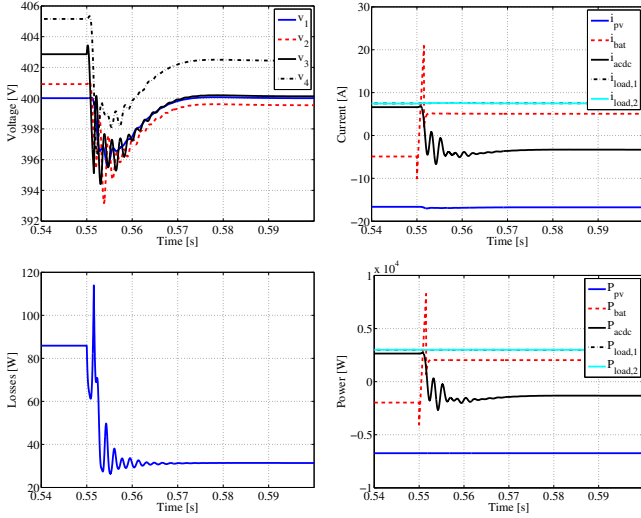


Fig. 7. Transient of voltage, current, load and power in Test case 2 in case of changing operational mode of BESS

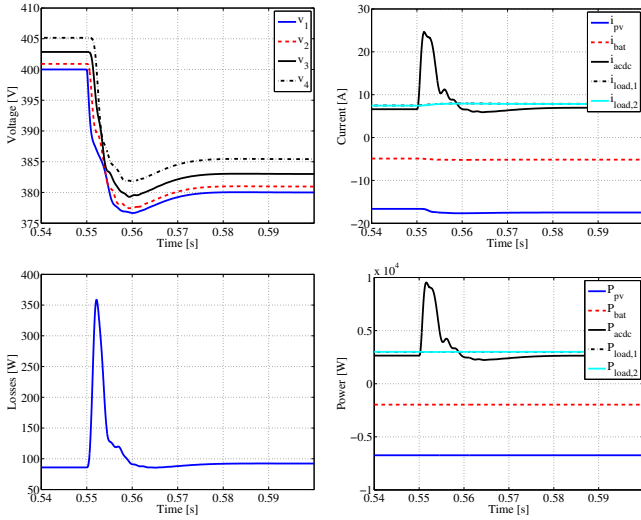


Fig. 8. Transient of voltage, current, load and power in Test case 3 in case of changing slack-bus voltage

Voltage at the other buses accordingly changes without any oscillation. A transient peak of power and current exists at the node installing AC-DC converter due to the capacitor filter which also causes transient of total losses.

## VII. CONCLUSION

A global model is obtained by linearizing sub-models and coupling them. The dynamic behavior of each component is plotted and evaluated if there is any transient occurring at a specific bus.

The proposed dynamic model is applied not only for transient analysis such as voltage, power, and current but also for evaluating total losses of system caused by converters in DC grids. Because control parameters of converters mainly affect the overall system, the dynamic model is also an alternative assessment tool to tune the parameters of converters.

- [1] B. Zahedi, S. Member, and L. E. Norum, "Modeling and Simulation of All-Electric Ships With Low-Voltage DC Hybrid Power Systems," *IEEE Transactions on Power Electronics*, vol. 28, no. 10, pp. 4525–4537, 2013.
- [2] C. H. Rivetta, A. Emadi, S. Member, G. A. Williamson, and R. Jayabalan, "Analysis and Control of a Buck DC-DC Converter Operating With Constant Power Load in Sea and Undersea Vehicles," *IEEE Transactions on Industrial Applications*, vol. 42, no. 2, pp. 559–572, 2006.
- [3] A. Yazdani, P. P. Dash, and S. Member, "A Control Methodology and Characterization of Dynamics for a Photovoltaic (PV) System Interfaced With a Distribution Network," *IEEE Transaction on Power Delivery*, vol. 24, no. 3, pp. 1538–1551, 2009.
- [4] J. Beerten, S. Cole, and R. Belmans, "Generalized Steady-State VSC MTDC Model for Sequential AC/DC Power Flow Algorithms," *Power Systems, IEEE Transactions on*, vol. 27, no. 2, pp. 821–829, 2012.
- [5] M. Brenna, C. Bulac, G. C. Lazaroiu, S. Member, and E. Tironi, "DC Power Delivery in Distributed Generation Systems," in *International Conference on Harmonics and Quality of Power, 2008. ICHQP 2008. 13th*, 2008, pp. 1–6.
- [6] C. Rivetta, "Large-Signal Analysis of a DC-DC Buck Power Operating with a Constant Power Load," in *Industrial Electronics Society, 2003. IECON '03. The 29th Annual Conference of the IEEE*, no. 1, 2003, pp. 732–737.
- [7] A. Kwasinski and P. T. Krein, "Passivity-Based Control of Buck Converters with Constant-Power Loads," in *Power Electronics Specialists Conference, 2007. PESC 2007. IEEE, 2007*, pp. 259–265.



# References

- [1] ABB. ABB Onboard DC Grid. URL <http://www.abb.com/cawp/seitp202/12314897e272c132c1257c6d002fc268.aspx>.
- [2] Thomas Ackermann, Göran Andersson, and Lennart Söder. Distributed generation: a definition. *Electr. Power Syst. Res.*, 57(3):195–204, April 2001. ISSN 03787796. doi: 10.1016/S0378-7796(01)00101-8. URL <http://www.sciencedirect.com/science/article/pii/S0378779601001018>.
- [3] A Agustoni, M Brenna, and E Tironi. Proposal for a high quality DC local distribution network with photovoltaic generation and storage systems. In *7th Int. Conf. Electr. POWER Qual. Util.*, pages 17–19, 2003.
- [4] Alessandro Agustoni, Enrico Borioli, Morris Brenna, Giuseppe Simioli, Enrico Tironi, and Giovanni Ubezio. LV DC distribution network with distributed energy resources: analysis of possible structures. 2005.
- [5] Michael Bahrman and Per-Erik Bjorklund. The New Black Start: System Restoration with Help from Voltage-Sourced Converters. *IEEE Power Energy Mag.*, 12(1):44–53, January 2014. ISSN 1540-7977. doi: 10.1109/MPE.2013.2285592. URL <http://ieeexplore.ieee.org/articleDetails.jsp?arnumber=6684690>.
- [6] ME Baran and NR Mahajan. DC distribution for industrial systems: opportunities and challenges. *Ind. Appl. IEEE ...*, 2003. URL [http://ieeexplore.ieee.org/xpls/abs\\_all.jsp?arnumber=1248241](http://ieeexplore.ieee.org/xpls/abs_all.jsp?arnumber=1248241).
- [7] Jef Beerten. *Modelling and Control of DC Grids (Modellering en controle van DC netten)*. PhD thesis, 2013.
- [8] Ulrich Boeke, Roland Weiß, Anton Mauder, Luc Hamilton, and Leopold Ott. White Paper Efficiency Advantage Advantages of +/- 380 V DC Grids. Technical report, 2014.
- [9] E. Borioli, M. Brenna, R. Faranda, and G. Simioli. Comparison between the electrical capabilities of the cables used in LV AC and DC power lines. In *2004 11th Int. Conf. Harmon. Qual. Power (IEEE Cat. No.04EX951)*, pages 408–413. IEEE, 2004. ISBN 0-7803-8746-5. doi: 10.1109/ICHQP.2004.1409390. URL <http://ieeexplore.ieee.org/lpdocs/epic03/wrapper.htm?arnumber=1409390>.

- [10] Morris Brenna, Enrico Tironi, and Giovanni Ubezio. Proposal of a local dc distribution network with distributed energy resources. In *Harmon. Qual. Power, 2004. 11th Int. Conf.*, pages 397–402. IEEE, 2004.
- [11] Johannes Brombach, Arno Lucken, Brice Nya, Martin Johannsen, and Detlef Schulz. Comparison of different electrical HVDC-architectures for aircraft application. In *Electr. Syst. Aircraft, Railw. Sh. Propuls. (ESARS), 2012*, pages 1–6. IEEE, 2012.
- [12] V.A. Caliskan, O.C. Verghese, and A.M. Stankovic. Multifrequency averaging of DC/DC converters. *IEEE Trans. Power Electron.*, 14(1):124–133, 1999. ISSN 08858993. doi: 10.1109/63.737600. URL <http://ieeexplore.ieee.org/lpdocs/epic03/wrapper.htm?arnumber=737600>.
- [13] K. Clement-Nyns, E. Haesen, and J. Driesen. The Impact of Charging Plug-In Hybrid Electric Vehicles on a Residential Distribution Grid. *IEEE Trans. Power Syst.*, 25(1): 371–380, February 2010. ISSN 0885-8950. doi: 10.1109/TPWRS.2009.2036481. URL <http://ieeexplore.ieee.org/articleDetails.jsp?arnumber=5356176>.
- [14] Colin Debruyne, Bart Verhelst, Jan Desmet, and Lieven Vandeveld. Technical SWOT analysis of decentralised production for low voltage grids in Flanders, 2012. URL <https://biblio.ugent.be/publication/2109738/file/2109739.pdf>.
- [15] Department of Defense. Aircraft Electric Power Characteristics MIL-STD-704F. Standard, 2004.
- [16] Electric Power Research Institute. The Integrated Grid: Realizing the Full Value of Central and Distributed Energy Resources. Technical report, Electric Power Research Institute, 2014.
- [17] A. Emadi. Modelling and analysis of multi-converter DC power electronic systems using the generalized state space averaging method. In *IECON'01. 27th Annu. Conf. IEEE Ind. Electron. Soc. (Cat. No.37243)*, volume 2, pages 1001–1007. IEEE, 2001. ISBN 0-7803-7108-9. doi: 10.1109/IECON.2001.975908. URL <http://ieeexplore.ieee.org/articleDetails.jsp?arnumber=975908>.
- [18] A. Emadi, A. Khaligh, C.H. Rivetta, and G.A. Williamson. Constant Power Loads and Negative Impedance Instability in Automotive Systems: Definition, Modeling, Stability, and Control of Power Electronic Converters and Motor Drives. *IEEE Trans. Veh. Technol.*, 55(4):1112–1125, July 2006. ISSN 0018-9545. doi: 10.1109/TVT.2006.877483. URL <http://ieeexplore.ieee.org/articleDetails.jsp?arnumber=1658410>.
- [19] Kristof Engelen, Erik Leung Shun, Pieter Vermeyen, Ief Pardon, Reinhilde D’hulst, Johan Driesen, and Ronnie Belmans. Small-scale residential dc distribution systems. In *IEEE Benelux Young Res. Symp. Electr. Power Eng.* sn, 2006.

- [20] T Esum and PL Chapman. Comparison of photovoltaic array maximum power point tracking techniques. *IEEE Trans. ENERGY ...*, 2007. URL [http://www.mz3r.com/fa/wp-content/uploads/2012/02/books/photovoltaic\\_papers/comparison-of-photovoltaic-array-maximum-power-techniques-point-tracking-techniques.pdf](http://www.mz3r.com/fa/wp-content/uploads/2012/02/books/photovoltaic_papers/comparison-of-photovoltaic-array-maximum-power-techniques-point-tracking-techniques.pdf).
- [21] European Parliament and European Council. Directive 2006/95/EC. Technical Report 9, 2006.
- [22] European Telecommunication Standards Institute. ETSI EN 300 132-3-1 Final Draft. 1:1–31, 2011.
- [23] CC Fang and EH Abed. Sampled-data modeling and analysis of closed-loop PWM DC-DC converters. *Circuits Syst. 1999. ISCAS'99. ...*, 1999. URL [http://ieeexplore.ieee.org/xpls/abs\\_all.jsp?arnumber=777523](http://ieeexplore.ieee.org/xpls/abs_all.jsp?arnumber=777523).
- [24] O. Fethi, L.-A. Dessaint, and K. Al-Haddad. Modeling and simulation of the electric part of a grid connected micro turbine. In *IEEE Power Eng. Soc. Gen. Meet. 2004.*, volume 2, pages 2213–2220. IEEE. ISBN 0-7803-8465-2. doi: 10.1109/PES.2004.1373274. URL <http://ieeexplore.ieee.org/articleDetails.jsp?arnumber=1373274>.
- [25] Gene F. Franklin, J. David Powell, and Abbas Emami-Naeini. *Feedback control of dynamic systems*. Pearson Education, New Jersey, 6th edition, 2010. ISBN 9780135001509.
- [26] E W Gholdston, K Karimi, F C Lee, J Rajagopalan, Y Panov, and B Manners. Stability of large DC power systems using switching converters, with application to the International Space Station. In *Energy Convers. Eng. Conf. 1996. IECEC 96., Proc. 31st Intersoc.*, volume 1, pages 166–171. IEEE, 1996.
- [27] VB Giel, TD Mai, and J Driesen. Modeling Dynamics of Electric and Electronic Components in DC Distribution Grids. *status Publ.*, 2014. URL <https://lirias.kuleuven.be/handle/123456789/451741>.
- [28] Hongwen He, Rui Xiong, and Jinxin Fan. Evaluation of Lithium-Ion Battery Equivalent Circuit Models for State of Charge Estimation by an Experimental Approach. *Energies*, 4(12):582–598, March 2011. ISSN 1996-1073. doi: 10.3390/en4040582. URL <http://www.mdpi.com/1996-1073/4/4/582>.
- [29] International Energy Agency. Tracking Clean Energy Progress 2014 Tracking Clean Energy Progress 2014. Technical report, 2014.
- [30] International Energy Association. Global EV Outlook. (April):41, 2013.
- [31] B.K. Johnson and R. Lasseter. An industrial power distribution system featuring UPS properties. In *Proc. IEEE Power Electron. Spec. Conf. - PESC '93*, pages 759–765. IEEE, 1993. ISBN 0-7803-1243-0. doi: 10.1109/PESC.1993.472009. URL <http://ieeexplore.ieee.org/lpdocs/epic03/wrapper.htm?arnumber=472009>.

- [32] Jackson John Justo, Francis Mwasilu, Ju Lee, and Jin-Woo Jung. AC-microgrids versus DC-microgrids with distributed energy resources: A review. *Renew. Sustain. Energy Rev.*, 24:387–405, 2013.
- [33] T Kaipia, J Lassila, J Partanen, and J Lohjala. Principles and tools for the 20/1/0.4 kV distribution network planning. In *Proc. Nord. Nord. Distrib. Asset Manag. Conf. 2006*, 2006.
- [34] Tero Kaipia, Pasi Salonen, Jukka Lassila, and Jarmo Partanen. Possibilities of the low voltage DC distribution systems. In *Nord. Nord. Distrib. Asset Manag. Conf.*, 2006.
- [35] H. Kakigano, Y. Miura, T. Ise, and R. Uchida. DC Voltage Control of the DC Microgrid for Super High Quality Distribution. In *2007 Power Convers. Conf. - Nagoya*, pages 518–525. IEEE, April 2007. ISBN 1-4244-0843-1. doi: 10.1109/PCCON.2007.373016. URL <http://ieeexplore.ieee.org/lpdocs/epic03/wrapper.htm?arnumber=4239206>.
- [36] H Kakigano, M Nomura, and T Ise. Loss evaluation of DC distribution for residential houses compared with AC system. In *Power Electron. Conf. (IPEC), 2010 Int.*, pages 480–486. IEEE, 2010.
- [37] Hiroaki Kakigano, Yushi Miura, and Toshifumi Ise. Low-voltage bipolar-type DC microgrid for super high quality distribution. *Power Electron. IEEE Trans.*, 25(12):3066–3075, 2010.
- [38] Hiroaki Kakigano, Yushi Miura, and Toshifumi Ise. Distribution voltage control for dc microgrids using fuzzy control and gain-scheduling technique. 2013.
- [39] Per Karlsson and Jörgen Svensson. DC bus voltage control for a distributed power system. *Power Electron. IEEE Trans.*, 18(6):1405–1412, 2003.
- [40] Hassan K Khalil and J W Grizzle. *Nonlinear systems*, volume 3. Prentice hall Upper Saddle River, 2002.
- [41] M.R. Kuhn, Y. Ji, H.D. Joos, and J. Bals. An approach for stability analysis of nonlinear electrical network using antioptimization. In *2008 IEEE Power Electron. Spec. Conf.*, pages 3873–3879. IEEE, June 2008. ISBN 978-1-4244-1667-7. doi: 10.1109/PESC.2008.4592560. URL <http://ieeexplore.ieee.org/articleDetails.jsp?arnumber=4592560>.
- [42] P Kundur, NJ Balu, and MG Lauby. Power system stability and control. 1994. URL <http://www.academia.edu/download/30389105/invitation.pdf>.
- [43] Prabha Kundur, John Paserba, Venkat Ajarapu, Göran Andersson, Anjan Bose, Claudio Canizares, Nikos Hatziargyriou, David Hill, Alex Stankovic, Carson Taylor, and Others. Definition and classification of power system stability IEEE/CIGRE joint task force on stability terms and definitions. *Power Syst. IEEE Trans.*, 19(3):1387–1401, 2004.

- [44] J Lago, J Moia, and ML Heldwein. Evaluation of power converters to implement bipolar DC active distribution networksDC-DC converters. *Energy Convers. Congr. ...*, 2011. URL [http://ieeexplore.ieee.org/xpls/abs\\_all.jsp?arnumber=6063879](http://ieeexplore.ieee.org/xpls/abs_all.jsp?arnumber=6063879).
- [45] Jackson Lago and Marcelo Lobo Heldwein. Operation and control-oriented modeling of a power converter for current balancing and stability improvement of DC active distribution networks. *Power Electron. IEEE Trans.*, 26(3):877–885, 2011.
- [46] William S Levine. *The control handbook*. CRC press, 1996.
- [47] J. Mahdavi, A. Emaadi, M.D. Bellar, and M. Ehsani. Analysis of power electronic converters using the generalized state-space averaging approach. *IEEE Trans. Circuits Syst. I Fundam. Theory Appl.*, 44(8):767–770, 1997. ISSN 10577122. doi: 10.1109/81.611275. URL <http://ieeexplore.ieee.org/articleDetails.jsp?arnumber=611275>.
- [48] D. Maksimovic, A.M. Stankovic, V.J. Thottuvelil, and G.C. Verghese. Modeling and simulation of power electronic converters. *Proc. IEEE*, 89(6):898–912, June 2001. ISSN 00189219. doi: 10.1109/5.931486. URL <http://ieeexplore.ieee.org/lpdocs/epic03/wrapper.htm?arnumber=931486>.
- [49] D. Manz, R. Walling, N. Miller, B. LaRose, R. D’Aquila, and B. Daryanian. The Grid of the Future: Ten Trends That Will Shape the Grid Over the Next Decade. *IEEE Power Energy Mag.*, 12(3):26–36, May 2014. ISSN 1540-7977. doi: 10.1109/MPE.2014.2301516. URL <http://ieeexplore.ieee.org/lpdocs/epic03/wrapper.htm?arnumber=6802820>.
- [50] Didier Marx, Pierre Magne, Babak Nahid-Mobarakeh, Serge Pierfederici, and Bernard Davat. Large signal stability analysis tools in DC power systems with constant power loads and variable power loads - A review. *Power Electron. IEEE Trans.*, 27(4): 1773–1787, 2012.
- [51] J.-M. Meyer and A. Rufer. A DC Hybrid Circuit Breaker With Ultra-Fast Contact Opening and Integrated Gate-Commutated Thyristors (IGCTs). *IEEE Trans. Power Deliv.*, 21(2):646–651, April 2006. ISSN 0885-8977. doi: 10.1109/TPWRD.2006.870981. URL <http://ieeexplore.ieee.org/articleDetails.jsp?arnumber=1610674>.
- [52] R D Middlebrook. Topics in multiple-loop regulators and current-mode programming. *Power Electron. IEEE Trans.*, (2):109–124, 1987.
- [53] MIT. William Stanley and the invention of the transformer, 2002. URL <http://web.mit.edu/invent/iow/stanley.html>.
- [54] N Mohan and TM Undeland. *Power electronics: converters, applications, and design*. John Wiley and Sons, 2007. URL <http://scholar.google.be/scholar?hl=nl&q=power+electronics+mohan&btnG=&lr=#0>.

- [55] Thabit Salim Nasser, Zakaria Ziadi, Atsushi Yona, Tomonobo Senjyu, and Mamdouh Abdel-Akher. Comprehensive analysis of DC smart grid operation. In *Power Energy (PECon), 2012 IEEE Int. Conf.*, pages 880–885. IEEE, 2012.
- [56] Stavros Papathanassiou. A benchmark low voltage microgrid network. (April): 1–8, 2005. URL [http://www.researchgate.net/publication/237305036\\_A\\_BENCHMARK\\_LOW\\_VOLTAGE\\_MICROGRID\\_NETWORK/file/60b7d5269306c54780.pdf](http://www.researchgate.net/publication/237305036_A_BENCHMARK_LOW_VOLTAGE_MICROGRID_NETWORK/file/60b7d5269306c54780.pdf).
- [57] Antonino Riccobono and Enrico Santi. Comprehensive review of stability criteria for DC distribution systems. In *Energy Convers. Congr. Expo. (ECCE), 2012 IEEE*, pages 3917–3925. IEEE, 2012.
- [58] Daniel Salomonsson. *Modeling, control and protection of low-voltage dc microgrids*. PhD thesis, KTH, 2008.
- [59] Daniel Salomonsson, Lennart Soder, and Ambra Sannino. Protection of low-voltage DC microgrids. *Power Deliv. IEEE Trans.*, 24(3):1045–1053, 2009.
- [60] S.R. Sanders, J.M. Noworolski, X.Z. Liu, and G.C. Verghese. Generalized averaging method for power conversion circuits. *IEEE Trans. Power Electron.*, 6(2):251–259, April 1991. ISSN 08858993. doi: 10.1109/63.76811. URL <http://ieeexplore.ieee.org/articleDetails.jsp?arnumber=76811>.
- [61] A. Sannino, G. Postiglione, and M.H.J. Bollen. Feasibility of a DC network for commercial facilities. *IEEE Trans. Ind. Appl.*, 39(5):1499–1507, September 2003. ISSN 0093-9994. doi: 10.1109/TIA.2003.816517. URL <http://ieeexplore.ieee.org/articleDetails.jsp?arnumber=1233614>.
- [62] MR Michael Starke, Fangxing Li, Leon M. Tolbert, and Burak Ozpineci. AC vs. DC distribution: Maximum transfer capability. In *2008 IEEE Power Energy Soc. Gen. Meet. - Convers. Deliv. Electr. Energy 21st Century*, pages 1–6. IEEE, July 2008. ISBN 978-1-4244-1905-0. doi: 10.1109/PES.2008.4596730. URL <http://ieeexplore.ieee.org/lpdocs/epic03/wrapper.htm?arnumber=4596730>[http://ieeexplore.ieee.org/xpls/abs\\_all.jsp?arnumber=4596730](http://ieeexplore.ieee.org/xpls/abs_all.jsp?arnumber=4596730).
- [63] SD Sudhoff. DC stability toolbox 3.0, 2008. URL [https://engineering.purdue.edu/ECE/Research/Areas/PEDS/dc\\_stability\\_toolbox](https://engineering.purdue.edu/ECE/Research/Areas/PEDS/dc_stability_toolbox).
- [64] F. Vasca and L. Ianneli. *Dynamics and Control of Switched Electronic Systems*. Springer London, 2012. ISBN 1-4471-2884-2.
- [65] W Yan, M Braun, and J von Appen. Operation strategies in distribution systems with high level PV Penetration. *Sol. world ...*, 2011. URL [https://www.bayernwerk.de/pages/eby\\_de/Innovationen/Smart\\_Grid/V0e\\_Projektbeschreibung/Operation\\_Strategies\\_in\\_Distribution\\_Systems\\_with\\_High\\_Level\\_PV\\_Penetration\\_SolarWorldConference\\_201109.pdf](https://www.bayernwerk.de/pages/eby_de/Innovationen/Smart_Grid/V0e_Projektbeschreibung/Operation_Strategies_in_Distribution_Systems_with_High_Level_PV_Penetration_SolarWorldConference_201109.pdf).

- [66] Amirnaser Yazdani and Prajna Paramita Dash. A control methodology and characterization of dynamics for a photovoltaic (PV) system interfaced with a distribution network. *Power Deliv. IEEE Trans.*, 24(3):1538–1551, 2009.
- [67] Amirnaser Yazdani and Reza Iravani. *Voltage-Sourced Converters in Power Systems: Modeling, Control, and Applications*. Wiley, 2010. ISBN 0470551569. URL [http://books.google.be/books/about/Voltage\\_Sourced\\_Converters\\_in\\_Power\\_Syst.html?id=\\_x\\_4Cu-BKwkC&pgis=1](http://books.google.be/books/about/Voltage_Sourced_Converters_in_Power_Syst.html?id=_x_4Cu-BKwkC&pgis=1).
- [68] RD Zimmerman. MATPOWER: Steady-state operations, planning, and analysis tools for power systems research and education. *Power Syst. IEEE ...*, 2011. URL [http://ieeexplore.ieee.org/xpls/abs\\_all.jsp?arnumber=5491276](http://ieeexplore.ieee.org/xpls/abs_all.jsp?arnumber=5491276).